Local Dispersion Behaviour at Marylebone Road Monitoring Site

Bryn Noel Ubald
Aerospace Engineering MEng

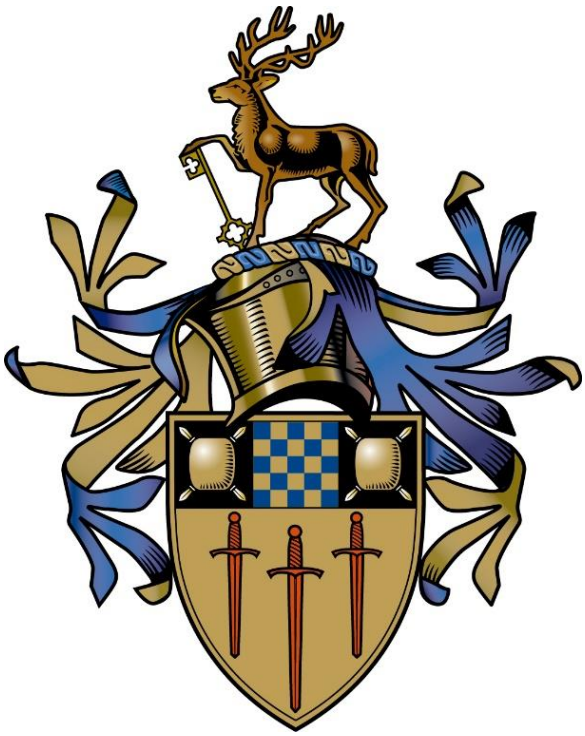

A dissertation
submitted in partial fulfilment of the
requirements for the degree of
Aerospace Engineering MEng

Department of Mechanical Engineering Sciences
Faculty of Engineering and Physical Sciences
University of Surrey

Project Report
May 2015

Project Supervisor: Professor Alan Robins

Abstract

One method of modelling the dispersion behaviour for the purpose of understanding the physical processes involved in an urban environment, is through the use of a wind tunnel. This present study seeks to model dispersion behaviour in a region surrounding Marylebone Road, London. This area is of particular interest as it is recorded as being one of the most polluted roads in central London and also due to the long standing presence of an air pollution monitoring station. The primary aim of this report is to use wind tunnel modelling to evaluate the impact of the monitoring station on measurements taken at the field site. The secondary aim is to investigate the spatial relationship between the dispersion of air pollutants and several areas of interest, while also gathering good quality data that can be used for validating computational models.

In order to meet these objectives, two sets of experiments were completed. The first set of experiments took concentration measurements encompassing the top and road facing surfaces of the monitoring station with and without the station in place to understand its impact on the flow. The second set of experiments took concentration measurements at the centre of the station with a tracer gas being released at different locations across the site (also called forward modelling). This was repeated with the tracer gas released at the centre of the station, while concentration measurements were taken across the site at an inverted wind direction (also called inverse modelling), to understand the level of similarity between the two cases.

The results in this report shows that the presence of the station does not impact the results across the top surface significantly, which is promising as data sampling in the field occurs over devices located across the top surface. The front surface, on the other hand, showed a substantial reduction in concentration with the station in place. The second set of results showed a cluster of points at close proximity to the station within which concentration contributions were at their peak for all wind directions. The concentrations from the forward and inverse scenarios show no significant resemblance for the most part with a substantial decline in peak concentration with the latter. The quality of the data verified, hence, the data from this study can be added to existing datasets for the validation of computational models.

Acknowledgements

I would like to take this opportunity to thank the following people for their assistance and contribution to this project.

Firstly, I would like to express my sincerest gratitude to Professor Alan G Robins for guiding me throughout the project and providing me with continuous advice and his willingness to help even when busy with other work, leading to the successful completion of this project.

I would also like to thank Dr Paul Hayden for his continuous help with the running of the wind tunnel and ingenious solutions to issues with regards to the tunnel.

I would also like to thank Dr Paul Nathan and Dr Allan Wells for their assistance with the data acquisition and manufacture of the models respectively.

In addition to the technical support, I would finally like to thank my family and friends for their continuous support throughout my time at the University of Surrey.

Table of Contents

List of Tables

List of Figures

List of Nomenclature

Abbreviations

ABL	Atmospheric Boundary Layer
ADMS	Atmospheric Dispersion Modelling System
AURN	Automatic Urban and Rural Network
BL	Boundary Layer
CERC	Cambridge Environmental Research Consultant
CFD	Computational Fluid Dynamics
DAPPLE	Dispersion of Air Pollution and its Penetration into the Local Environment
DNS	Direct Numerical Simulation
EnFlo	Environmental Flow Research Centre
EPSRC	Engineering and Physical Sciences Research Council
EVM	Eddy Viscosity Model
FA	Free Atmosphere
FFID	Fast Flame Ionisation Detector
FID	Flame Ionisation Detector
LDA	Laser Doppler Anemometry
LES	Large Eddy Simulation
LHS	Left Hand Side
OSPM	Operational Street Pollution Model
PBL	Planetary Boundary Layer
PDF	Probability Distribution Function
ppm	Parts per million
RANS	Reynolds-Averaged Navier-Stokes
RHS	Right Hand Side
RMS	Root Mean Square
RSM	Reynolds Stress Model
SNM	Street Network Model

Greek Symbols

σ_y	Standard deviation of the concentration distribution in the crosswind direction
σ_z	Standard deviation of the concentration distribution in the vertical direction

Latin Symbols

C	Source gas emission concentration
C*	Dimensionless mean concentration
C_{ppm}	Mean concentration in parts per million
H	Effective stack height
H_{BH}	Average building height
Q, Q_{trace}	Volumetric source emission rate
R	Straight line distance
U	Average wind speed at stack height
U_{REF}	Reference velocity at boundary layer
x	Positive axis along flow direction
y	Crosswind distance from plume centreline
z	Height from ground level

1. INTRODUCTION

A risk assessment conducted by World Health Organisation (2006) argues that annual premature deaths of more than two million can be attributed to the effects of air pollution where more than half of the impact is caused by inhabitants from developing countries. One of the major sources of pollution is traffic emission in urban areas where people are exposed to severe levels of pollutants (Kakosimos et al., 2010). Therefore, air quality is especially important considering the direct health implications from traffic pollutions with building design and layout of road networks being key deciding factors (Di Sabatino, 2008).

There are air quality standards in place set by each country for improving the environment each of which can have far reaching benefits. Air pollution has been monitored in one way or another over the past 60 years in the UK. There are issues with the monitoring methods and techniques used for monitoring air quality particularly in large urban environments due to the increasing complexity of street networks which makes the measurement and analysis of pollutant dispersion in the field an increasingly difficult and time consuming task.

By the late 1990s, all monitoring sites were consolidated into one programme known as the Automatic Urban and Rural Network (AURN) which exists to this day. The AURN currently consists of 127 monitoring sites spread throughout the UK. These sites continuously monitor air quality to assess compliance with various air quality standards and to aid in the development of future policies regarding air quality amongst many others (DEFRA, 2011). Concurrently, several studies have been conducted to model and understand the release and dispersion of pollutants into the atmosphere. The results of modelling studies are used by meteorologists for weather forecasting and to warn of natural disasters. The region that may be contaminated following the release of a hazardous material and the movement of the pollutant is extremely important for the purpose of emergency planning and training (Wood, 2010).

An important project completed previously is the multidisciplinary Dispersion of Air Pollution and its Penetration into the Local Environment (DAPPLE) project. It originally started as a four year UK project in 2002 conducted by a consortium of six universities and funded by Engineering and Physical Sciences Research Council (EPSRC) to understand the physical processes affecting pollutant dispersion, the impact on individual exposure and to understand the relationship between pollutant releases and areas of interest (source-receptor relationship). The project used a combination of field experiments, wind tunnel and computer simulations to understand these aspects of flow behaviour. Additional funding was received from the Home Office which extended the project for another three years where the focus shifted towards addressing potential terrorist activities in London and in other environments of a similar nature (University of Surrey, 2015). A series of smaller experiments have since been completed to supplement the results from the project. The greater objective of the project is to aid in the development of safer, more sustainable cities throughout the world (Arnold, 2004).

The DAPPLE project specifically targeted the intersection between Marylebone Road and Gloucester Place as it has been identified as one of the most polluted regions in London due to the high level of traffic flow in the region (Arnold, 2004). As a consequence, Marylebone Road has very poor air quality with pollution levels that by far exceeds the limit set by the European Union Air Quality Directive. This site is of particular importance as it hosts an air pollution monitoring station which has been in operation for an extensive period of time and has been the basis of several independent studies (Crosby, 2014). Full scale dispersion experiments were conducted in this region during 2003, 2004, 2007 and 2008 to monitor pollutant dispersion from a street level release (Wood, 2010). Similarly, wind tunnel experiments as well as computational simulations have been conducted of the site over this time period.

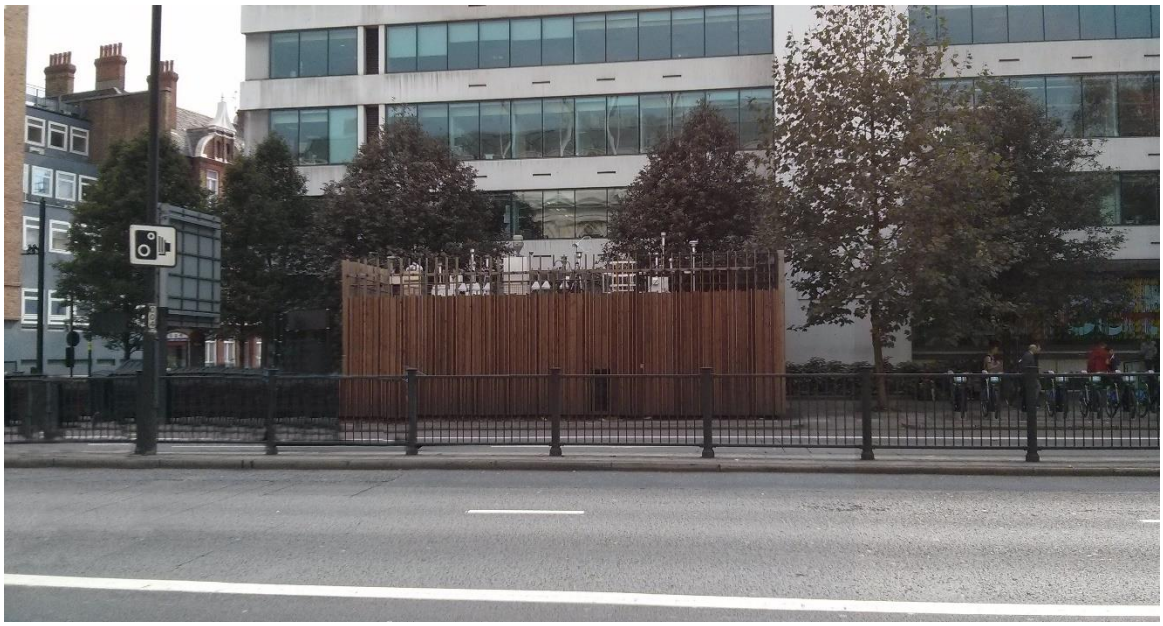

Figure 1: *Front side of monitoring station along Marylebone Road.*

Figure 1 displays the road facing side of the monitoring station placed along Marylebone Road, opposite Madam Tussauds. The station is located 1.5 m away from the road, with data sampled at a height of approximately 2.5 m (King's College London, 2015). This station is a part of AURN and has been integral to the DAPPLE project as it enabled the comparison of wind tunnel and computationally modelled simulations with onsite measurements. It measures a wide range of gaseous and particulate pollutants and also records meteorological data. These measurements are used to help understand people's exposure to pollution close to roads; to assess the emissions from different vehicles, and to help understand the influence of the weather on air quality. It should be noted that the data from these monitoring stations only provide coverage over a limited area and can be extremely resource intensive to obtain.

There are several issues present with the methods currently used to understand dispersion behaviour. Primarily, the use of monitoring stations such as the one in the DAPPLE is a time consuming and extremely difficult process due to the number of field experiments required to find a useful underlying distribution. This issue is compounded by the fact that field experiments are not repeatable or statistically steady for a long period of time owing to the variations in atmospheric conditions (Robins et al., 2010). Hence, a considerable amount of resources have been dedicated to

research that models different sites through the use of wind tunnel simulations and computational models which are capable of producing results that are both repeatable and statistically steady to a certain extent.

The issue this report aims to tackle is one where the dispersion process within a small scale in an urban environment is not well understood. The DAPPLE consortium project, and thus, by extension, this study, aims to conduct a series of experiments that will enable a better understanding of the physical processes that can be seen in a small scale (Arnold, 2004).

More precisely, the purpose of this study is to simulate the real world conditions around the Marylebone road air quality monitoring station within a wind tunnel and to understand the relationship between pollutant release locations and concentration measurements within a street network layout. This will be useful for the dispersion modelling community as it will extend the DAPPLE consortium research project and improve upon existing remote sensing results and also help add to existing datasets for validating different computational models (Arnold, 2004).

This report covers a range of experiments that were conducted for this purpose. The first set of experiments analyse the impact of the monitoring station on concentration measurements through the use of contour plots and ratios that compare results with and without the station in the tunnel. The second set of experiments establishes source-receptor relationships through the use of tracer gas releases for several wind directions and also inverts the positioning of the source and receptor to find the level of similarity between the two.

This report has been divided into six parts. Chapter 2 briefly introduces a review of existing literature pertinent to the field of pollutant dispersion behaviour and includes certain results from previous DAPPLE work that enables comparative analysis with results from this study. Chapter 3 presents the Environmental Flow Research Centre (EnFlo) wind tunnel located at the University of Surrey which was used for gathering data throughout this study. This chapter also lists the assumptions made in creating a scale wind tunnel model of the DAPPLE site and introduces the coordinate system and sign conventions used throughout the report. Chapter 4 details the procedure, the type of experiments conducted and the reasons for their conducting them. Chapter 5 presents the results, analyses them and compares them to the previous work briefed in Chapter 2. Finally, Chapter 6 provides a summary of the results and details a set of recommendations for further study.

2. BACKGROUND LITERATURE

Field dispersion modelling of pollutants is inherently difficult due to rapidly varying environmental conditions. Thus, in field experiments, repeat experiments are impractical and the results are not statistically steady for a reasonable amount of time. Therefore, several other methods have been developed that are able to predict the flow to a good degree such as wind tunnel modelling and computational simulations. Conversely, however, certain aspects of the real world cannot be modelled in a lab or in a computer simulation, although the advantage is that the results are repeatable and statistically steady. These experiments are conducted in order to understand the physical process behind pollutant dispersion and to gather accurate data for validating computational models. This section presents a detailed review of the relevant theory, factors to consider, different methods of dispersion modelling and existing research in this area of study as follows:

- Urban Street Modelling
- Computational Modelling
- Wind Tunnel Modelling
- DAPPLE Project

2.1. Urban Street Modelling

This section introduces and describes aspects of pollutant release and dispersion in an urban environment and considerations for modelling such an environment.

2.1.1. URBAN METEOROLOGY

The Earth's atmosphere is divided into five distinct layers as depicted in Figure 2, with a combination of gases, particles and water. There are no clear transitional regions between these layers and there is no definite upper limit as this can vary.

The layer closest to the planet is called the troposphere, it extends to a range of 10-20 km from the Earth's surface (Oke, 1988). A transitional region called the tropopause separates it from the stratosphere as shown in Figure 3. The upper section of the stratosphere hosts a significant portion of the ozone layer which absorbs harmful radiation resulting in an increase in temperature at this level.

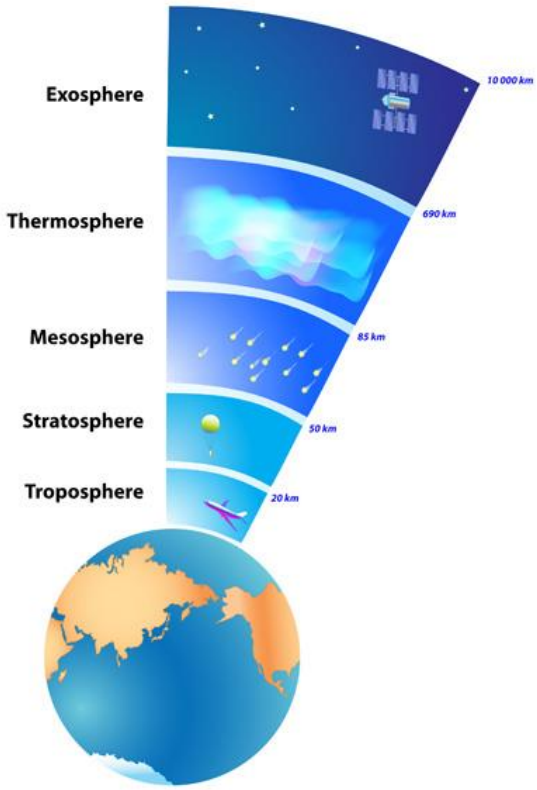

Figure 2: *Atmospheric Layers (Exploring the Environment Project, 2015)*

The mesosphere follows the stratosphere where the temperatures decline sharply as ozone concentrations and water vapour content are negligible, followed by the thermosphere where temperatures increase due to the ionisation of the remaining air particles by absorption of solar radiation. The most remote layer is the exosphere which transitions between the atmosphere and interplanetary space (NASA, 2010).

2.1.1.1. Atmospheric Boundary Layer

The part of the troposphere that is responsible for all atmospheric processes such as evaporation, convection, rain, etc. is called the atmospheric boundary layer (ABL) or planetary boundary layer (PBL). It is the lowest part of the troposphere and is where all land based life forms inhabit (Moreira and Vilhena, 2009).

A definition provided by Stull (1988) for the boundary layer (BL) states that it is the part of the troposphere where the earth's surface has the largest impact and it responds to influences such as surface roughness, heat transfer and pollutant emission within a timescale of an hour or less, while Garratt (1994) provides a similar description, but refers to timescales of less than a day. The remainder of the troposphere is called the free atmosphere (FA) as illustrated in Figure 3 (Stull, 1988).

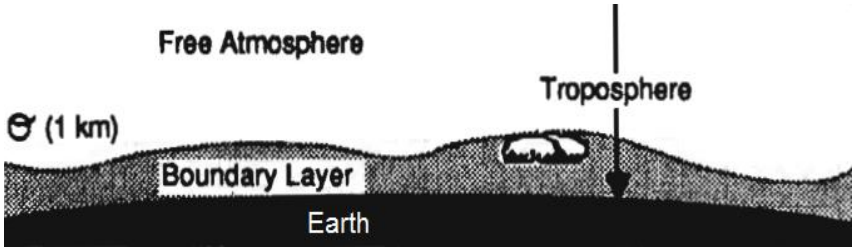

Figure 3: *Troposphere division into a boundary layer and the free atmosphere (Stull, 1988)*

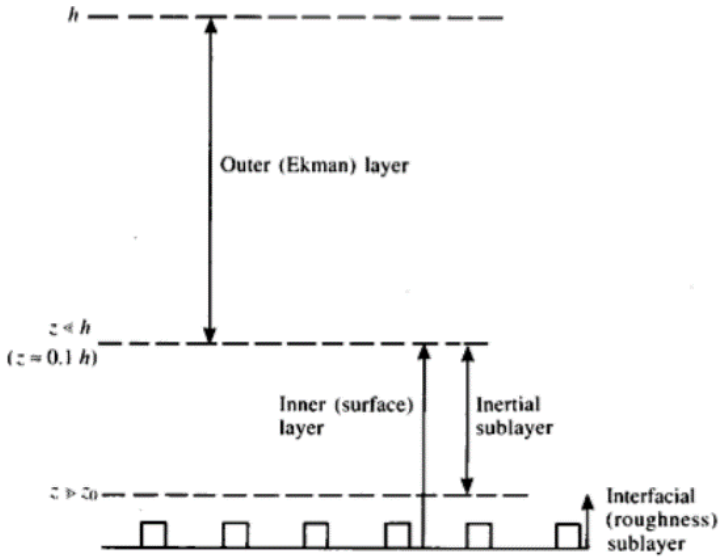

Figure 4: *Schematic structure of atmospheric boundary layer (Garratt, 1994)*

The atmospheric boundary layer is turbulent by nature, where turbulence is generated by wind shear due to frictional drag causing the air velocity at the surface to become zero (Stull, 1988). Due to this turbulence, the flow breaks up into eddies that transport heat, mass and momentum in the

vertical direction. The free atmosphere is governed by atmospheric processes at large scales such as horizontal pressure gradients and atmospheric disturbances and is laminar in most cases (Moreira and Vilhena, 2009).

The atmospheric boundary layer itself can be divided into inner and outer regions as illustrated in Figure 4, where h is the boundary-layer depth, z is the height above the surface and z_0 is the aerodynamic roughness length (height where mean wind is zero). The inner layer extends from the ground up to a height of 120-150 m while the outer layer extends from the top of the inner layer to the start of the free atmosphere. This layer is responsible for the transportation of pollutants as most pollutant sources are located near the earth's surface. There exists a transitional region between the two layers, with a variable altitude that depends on surface location and time of day (Moreira and Vilhena, 2009).

In the outer layer (also called Ekman layer), the important aspect to consider is the Coriolis force (object deflection caused by a rotating frame of reference) caused by the Earth's rotation, and to some extent, the surface irregularities. In the inner layer (also called surface layer), however, flow is mainly dependent on the surface characteristics rather than the rotation of the Earth. The region that is directly influenced by the surface features is the interfacial sublayer, which is the region directly above the roughness elements. In this layer, molecular diffusion is an important process where mass and heat are transferred between the surface and the air (Garratt, 1994).

A stable boundary layer (stably stratified atmospheric boundary layer) is formed generally during the night when the Earth's surface is cooler than the air due to surface cooling by the upward flux of infrared radiation and the absence of turbulent effects, resulting in little vertical mixing (Geernaert, 2003). Hence, pollutants disperse very little in the vertical but more rapidly in the horizontal direction. On the contrary, a convective boundary layer (unstably stratified atmospheric boundary layer) usually forms during the day when the surface is heated up by solar radiation which produces thermal instability, resulting in a large amount of vertical mixing (Bonner et al., 2010). This in turn results in the pollutant rapidly traversing up and down in the vertical direction before becoming uniformly distributed over time. Stable layers typically have a height of 100 m (Stull, 1988; Garratt, 1994).

A neutral boundary layer forms with the absence of thermal effects. This is mostly seen in windy conditions where the wind drives strong turbulence levels that keeps the ground in thermal equilibrium with the Earth's surface. The inclusion of complete cloud cover that blocks solar radiation will also aid in the formation of a neutral boundary layer. The depth of this type of boundary layer is typically 1 km, depending on wind speeds (Garratt, 1994).

Under convective conditions, an unstable boundary layer is formed. The top of the atmospheric boundary layer is capped by a stable layer (also called inversion layer) that turbulent motions generated in the inner layer are unable to penetrate, although, they may start to erode the base of the inversion layer. Thus, pollutants are trapped below this layer and the free atmosphere concentration levels remain very low which can cause high levels of pollution in certain areas. The height of the stable layer is generally below 2-3 km (Stull, 1988; Garratt, 1994).

2.1.1. POLLUTION AND DISPERSION

Pollutants are transported and diffused at the atmospheric boundary layer (Moreira and Vilhena, 2009). Five characteristic scales are generally used when characterising the pollutant dispersion phenomena: continental scale (~1000 km), regional scale (~100 km), urban scale (~10 km), neighbourhood scale (~1 km), and the street scale (~100 m) (Soulhac et al., 2011; Britter and Hanna, 2003).

The regional scale is influenced by the urban environment, where the buildings act as roughness elements that decelerate and deflect the flow. The urban scale encompasses the average diameter of an urban city, at this scale, the variations in concentration and dispersion have mainly been averaged out by buildings and most of the pollutant cloud travelling this distance will be above the buildings. In the neighbourhood scale, the flow within the urban canopy is important as flow variations can be large depending on building density in the areas under study. The street scale considers pollutant dispersion along a few streets or within an intersection, e.g. where monitoring stations have been located (Britter and Hanna, 2003).

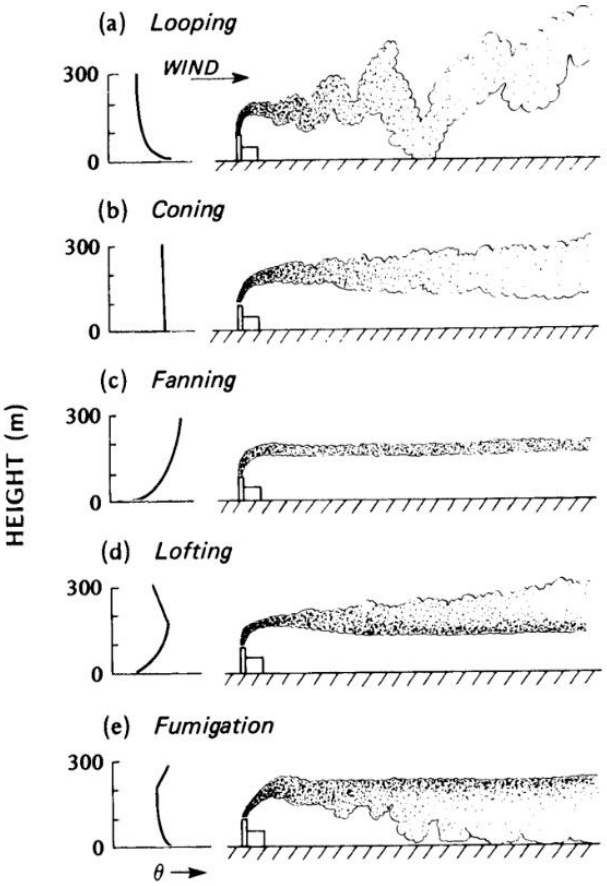

Figure 5: *Plume patterns under different stability conditions. (Oke, 1988)*

Patterns of pollutant release and dispersion from a stack can be classified into five basic types as illustrated in Figure 5. Di Sabatino et al. (2003) suggests that at lower wind speeds, traffic produced turbulence is important and Britter and Hanna (2003) states that the major pollutant source within a city are traffic emissions. In general, the best conditions for pollutant dispersion is with strongly unstable boundary layers, i.e. during high temperature conditions and the worst dispersion occurs with a stable boundary layer where there is a temperature inversion and turbulence is suppressed.

Pollutants diffuse into the atmosphere when eddies formed by an unstable boundary layer are smaller than the plume release and when larger, the pollutants are advected. Wind speed is clearly a factor when trying to determine pollutant dispersion as higher wind speeds will lead to greater mixing (due to higher turbulence generation), further travel and can reduce plume height from elevated stacks. Furthermore, pollutant dispersion is sensitive to variable wind direction in an urban environment as it dictates the path of the pollutants (Xie, 2011).

2.1.2. WIND FLOW AROUND BUILDINGS

Numerous studies have been conducted to understand the airflow around buildings. Wind tunnel studies using a cube (Figure 6) have shown that as long as the upwind conditions (wind, topography, perturbations due to other buildings) are simulated, the modelling can provide good approximations to conditions observed in the field. The presence of a building requires considerations of thermal, moisture and aerodynamic modification to the surrounding flow (Oke, 1988).

2.1.2.1. Isolated Buildings

Air flow around a large bluff body such as a building has several contributing factors and can be difficult to predict especially for buildings in close proximity to each other. Thus, the spacing between buildings as well as the building density have a significant impact on pollutant dispersion (Oke, 1988).

The flow is modified even before reaching the building due to pressure build-up caused by air that acts against the building. The highest pressure is located at the upper middle part of the wall, called the stagnation point outwards from which the pressure decreases (Oke, 1988). This effect is more apparent with tall buildings where strong winds can cause faster moving air that hits the upper middle part to deflect downwards due to the pressure difference.

The three main zones that can be identified for an idealised flow around a building are illustrated in Figure 6 and are as follows (Eisenbud and Gesell, 1997):

- The displacement zone, the volume where the air is deflected around the solid building.
- The cavity, a region of recirculation formed when flow over the roof top separates - located immediately after the building, also known as an eddy zone, where it is possible for the accumulation of high pollutant concentration.
- The wake, located downwind from the building which is a region of high turbulence, where pollutants are mixed more rapidly.

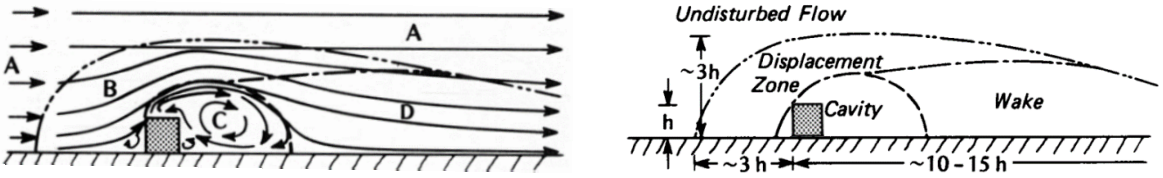

(a) (b)

Figure 6: *Airflow around isolated flat-roofed building in a wind tunnel, (a) Side view showing streamlines and flow zones. [A-undisturbed flow, B-displacement zone, C-cavity, D-wake] (b) Side view showing generalised flow zones, where h is the height of the building (Oke, 1988)*

(a) (b)

Figure 7: *Flow pattern around a building diagonal to the wind, (a) flow pattern with building normal to the flow, (b) flow pattern with building faced diagonally against the flow (Oke, 1988)*

There can be variations on this theme depending on the building shape and orientation. Figure 7a shows the flow field around a cuboid shaped building directly facing the flow. The sharp corners at the edges accelerates the flow across the sides and top, separating it from the surface. The accelerating flow creates a change in pressure which causes flow reversal, forming the double eddy circulation. If the building were to face the wind diagonally as shown in Figure 7b, the strength of the suction zone across the trailing edge of the roof would reduce. However, the leading edge would have a vastly stronger suction zone due to the formation of high strength vortices. In either case, the double eddy pattern found downstream of the building would still exist. Another variation occurs with tall buildings that usually reduces the wind speed compared to the isolated case due to the larger area exposed to the flow. Even if the edges of the buildings were smoothed, the basic pattern shown in Figure 7 would remain, but the flow would be less disturbed (Oke, 1988).

2.1.2.1. Building Arrays

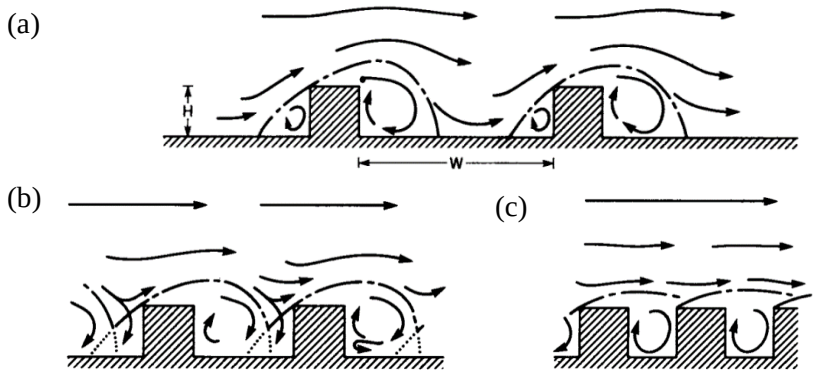

Figure 8: *Flow patterns associated with varied building spacing, (a) large spacing, (b) close spacing, (c) narrow spacing (Oke, 1988)*

Groups of buildings separated by narrow spaces between them form street canyons. They can trap incoming and outgoing radiation and affect the flow in the region. The effect is dependent on the height and distance between the buildings, characterised by the height to width ratio (H/W), where H is the average building height and W is the along-wind spacing. This is an important factor in urban environments. When buildings are widely spaced (H/W<0.4), the flow pattern behaves in the same manner as isolated buildings as shown in Figure 8a. With a spacing of H/W ~ 0.7, the wake from a building will affect those located downstream, creating a highly complex flow as shown in Figure 8b. As the spacing reduces to a greater degree, the flow starts to skim on top of the buildings (illustrated in Figure 8c) which generates vortices within the spacing (Oke, 1988; Vardoulakis et al., 2003).

Di Sabatino et al. (2008) states that the worst case scenario for air pollutants is when the wind direction is perpendicular to the street, as this allows the pollutant to dilute and escape from the street canyons. It also demonstrates that for parallel and 45° wind directions, variations in ambient wind direction could have a large impact on the mean flow recirculation and thus in turn, pollutant distribution. (Di Sabatino et al., 2008; Zhang et al., 2005). With flow acts at an angle to a street, the flow can be resolved into two components that acts along two different axes. The first, generates vortices as shown in all Figure 8, while the second channels the flow along the street, creating what is known as helical vortices. Furthermore, depending on geometry of street network, even a slight

variation in wind direction can lead to flow reversal within a street section. Further, more extensive write-ups on the effect of buildings on dispersion can be found in Hunt (1978), Hosker (1984), and Foster (1985).

2.2. Computational Modelling

There are several techniques other than physical testing used to model flow across surfaces such as CFD and more specific to modelling pollutant emissions - dispersion models. Such techniques model factors affecting pollutant dispersion or industrial emissions such as wind speed and direction and atmospheric turbulence to predict downwind concentration levels in urban street networks. Due to the rapid speed at which results can be generated from dispersion models, they are used in emergency situations to find the worst case scenarios and plan for it. Computational models draw on input data/constants from wind tunnel experiments and to some extent, field studies to accurately predict flow behaviour for a range of environmental conditions.

2.2.1. GAUSSIAN BASED DISPERSION MODELS

Pollutant dispersion models are used to monitor and assess the effect of pollutant emission in urban areas and also to aid in urban planning and traffic management (Kakosimos et al., 2010). Since their inception in the early twentieth century, these models were designed based on emissions from point sources (e.g. smoke stacks) and wind statistics to estimate downwind deposition and human exposure levels (Geernaert, 2003).

Several models have been developed solely for this purpose such as Airviro, ADMS and USEPA models (Mitchell et al., 2002). The ADMS model is used extensively in this field of research throughout Europe, especially the UK amongst other countries (Carruthers and Hunt, 2008). The basis of many such models is the Gaussian model where the plume dispersion is assumed to occur by diffusion perpendicular to the direction of the mean wind. The most general form of the Gaussian dispersion equation is (Allen and Durrenberger, 1995):

$$C(x,y,z,H) = \frac{Q}{2\pi U \sigma_y \sigma_z} exp\left[-\frac{y^2}{2{\sigma_y}^2}\right]\left\{exp\left[-\frac{(z-H)^2}{2{\sigma_z}^2}\right] + exp\left[-\frac{(z+H)^2}{2{\sigma_z}^2}\right]\right\} \quad (1)$$

Where:

C is the emission concentration (g/m^3)

Q is the source emission rate (g/s)

U is the average wind speed at stack height (m/s)

σ_y, σ_z are standard deviations of the concentration distributions in the crosswind and vertical directions respectively (m)

H is the effective stack height (m)

x is the distance downwind from the stack (m)

y is the crosswind distance from the plume centreline (m)

z is the vertical distance from ground level (m)

There are certain assumptions in place with Gaussian models as listed below (Allen and Durrenberger, 1995):

- The pollutant emission rate is constant.
- Dispersion conditions and wind speed are constant across height.
- Wind speeds are greater than 1 m/s.
- Plume is infinite with no knowledge of its history.
- Dispersion is negligible in the downwind direction.

The values for σ_y and σ_z in Equation (1) vary depending on surface height, surface roughness and atmospheric conditions. These values are determined based on the level of stability of the atmosphere ranging from Class A for extremely unstable to Class F for moderately stable conditions. In general, Gaussian models assume that the plume is spread primarily by diffusion with a Gaussian distribution along the mean wind direction and so, averages out all the turbulence motion. Their advantage is that they can produce results very quickly and can work on standard PCs without the use of supercomputers. The accuracy of Gaussian based models decreases rapidly over distances of 10-20 km and is best used in regions with little topographical features (Allen and Durrenberger, 1995; Fenger et al., 1998).

2.2.1.1. ADMS

The Atmospheric Dispersion Modelling System (ADMS) is a popular short range air dispersion model capable of calculating pollutant concentrations at different locations. It is capable of modelling dispersion from both buoyant and neutrally buoyant gas releases from point (e.g. chimney stack) and line sources (e.g. traffic emissions) into the atmosphere. It was developed by a consortium led by Cambridge Environmental Research Consultant (CERC) (Carruthers and Hunt, 2008).

Mitchell et al. (2002) states that ADMS uses boundary layer similarity profiles to model the variation in turbulence within the boundary layer and a skewed-Gaussian plume air dispersion model to determine the vertical height of pollutant concentrations from either continuous or discrete plume releases under unstable conditions.

ADMS employs a modular approach where several independently functioning modules are operated via a common control program as illustrated in Figure 9. Each module is a part of the entire dispersion process and as such, can be updated and modified without interfering with the other modules (Carruthers et al., 1994). Thus, depending on the modules in use, ADMS can model urban environments, roads, airports and industrial emissions (CERC, 2015).

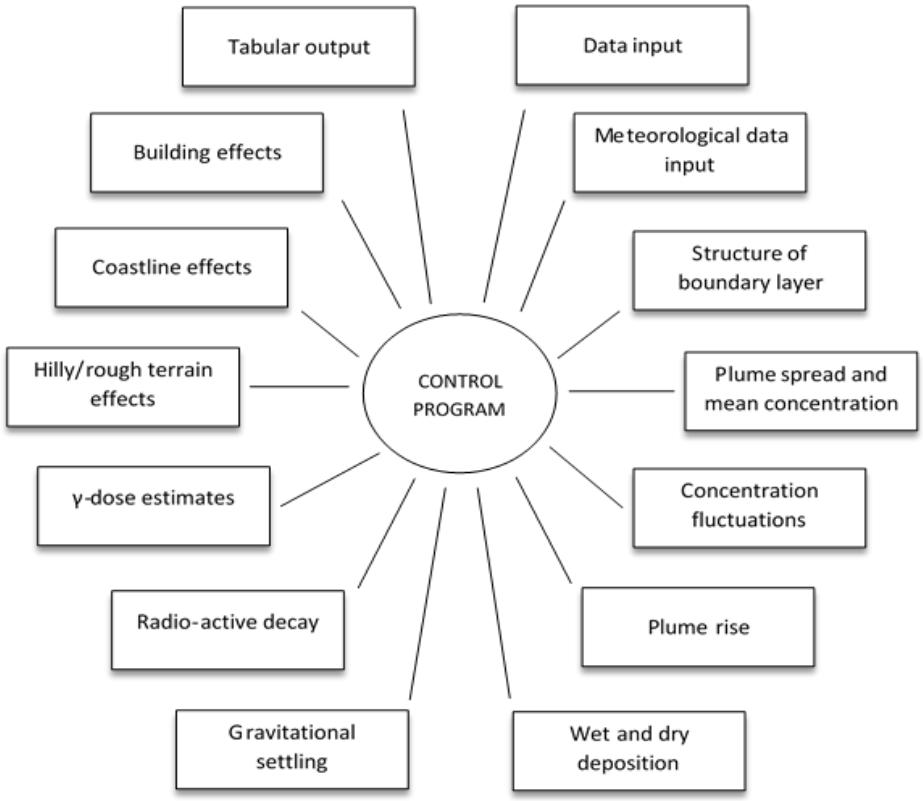

Figure 9: *Components of ADMS adapted from (Carruthers et al., 1994)*

The inputs to the system are pollutant emission parameters such as source location, height and rate, followed by meteorological conditions such as wind speed, direction and turbulence levels in the atmosphere. Topographical data can also be entered such as terrain levels and the presence of buildings/obstructions. This provides an output consisting of concentration levels averaged over a specified period and graphical outputs such as contour plots which visualise the concentration field over a specified region. Figure 10 illustrates some of the conditions ADMS is capable of modelling (Carruthers and Hunt, 2008).

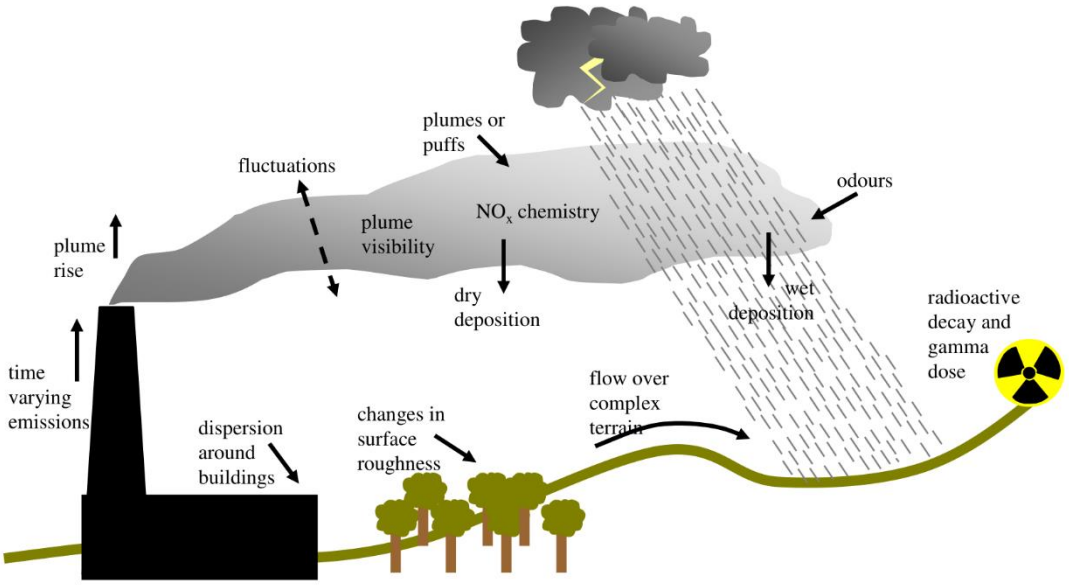

Figure 10: *Conditions ADMS is capable of modelling. (Carruthers and Hunt, 2008)*

One aspect of interest is the impact of traffic emissions and accidental toxic releases into the atmosphere in areas within a city with roads surrounded by buildings. For such a case, ADMS models local air quality around complex building structures by simplifying the buildings as cuboids before evaluating the flow field, as shown in Figure 11. ADMS has the advantage of accounting for emissions released at the same time from different locations. Thus, it is one of the most widely used tools for air quality monitoring in urban areas unless the terrain and buildings are of a more complicated structure. In general, Namdeo and Colls (1996) argues that Gaussian based dispersion methodology works better with roads in open space on flat terrain and that other Gaussian based dispersion models such as the CALINE and HIWAY series are unable to deal with stationary source emissions (Mitchell et al., 2002).

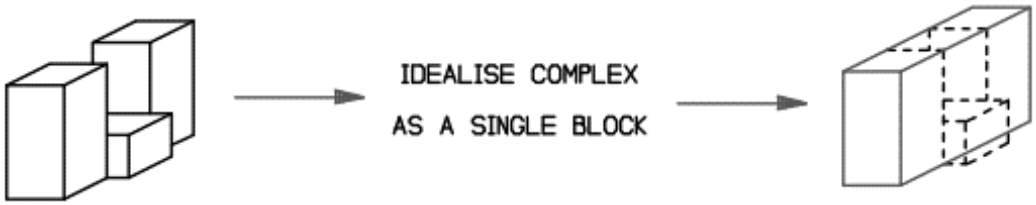

Figure 11: *Complex building structure simplified to a single cuboid for modelling*

One of the modules available is a street canyon building module which uses the Danish Operational Street Pollution Model (OSPM) model to calculate flow recirculation and the impact of traffic produced turbulence in street canyons (Kakosimos et al., 2010). Majority of the earlier work on OSPM was conducted by Berkowicz (2000). This module is activated when the street aspect ratio between the average building height bordering one street and its width is larger than 0.5. In other cases, the semi-Gaussian distribution is used throughout (Soulhac et al., 2011). The street canyon modelling omits junctions, assuming a straight road with a continuous line of buildings on either side. The greatest drawback of ADMS is its inability to deal with complex building structures – it is only capable of modelling simple buildings. Its strength lies in predicting dispersion when source and receptors are in the same street canyon.

ADMS has been validated and compared with other Gaussian type models such as AERMOD and ISC3, using datasets from throughout the world by Hanna et al. (2001) and Carruthers et al. (1994). This study finds that ADMS gives significantly better performance than ISC3 and slightly better results in the four performance measures considered over all experiments conducted. Carruthers et al. (1999) also conducted a study comparing the predictions from the ADMS building module to a series of wind tunnel simulations of chemical warehouse fires which showed that the building module was able to replicate features observed in the wind tunnel simulations.

The ADMS module has also been compared to a range of other field tests and wind tunnel experiments that considered a range of scenarios such as ground/high level releases, passive and buoyant releases, with buildings and terrain among others (Carruthers and Hunt, 2008). These studies have found that the ADMS model predictions are most valid over a flat terrain without any buildings which is in agreement with Namdeo and Colls (1996).

2.2.2. STREET NETWORK MODELS

The street network model (SNM) concept uses the decomposition of the urban atmospheric boundary layer into the external atmospheric flow and the urban canopy within which pollutants are well mixed. The concentrations are determined by the geometry of the street and intersections (Soulhac et al., 2011; Soulhac et al., 2012).

2.2.2.1. SIRANE

SIRANE is the first urban dispersion model created based on the concept of a street network. It simulates pollutant dispersion from both line and point sources at the district scale and models the effects of small details on buildings such as doors, chimneys, balconies, etc. as a uniformly distributed wall roughness. This is because it would be unrealistic to build data sets that account for such intricate details (Soulhac et al., 2012).

SIRANE uses a quasi-steady approximation where the time step is assumed to be one hour based on the definition of the boundary layer by Stull (1988). Pollutant dispersion is computed for each time step independent to the previous time step assuming steady conditions, i.e. contribution from previous time steps are not considered. Thus, the model will not account for the possibility of pollutant accumulation within the urban canopy over a period of several hours which is possible in case of calm wind conditions (Soulhac et al., 2011).

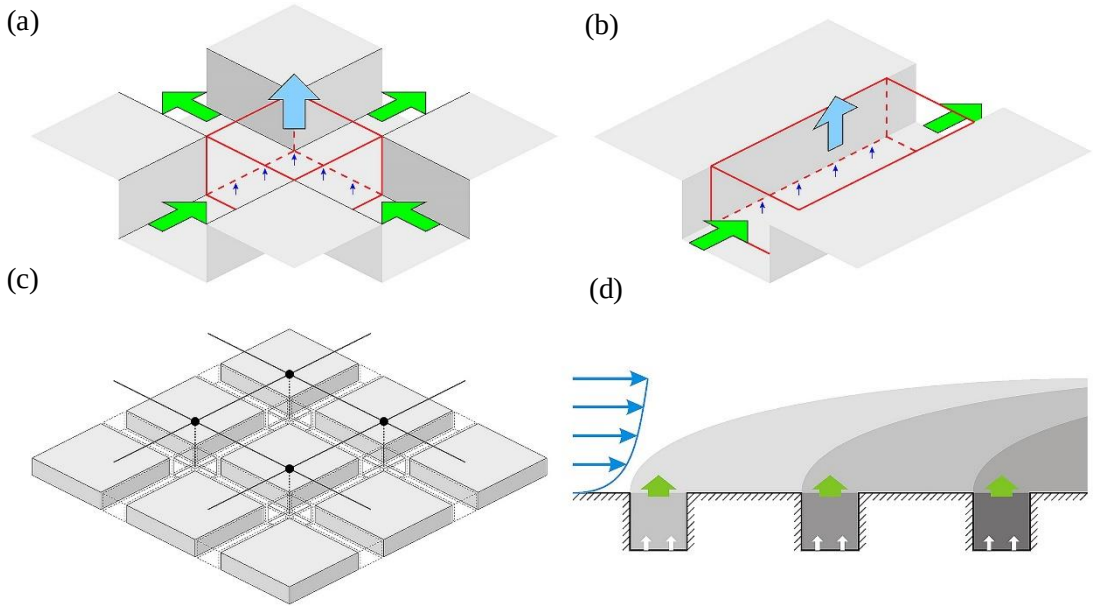

Figure 12: *Components of the SIRANE model, (a) District modelled as a network of streets, (b) Box model for each street, showing a mass flux, (c) Mass flux at street intersections, (d) Modified Gaussian plume model for roof level releases. (Soulhac et al., 2011)*

The urban canopy is represented by a network of connected streets, modelled as a network of boxes (Figure 12a) and isolated spaces (e.g. courtyards). The following three mechanisms are considered by SIRANE to compute the mean concentrations along each street (Soulhac et al., 2011):

- Convective mass transfer along street due to mean wind along their axis (Figure 12b).
- Turbulent transfer across the interface between the street and the atmospheric boundary layer (Figure 12b).
- Convective transport at street intersections (Figure 12c).

The external atmospheric flow is idealised as a boundary layer flow over a rough surface (where the urban canopy is modelled as the rough surface). This approach works well in cases of high building density, but not when modelling areas with large open spaces. Street network models work best with a dense building population and as the spacing between buildings increases, the urban canopy seeps in between the buildings which invalidates the modelling assumptions (Soulhac et al., 2011).

At street intersections, the flow is modelled as two distinct fluxes of air. A flux in the vertical between the urban canopy and the external atmosphere and a flux in the horizontal from one street to another. The horizontal flux is estimated assuming the intersection is two-dimensional, i.e. the height is not a consideration and the vertical flux is modelled by a mass balance of air entering/exiting the box section (Figure 12b). Pollutant dispersion into the external atmosphere from roof level releases are modelled using the Gaussian model introduced in section 2.2.1 (Figure 12d) (Soulhac et al., 2011; Carpentieri et al., 2012).

Since ADMS simply adds all the values from each street canyon at an intersection rather than considering the flow effect from each intersection, street network models can handle intersections better than ADMS. However, ADMS provides better results in other cases, such as when dealing with single street canyons (Salem, 2000).

Several validation studies of the SIRANE model have been completed, both against field studies, as well as wind tunnel measurements. The model was compared against field experiments from major European cities such as the 6th arrondissement of Lyon, Turin, Milan, Florence and London (Berrone et al., 2012). The comparison with Lyon for example, was conducted by Soulhac et al. (2012) where the field study measured changes in traffic fluxes, meteorological conditions, pollutant concentration and background pollution data over a two week period. Wind tunnel studies were conducted by Carpentieri et al. (2012) analysing the effect of varying wind direction, source gas emission and slight changes in geometry. The results from these studies found good agreement in cases where the oncoming wind was diagonal to the street axis and less so with parallel flow. It also demonstrated that ground releases gave more comparable results than roof level releases.

2.2.3. COMPUTATIONAL FLUID DYNAMICS (CFD)

The goal of CFD is to predict the behaviour of a fluid using a combination of applied mathematics and physics to solve the Navier-Stokes equations. CFD allows for modelling of complex building structures that Gaussian based models are unable to, as mentioned previously.

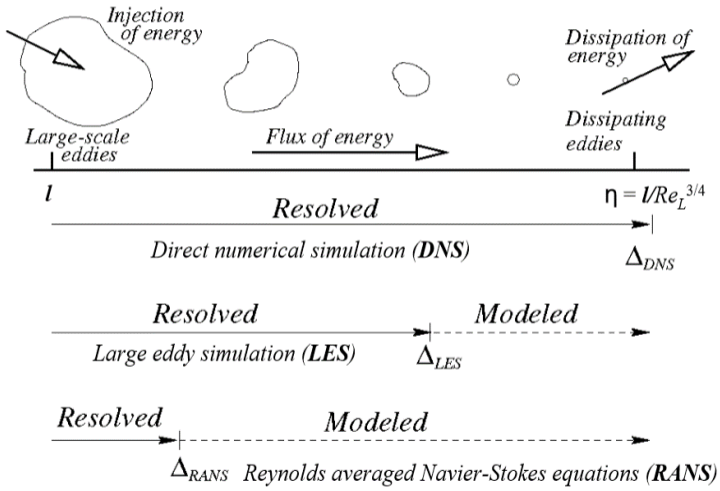

Figure 13: *Turbulent flow prediction methods (Bakker, 2006)*

Turbulence consists of coherent structures, i.e. eddies of different length scales that exist at the same time. Energy enters turbulence at the largest scales, l through energy produced from mean flow gradients. These large eddies are unstable and so, breakdown into smaller and smaller eddies by inviscid processes. As the larger eddies breakdown into the smallest scales (known as Kolmogorov scale, η), energy is dissipated as heat due to viscosity. Different types of CFD methods either model or numerically simulates this breakdown of eddies as illustrated in Figure 13.

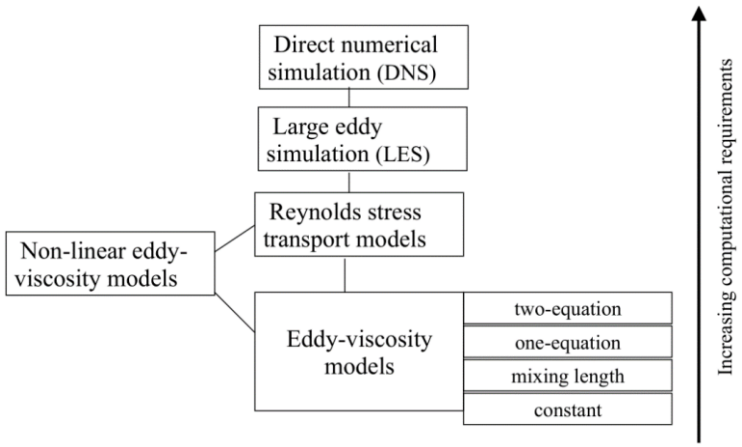

Figure 14: *Hierarchy of turbulence models*

CFD requires the selection of a turbulence model, and the accuracy of the models illustrated in Figure 14 depends on modelling choices, mesh quality and also the calibration of constants – all of which requires increasing computational power. The non-linear eddy-viscosity models (EVM) and Reynolds stress models (RSM) are both Reynolds-Averaged Navier-Stokes (RANS) based methods. They decompose the properties in the Navier-Stokes equations into mean and fluctuating parts and characterises turbulent flows in statistical terms. Such models simply average the flow

variables over time. Eddy-viscosity models use the Boussinesq hypothesis to describe the eddy viscosity using a number of equations and solve the Navier-Stokes equations (Sodja, 2007).

Large Eddy Simulation (LES) and Direct Numerical Simulation (DNS) are numerical approaches to the situation that directly solves the Navier-Stokes equations. DNS requires an increasing amount of computational power with Reynolds number as it numerically resolves down to the smallest scales – Kolmogorov scales, thus spending roughly 99% of its computational time on this scale. Bredberg (2001) claims that DNS is more accurate than wind tunnel measurements and is thus used to calibrate constants for the RANS models.

LES is an intermediary between RANS based models and DNS which numerically resolves eddies down to the inertial sub-range and models smaller eddies that are in the sub-grid scale. LES is more valid under separating and rotating flows than RANS models. Bredberg (2001) states that although RANS is limited with regards to the range of length scales it can model, it can deliver reasonable results for a wide range of flow types, but its performance is not much better than simple operational models (Xie and Castro, 2009). Thus, LES is generally used for urban modelling as it is capable of numerical simulation of the large scales which have the largest contribution to turbulent motion, but is also able to give reasonable results for the sub-grid scale by modelling.

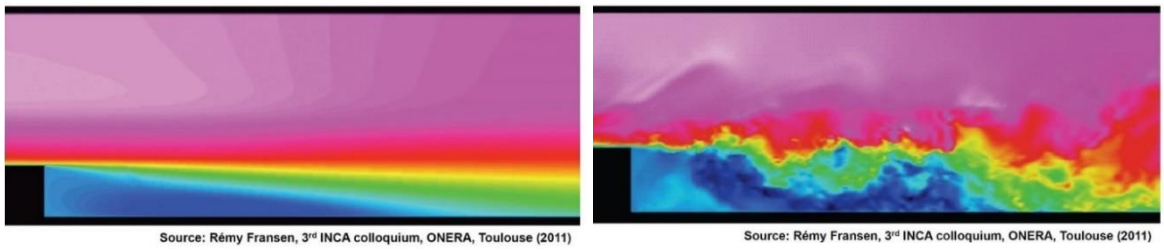

RANS LES

Figure 15: *A comparison between RANS and LES with a backward facing step*

LES provides more accurate results of recirculation zones than RANS as illustrated in the backward facing step example demonstrated in Figure 15 and according to Yuan et al. (2014), all RANS models tend to overestimate street level concentrations. Although work completed by Di Sabatino et al. (2007) suggests that a slightly modified k-ϵ model (a two-equation eddy viscosity model) is capable of delivering results similar to ADMS, Tominaga and Stathopoulos (2011) states that even the simplest of LES modelling provides more information on instantaneous concentration fluctuations than conventional RANS based models. Thus, LES is widely used for modelling urban environments to an appropriate amount of detail.

A study conducted by Riddle et al. (2003) comparing LES against ADMS observes that the results from ADMS simulations were satisfactory. However, LES is not recommended as an alternative to ADMS in all cases, but only when dealing with complex geometries due to the longer run times and intricacies involved with the setting up of each run. It should be noted that this study does not take into account stable or unstable atmospheric conditions and only applies to research conducted on neutral stability. This has been backed up by research conducted by Di Sabatino et al. (2007), comparing a slightly modified two-equation eddy-viscosity model against ADMS which found good agreement between the two results.

Table 1: *Classification of some commonly used dispersion models (Vardoulakis et al., 2003)*

Parametric						Numerical		
Empirical		Semi-empirical				Eulerian		Lagrangian Stochastic particle
Statistical	Receptor	Screening	Box	Street canyon	Gaussian	Microscale (CFD)	Urban scale	
Derwent and Middleton (1996)	COPREM	CAR International	STREET-SRI	OPBM	ADMS	PHOENICS	MEMO	GEM
	Karim and Ohno (2000)	AEOLUS Screen	MAPS	OSPM	ADMS-Urban	FLUENT	METRAS	Addison et al. (2000)
Stedman et al. (2001)		AEOLIUSQ	STREET BOX	AEOLIUS	INDIC AIRVIRO	STAR-CD	CALGRID	Jicha et al. (2000)
		STREET	Nicholson (1975)	SLAQ	TNO-Traffic	CFX-TASCflow		Xia and Leung (2001a, b)
		UK DMRB		OMG	CAR-FMI	PANACHE		
				Hotchkiss and Harlowe (1973)	PROKAS-V	MERCURE		
					HIWAY-2	CHENSI		
					CALINE4	MISKAM		
					APRAC	MIMO		
					PUFFER	MITRAS		
					AERMOD	ADREA-HF		
						FloVENT		

An extensive, but not exhaustive list of dispersion models can be found in Table 1. From left to right, the level of detail in the output increases, accompanied by an increase in computational time. It shows some of the very wide range of models that have been developed, of which only a few are used widely in practice. This is because there is no industrial standard for the use of CFDs and there are many different turbulent models which are more adept at predicting flows in certain conditions and less so in others. However, there are several guidelines in place for best practice such as the *COST* by Franke et al. (2007) for simulating flows in an urban environment and *Turbulence And Combustion Best Practice Guidelines* by Casey and Wintergerste (2000) for general CFD modelling.

2.3. Wind Tunnel Modelling

2.3.1. ATMOSPHERIC BOUNDARY LAYER SIMULATION

An important aspect of modelling pollution dispersion in cities is the simulation of the atmospheric boundary layer which requires the generation of a velocity and turbulence profile associated to planetary boundary layer data. The aim is to model the relevant turbulence scales. It requires the development of an artificial thick boundary layer through the use of either passive devices or a long fetch (downwind distance from change in surface feature) of roughness elements. Suitable tunnels have a length ranging from 15-20 m (e.g. Figure 16). A thicker boundary layer will enable better resolution through the use of larger scale models, whereas, when dealing with aerodynamic wind tunnels, to maximise flow uniformity, the boundary layer thickness must be minimised (Stull, 1988).

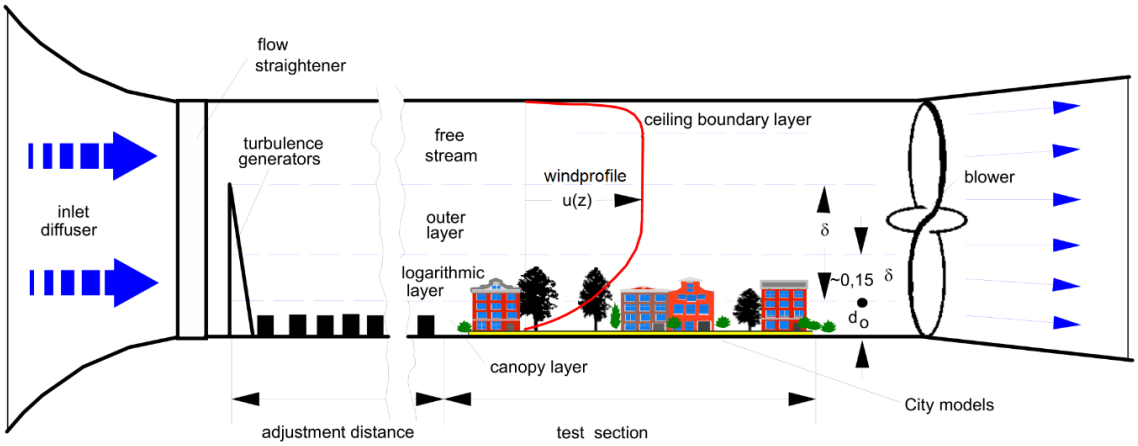

Figure 16: *Example wind tunnel modelling of atmospheric boundary layer flows (Fedorovich, 2015)*

A review of devices that can create a thick boundary layer can be found in Sargison et al. (2004), and an extensive report describing and analysing different atmospheric conditions in a wind tunnel can be found in Hunt and Fernholz (1975). Counihan (1971) developed the use of a fence and vortex generators and roughness elements further downstream to form a thick boundary layer. This option will reduce the fetch required for the boundary layer to develop before reaching the working model. This technique has gained wide acceptance and is used in tunnels such as the EnFlo tunnel at the University of Surrey and the WOTAN tunnel at the University of Hamburg. Irwin (1981) built on this technique to develop a simple design formula for the turbulence generators and came up with the recommended use of a set of triangular arrays with dimensions that can be built based on required boundary layer properties.

The report from Hunt and Fernholz (1975) summarises results and observations seen by thirty-eight researchers in a colloquium that discussed the simulation of atmospheric boundary layer in a wind tunnel. In particular, it mentions work completed by Dye which demonstrated the use of a short, 1.5 m, wind tunnel to model wind flow around a building. This method used a shear grid to generate the turbulence effect within the short distance. Stratified boundary layers can also be modelled in a wind tunnel with the use of inlet heaters and floor panels that can generate temperature profiles. Robins (2003) states that in general, for a wind tunnel experiment to be successful, the results must be under control, repeatable, statistically steady, with the ability to be fully determined.

Plate (1971) suggested an optimal design for the simulation of an atmospheric boundary layer. A tunnel with a working area of cross-section 2 x 1.5 m and length 10 m capable of running at wind speeds of 10 m/s. Hunt and Fernholz (1975) states that Cermak disagreed with the size and recommended a tunnel with a width of 3 m and length of 20 m where the extra width is used to prevent the walls from affecting the flow directed towards the working model. The recommendation of a wider section was echoed by other participants in the colloquium. All interested parties agreed that the size of the tunnel must be kept to a minimum while meeting the necessary criteria, as it would take too long to change the models and conduct different sets of experiments.

2.4. Review of the DAPPLE Project

Previous studies conducted considered an area of up to 1 km around the centre of the intersection between Gloucester Pl and Marylebone road. Field studies conducted in the area suggests that the predominant wind direction was SW-SSW with light winds averaging 2.5 m/s and a maximum daily temperature varying between 12 and 22 °C in April-May (Arnold et al., 2004; Wood et al., 2009). Earlier tracer dispersion studies conducted in 2007 considered a 500 m radius of the intersection with a mean building height of 21.6 m in the field of interest (Shallcross et al., 2010).

A combination of all the results from many field tests conducted by Shallcross et al. (2010) are shown in Figure 17. The concentration measurements taken were made dimensionless using the following equation and is plotted against a ratio of the distance between the source and receptor and average building height.

$$C^* = \frac{CU_H H^2}{Q} \tag{2}$$

Where:

C is the mean concentration in parts per million (ppm)

U_H is the mean velocity at roof level height (m)

H is the average building height (m)

Q is the volumetric flow rate from the source (m^3/s).

R is the straight line separation between the source and the receptor (m).

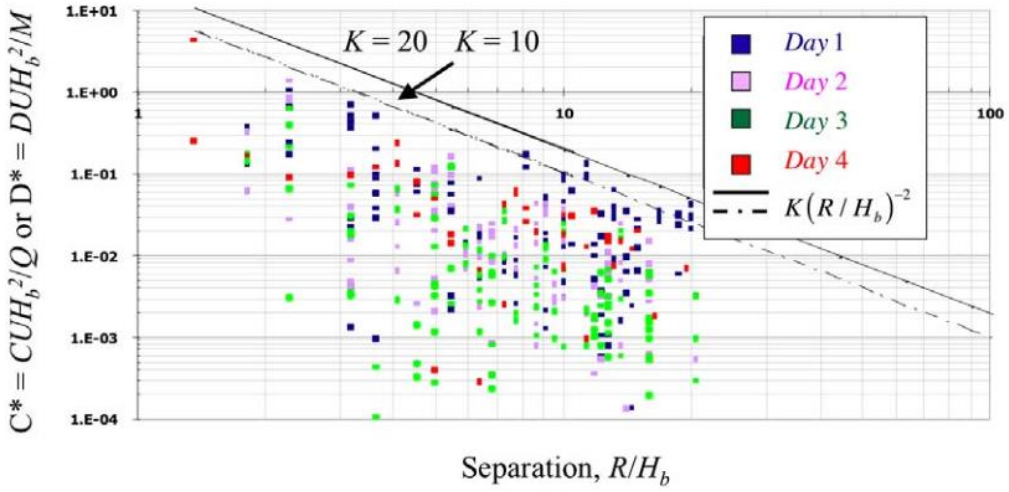

Figure 17: *Variation of non-dimensional concentration, C* from field studies plotted against source-receptor separation, R/H compared against the inverse-square decay law. (Shallcross et al., 2010)*

An upper bound can be seen with the data recorded in the field, with the data showing a decay of concentration with downstream distance. This upper bound was found to be consistent with the inverse square relationship shown in Equation (3) (where R is the straight line separation between

the source and the receptor) with constants n = -2 and K ranging from 10 to 20 (Shallcross et al., 2010).

$$C^* = K\left(\frac{R}{H}\right)^n \tag{3}$$

Wind tunnel testing completed by (Robins et al., 2010) considered a 300 m radius of the intersection with measurements taken of ground level concentrations for five wind directions. These studies used a scale model of 1:200 with varying amounts of detail (Robins et al., 2010). They were completed to help plan field experiments, conduct model evaluation and create detailed datasets. A combination of all data sets gathered in this study is plotted in Figure 18. It should be noted that this dataset uses a roof level speed that is roughly 0.28 that of the speed at the top of the BT Tower for non-dimensionalising the concentration results.

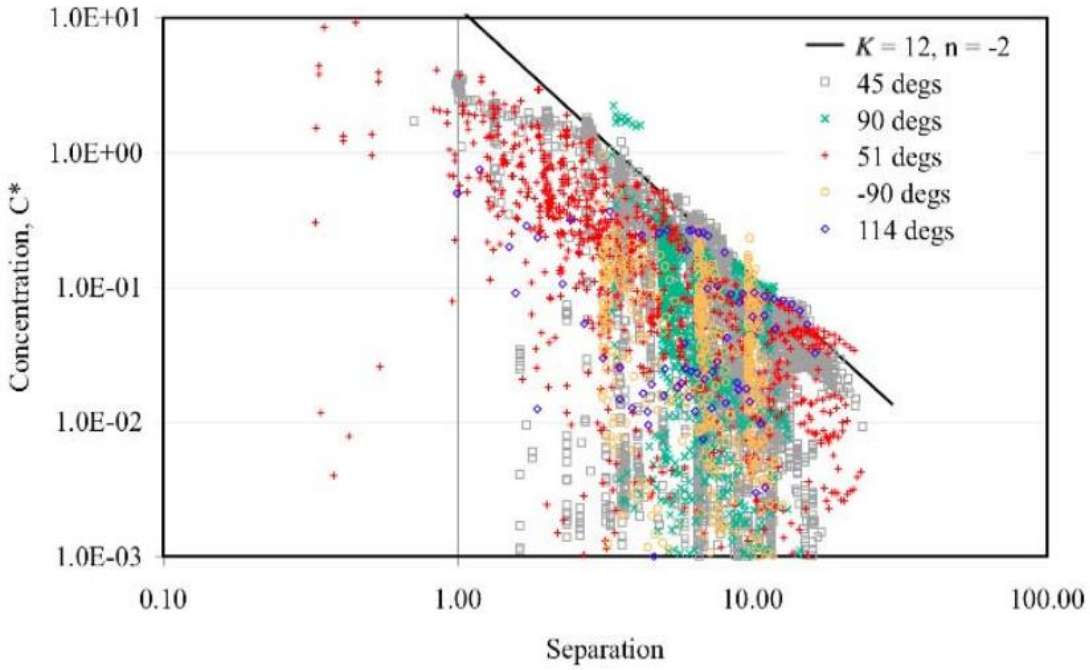

Figure 18: *Variation of non-dimensional concentration, C* from wind tunnel testing plotted against source-receptor separation, R/H for five wind directions compared against the inverse-square decay law. (Robins et al., 2010)*

The results plotted in Figure 18 shows an upper bound consistent with an inverse-square correlation for concentration decay downwind of the source as written in Equation (3). Sensitivity studies were also conducted which confirmed reliability of methods used and the model area considered. Initial results were gathered with buildings modelled as flat roofed blocks. Robins et al. (2010) justifies this simplification by stating that this level of complexity is consistent with the level of detail used in dispersion models and due to the successful completion of the sensitivity studies. These results and previous DAPPLE work have shown K=12 and n=-2 to be a good fit as a prediction of the upper bound in Equation (3) as a function of straight line distance, R. The results from the field work and wind tunnel experiments show good agreement. Ten buildings surrounding the central intersection were also modelled with greater architectural detail which did not significantly impact the dispersion patterns but did result in substantial changes to the concentration levels. The results

showed sensitivity to small changes in wind direction, primarily at near field locations and less so elsewhere (Robins et al., 2010).

In a similar manner, the standard deviations of the fluctuation measurements were plotted against separation distance as shown in Figure 19 which also showed an upper bound to the results, although, in this case, the constants were K = 6 and n = -2.

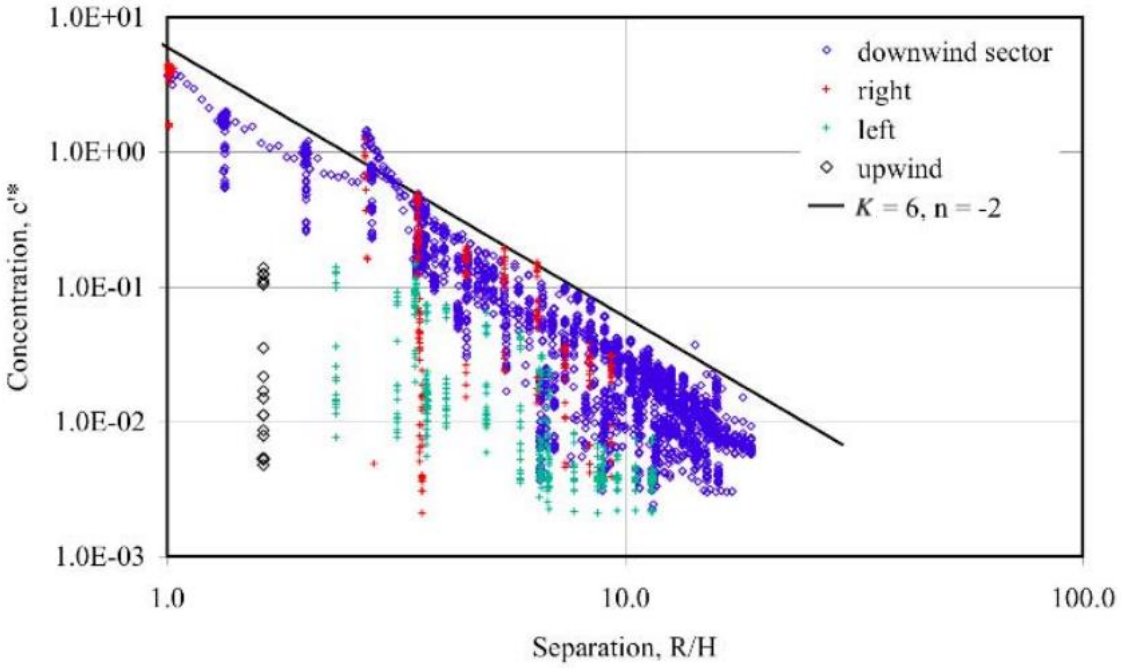

Figure 19: *Variation of non-dimensional standard deviation of concentration fluctuations, c'* from wind tunnel testing plotted against source-receptor separation, R/H for five wind directions compared against the inverse-square decay law. (Robins et al., 2010)*

Robins et al. (2010) states that it is not possible to directly compare field studies and wind tunnel simulations due to the inherent variability of the atmospheric conditions in the real world that makes it impossible to gather data for a prescribed set of conditions. However, the results shown in Figure 17 and Figure 18 gathered from field studies and wind tunnel simulations respectively both show an upper bound of a similar nature, which is more than mere coincidence.

Unpublished work by Ubald (2014) took concentration measurements across the top and road facing surfaces of the monitoring station, providing results shown in Figure 20. Measurements were taken at a distance of 7.5 mm off the surfaces of the station at two different wind directions both with and without the station in place to find out its impact on the results. These results were then non-dimensionalised with a U, reference velocity of 2 m/s; H, average building height of 0.106 m and the relevant trace gas flow rate.

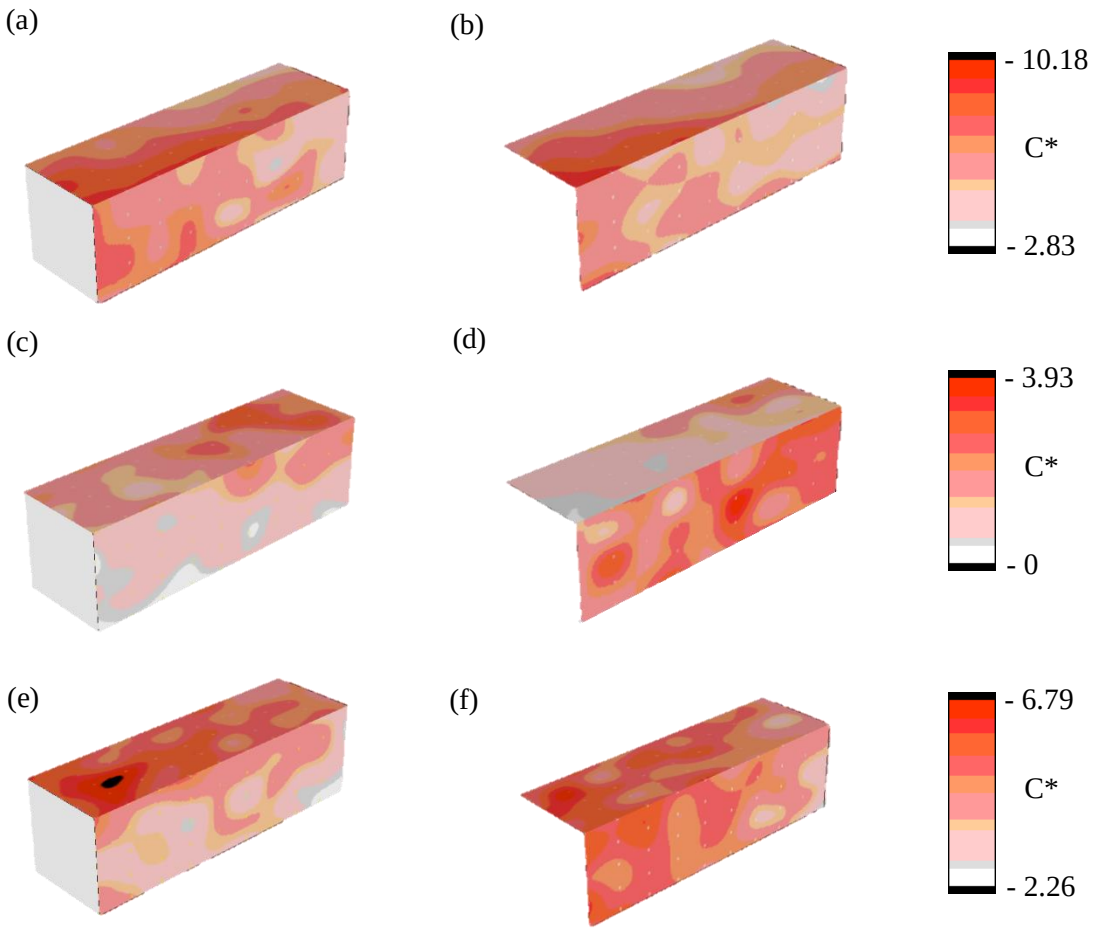

Figure 20: *Contour plots showing dimensionless concentration, C* across monitoring station surface, (a) Wind direction of -45° with source release at (0, -63) mm with the station in place (b) Wind direction of -45° with source release at (0, -63) mm without the station in place (c) Wind direction of -45° with source release at (0, 48) mm with the station in place (d) Wind direction of -45° with source release at (0, 48) mm without the station in place (e) Wind direction of -90° with source release at (-106, -63) mm with the station in place (f) Wind direction of -90° with source release at (-106, -63) mm without the station in place*

Work conducted by Xie et al. (2011, 2013) at the University of Southampton consisted of LES simulations of the DAPPLE site. With Xie et al. (2013) considering the effects of thermal stratification on dispersion - suggesting that its effects are not negligible in weakly unstable conditions (e.g. in London). This investigation showed good agreement between previous wind tunnel studies and LES results.

The study detailed in this report builds upon existing work to include more wind directions as well as extend the DAPPLE site and analyse dispersion behaviour in this extended site as stated in the introduction. Further information on the DAPPLE project, including figures, videos and reports can be found at www.dapple.org.uk.

3. EXPERIMENTAL MATERIALS

This section discusses the equipment used to simulate atmospheric conditions and take relevant measurements. The following equipment were either used or are recommended for future work as denoted by *.

- Atmospheric wind tunnel
- Concentration measurement
- Source gas
- Laser Doppler Anemometry*

3.1. EnFlo Wind Tunnel

All experiments were conducted in the EnFlo wind tunnel at the University of Surrey which was used to simulate a neutrally buoyant atmospheric boundary layer throughout the study. This open-circuit tunnel is also capable of simulating stratified boundary layers (stable and unstable) as described in Chapter 2. It has an operating speed ranging from 0.3 to 3.5 m/s and has a working section of length 20 m, width 3.5 m and height of 20 m (EnFlo, 2015).

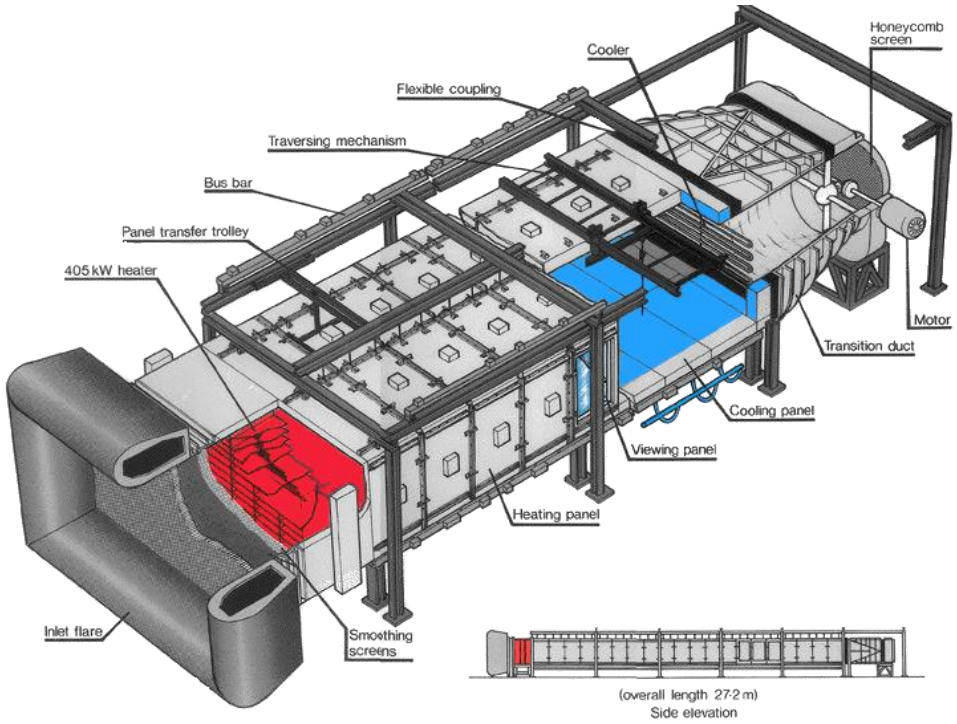

Figure 21: *3D view - EnFlo wind tunnel (EnFlo, 2015) [red – heated areas, blue – cooled areas]*

Figure 21 shows an overview of the capabilities of this tunnel. It is a 'suck-down' type tunnel as it has a motor at the end which sucks in air via the inlet flare after which it passes through a series of honeycomb meshes and smoothing screens that destroys any vortices in the flow and makes the flow uniform. Following the inlet flare is a 15 layer inlet flow heater which can generate vertical temperature profiles that can simulate different atmospheric conditions, complemented by floor heaters and heat exchangers at the end of the tunnel which can return the flow temperature back to ambient, if necessary (Robins et al., 2001).

To generate an atmospheric type boundary layer, five Irwin-type spires (Irwin, 1981) 1265 mm high, 150 mm wide and 10 mm across were placed at the inlet with a spacing of 660 mm. The spires are followed by surface roughness elements that generates a velocity profile similar to real life on-shore conditions. These elements have a height of 20 mm and width of 80 mm and were placed in a staggered pattern with a lateral and longitudinal spacing of 240 mm from the inlet through to the start of the model. This generated a boundary layer with thickness of roughly 1 m.

The reference velocity, U_{REF} was measured through the use a fixed ultrasonic anemometer located towards the end of the wind tunnel which inferred the velocity at the inlet without affecting the flow. Temperature conditions were also monitored towards the inlet and outlet through the use of thermocouple rakes.

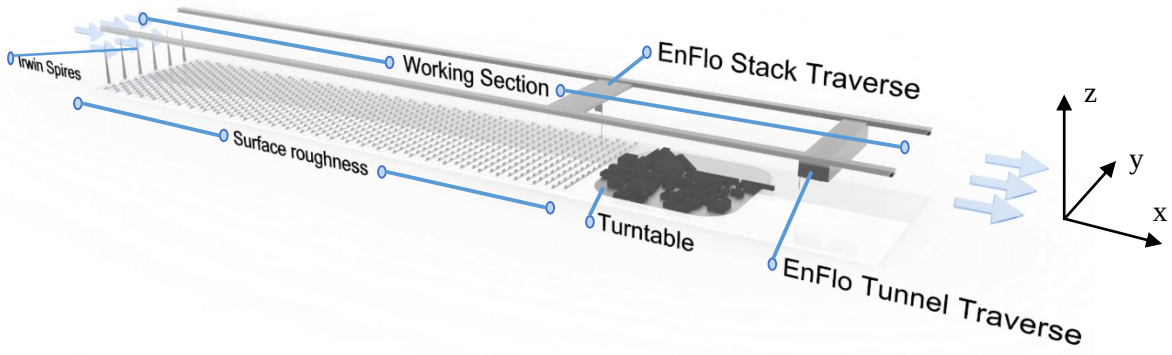

Figure 22: *Internal view of EnFlo tunnel*

Figure 22 illustrates the configuration used in this study. The surface roughness elements can be removed and other models can be placed in this location, if required. There is a turntable located 14 m downstream from the inlet which is capable of rotating from 0° to 360° to simulate different wind directions. Additionally, there are two traverses that hold equipment and measurement devices which can move along all three axes. Due to physical limitations and traverse set-up, movement restrictions were in effect, as shown below in Table 2.

Table 2: *Traverse boundaries*

Axis	EnFlo Stack Traverse (mm)		EnFlo Tunnel Traverse (mm)	
	Min	Max	Min	Max
x	-1500	1350	-1500	2300
y	-1000	980	-900	850
z	5	325	4	450

All of the equipment specified above are tied together through 'virtual instrument' software designed in-house with LABVIEW™. Spatially detailed data acquisition and time traces are recorded through the use of in-house devices which are then relayed into the LABVIEW™ software. Additionally, for this report, after post-processing of the data, results were imported and plotted via a custom made plugin in SketchUp. It should also be noted that all environmental conditions in the lab are always monitored and archived for future analysis.

Movement of the traverses are controlled via LABVIEW^{TM} as well. It recognises two different coordinate systems. The first is the model coordinate system where the positions are always relative to the origin in the model and does not change with rotation of the turntable. The second is the tunnel coordinate system where the positions are always relative to the origin in the tunnel.

3.2. Concentration measurement

The device used for sampling and measurement of the air concentration at various locations across the working section was an atmospheric HFR400 Fast Flame Ionisation Detector (FFID) provided by Cambustion of which a schematic view can be found in Figure 23. It uses the principle of a FID (Flame Ionisation Detector) where a sample gas with hydrocarbons are introduced through the 'Sample capillary' which flows into the hydrogen flame chamber. With the presence of hydrocarbons in the flame, ionisation occurs and the ions formed by burning are detected by the high voltage ion collector. The current across the collector is proportional to the ionisation rate which is also proportional to the hydrocarbon concentration in the sample gas (Cambustion, 2014). For a direct concentration measurement, the FFID (also called a receptor) must be calibrated against several fixed concentrations to provide a linear fit which in this study consisted of 0, 300, 600 and 900 ppm, at flow rates of 50, 50, 25 and 16.7 l/min respectively.

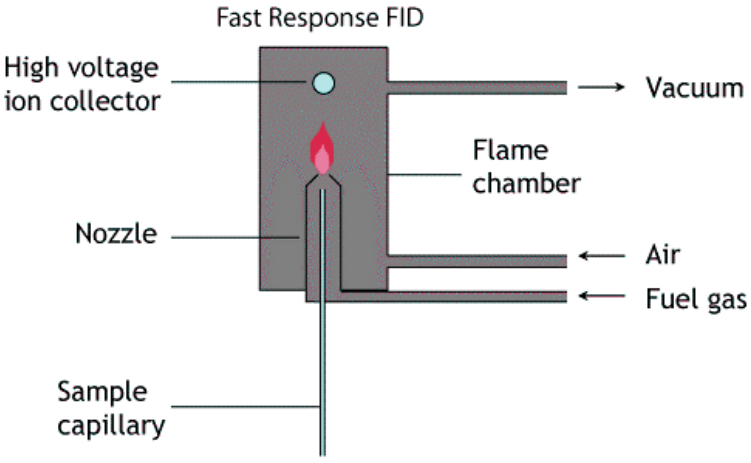

Figure 23: *Schematic view of FFID (Cambustion, 2014)*

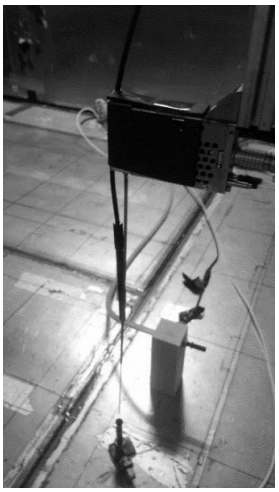

Figure 24: *FFID above calibration chimney stack*

A FFID improves upon the sampling time of a FID from seconds to milliseconds by isolating fluctuations in pressure at the sampling point, allowing for a constant flow of the sample gas into the FID (Cheng et al., 1998). Furthermore, a bespoke sample capillary with a height of 345 mm was used for clearance from the tallest building in the model.

A source diverter valve was used to divert the flow outside the tunnel before taking background measurements to prevent increasing the run time by having to wait for the emission rate to increase to required values repeatedly. This result was deducted automatically from the results with the FFID exposed to the plume. These measurements were repeated every 12 minutes to take into account subtle variations in lab conditions.

Figure 24 shows the device in operation, with the capillary inside a chimney stack that was placed at an arbitrary, but fixed position, downstream of the turntable (2101, 401, 70). This stack is used for routine calibration of the device every 2 hours to account for variations in lab conditions much like the background measurements. Each calibration is automatically compared to previous measurements and the percentage change in drift recorded with any significant increase requiring a repeat. A pen camera was also attached to the capillary to take automated pictures during calibration to ensure that it was immersed in the stack.

For reliable statistical data, concentrations were averaged over a period of 2.5 minutes throughout the study, with a sampling frequency of 400 Hz.

3.3. Emission system

As mentioned previously, the sample gas requires the presence of hydrocarbons for concentration measurement which is the tracer gas. For all experiments in this study, the source gas is 1.75% propane in compressed air unless otherwise specified. This mixture was released downwards via a vertical steel pipe connected to the EnFlo Stack traverse to simulate a passive release (the release pipe had a length of 1100 mm, with inner and outer dimensions of 4.25 mm and 6.1 mm respectively) as shown in Figure 25. The source gas was released at a rate of 1 l/min throughout the study, unless otherwise specified.

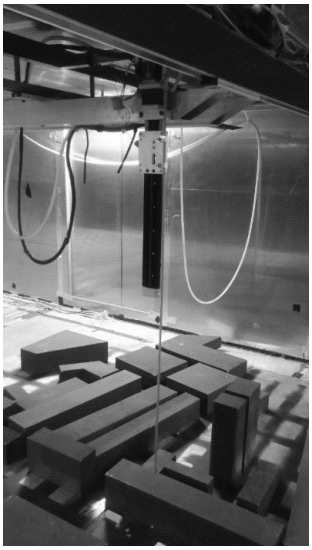

Figure 25: *Source releasing from "EnFlo Stack" traverse*

3.4. Laser Doppler Anemometry System (LDA)

An LDA system is used for velocity measurements of a fluid. The system used in the EnFlo tunnel is a two component system, capable of measurements along two axes, depending on probe placement (Dantec Dynamics, 2013). It is an optical method, hence, for optimum power output, the lasers must be aligned correctly through the fibre optic cables and into the tunnel (Zhang, 2010).

For velocity measurements, natural impurities in the air are not enough, as the particles must be large enough to scatter light, but small enough to follow the flow without affecting it. For this reason, a process known as ‘seeding’ is used. In the EnFlo tunnel, this process involves releasing a mixture of sugar and water towards the inlet as a mist that travels downstream and flows past the laser. It works by using the Doppler shift; as the light hits the sugar particle, the light is reflected back at a shifted frequency which is proportional to the flow velocity.

An LDA has the distinct advantage of not requiring calibration and being non-intrusive. However, they also have a limited lifespan, so their power levels must be monitored closely before the start of any experiment (Dantec Dynamics, 2013).

3.5. Wind Tunnel Model

The dispersion experiments were completed in the EnFlo tunnel using a 1:200 scale model of Marylebone Road, London, centred at the middle of Marylebone Road, opposite the Madam Tussauds dome (surrounding a 300 m radius) as shown in Figure 28. Building locations and dimensions were obtained from Infoterra and Google Earth which enabled the scale models to be built. The average building height in the study area is 21.28 m (ranging from 7 to 64 m). All buildings were assumed to have flat roofs with the height of the eaves (where the roof overhangs) taken as the building heights.

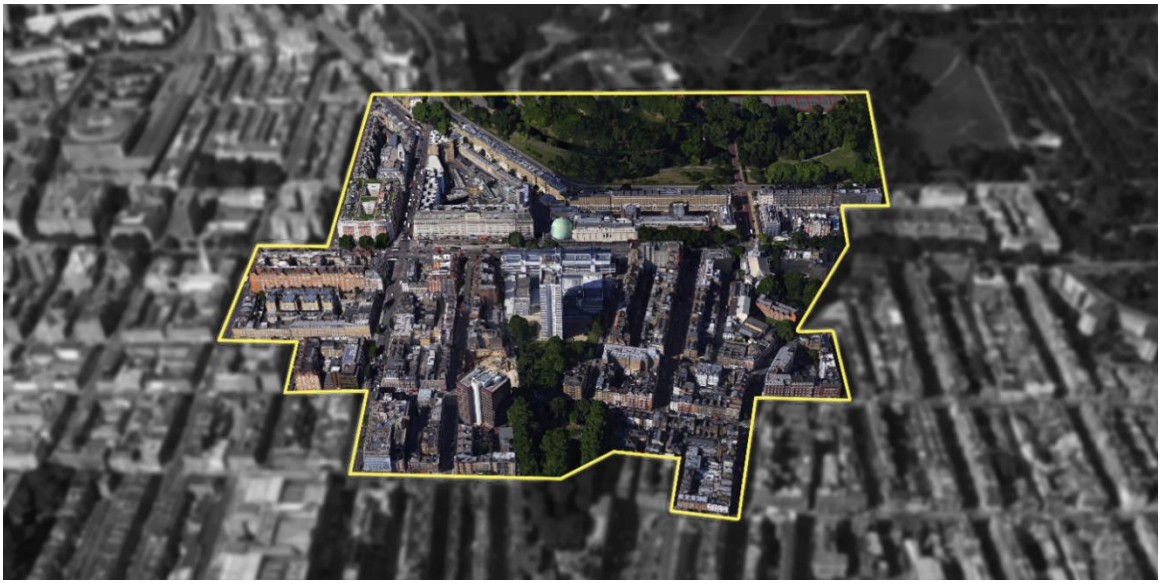

Figure 26: *Area of Marylebone Road under consideration in this study (Google Earth, 2015)*

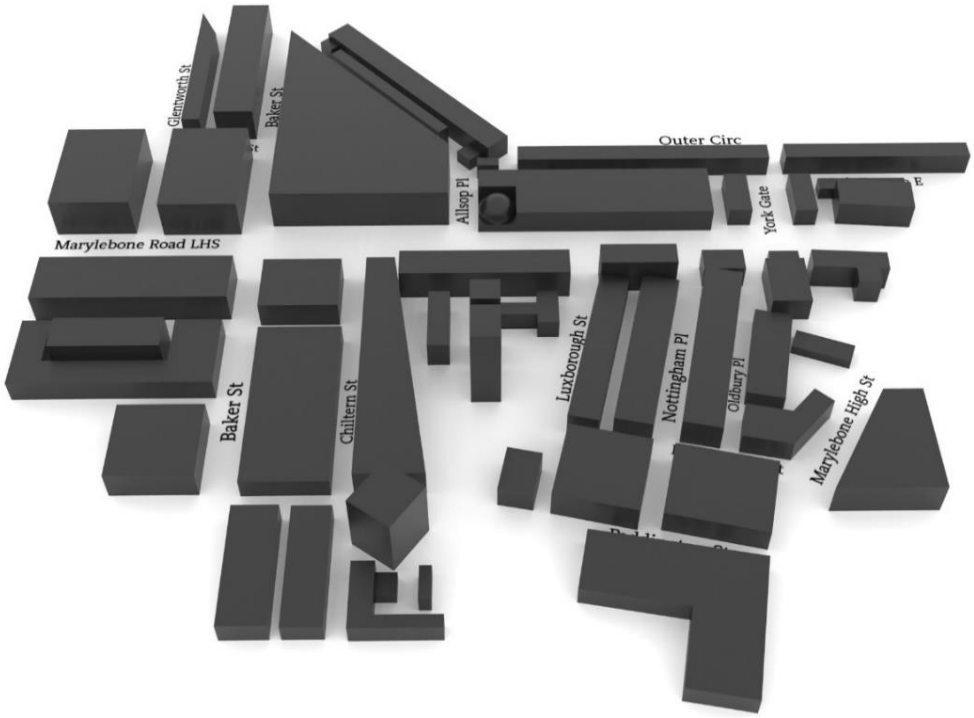

Figure 27: *Simplified 3D model of Marylebone Road and surroundings*

A satellite view of Marylebone Road is shown in Figure 26 with a yellow overlay showing the region under consideration. Figure 27 shows the simplified model that was then created of this region. A plan view of the site is shown in Figure 28 with the coordinate system and wind direction angles used throughout this report. The model coordinates are all in mm, with 0° defined as flow parallel to the x axis and rotation angle defined as negative south of Marylebone Road and positive elsewhere.

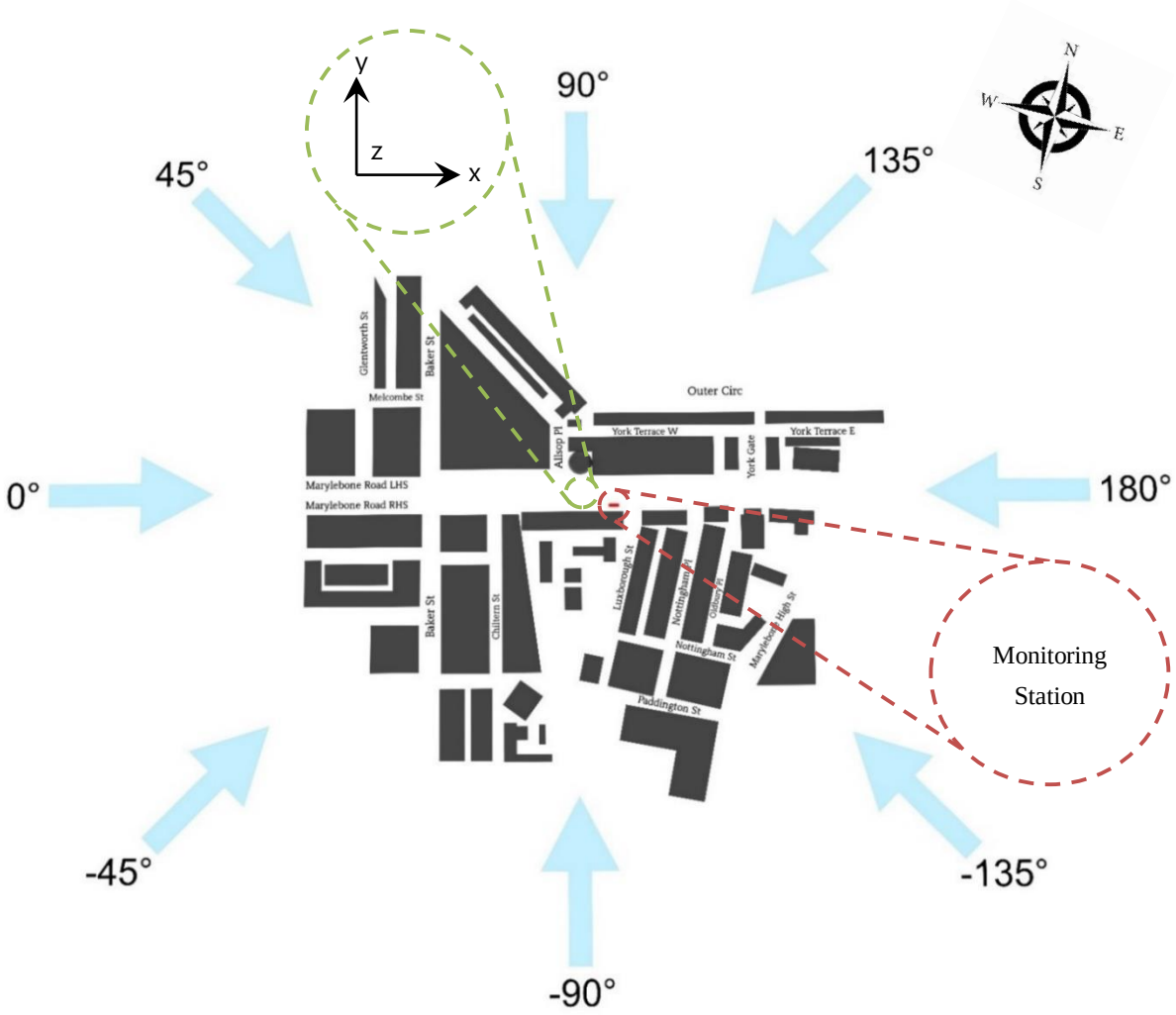

Figure 28: *Plan view of Marylebone Road site with coordinate system and wind directions*

Due to the possibility of the cables under the turntable twisting and causing an issue, the convention used in this report will be as shown in Figure 28 ranging from 0° to ±180°, with x, y and z denoting distances from the centre of Marylebone Road directly opposite Madam Tussauds dome along their respective axes.

This study does not consider the effect of trees on the model. Due to the size and traffic conditions, for source gas releases, Marylebone Road was split into two lanes consisting of a left (y=48) and a right (y=-63) hand side; all other roads were assumed to have a single lane. There is a monitoring station located across from Madam Tussauds as shown in Figure 28 which takes field measurements continuously and will also be modelled in this study as a cuboidal structure. The next chapter discusses the procedure used to gather results using the equipment detailed in this chapter.

4. EXPERIMENTAL PROCEDURE

The experimental procedure for this study is laid out in this section. This study consisted of two sets of experiments with the first set analysing the effect of the monitoring station on the results. The second set of experiments were subdivided into forward and inverse modelling scenarios to understand source-receptor relationships. All wind tunnel experiments were completed at a reference wind speed of 2 m/s, with a simulated neutral boundary layer.

4.1. Experiment Set 1 - Monitoring station

The first set of experiments consisted of a tracer gas release with concentration measurements taken by the FFID via longitudinal profiles across the top and road facing surfaces of the monitoring station as shown in Figure 29. Contrary to the unpublished work completed by Ubald (2014) which used a grid of 5 x 10 across the top and bottom surfaces with a constant distance of 7.5 mm from the surfaces, this study took measurements across a 11 x 8 grid along the top and a 11 x 7 grid along the front surface with the FFID kept 5 mm away from either surface. The changes from the previous experiment were made based on consideration of wind tunnel run-times, requirement of results at a higher resolution and at a closer distance to the surfaces.

A sensitivity analysis of the station was also conducted by taking measurements with and without the station in place to study its effect on the results.

This was completed at wind directions of 180°, -45° and -90° and two tracer gas release locations per wind direction which were on opposite sides of Marylebone Road compared to the two wind directions -45° and -90° and three source release locations considered in previous the previous study introduced in section 2.4. These wind directions were selected based on concentration measurements obtained from Ubald (2014), as the source release from either lane of Marylebone Road at the selected positions and wind directions have much higher changes in concentration than the any other.

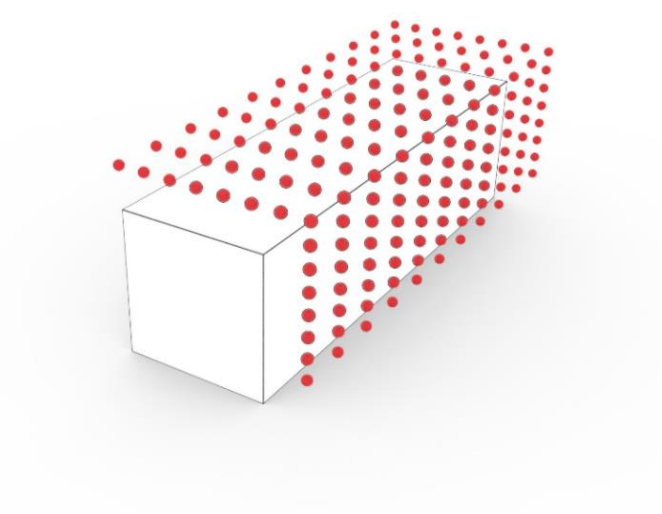

Figure 29: *Measurement points across station surface for Experiment Set 1*

The monitoring station is modelled as having dimensions of length 58 mm, width 17 mm and height 17.5 mm.

4.2. Experiment Set 2

4.2.1. FORWARD MODELLING

The forward modelling scenario consisted of the FFID kept fixed at (202.5, -74, 10) mm which is the approximate centre of the monitoring station across x and y in model coordinates. The source was moved across each of the roads and areas of empty space at a height of 10 mm with the results at each point being averaged over 2.5 minutes.

The spacing between measurement points were determined by analysing unpublished work completed by Ubald (2014), where a similar number of measurement points were used, but the resolution varied by transitioning the spacing from 20 mm up to 150 mm smoothly to reflect high to poor concentration regions. Figure 30 shows the measurement points for the 180° case, the measurement points for the other wind directions can be found in Appendix A (Figure A1 to Figure A3).

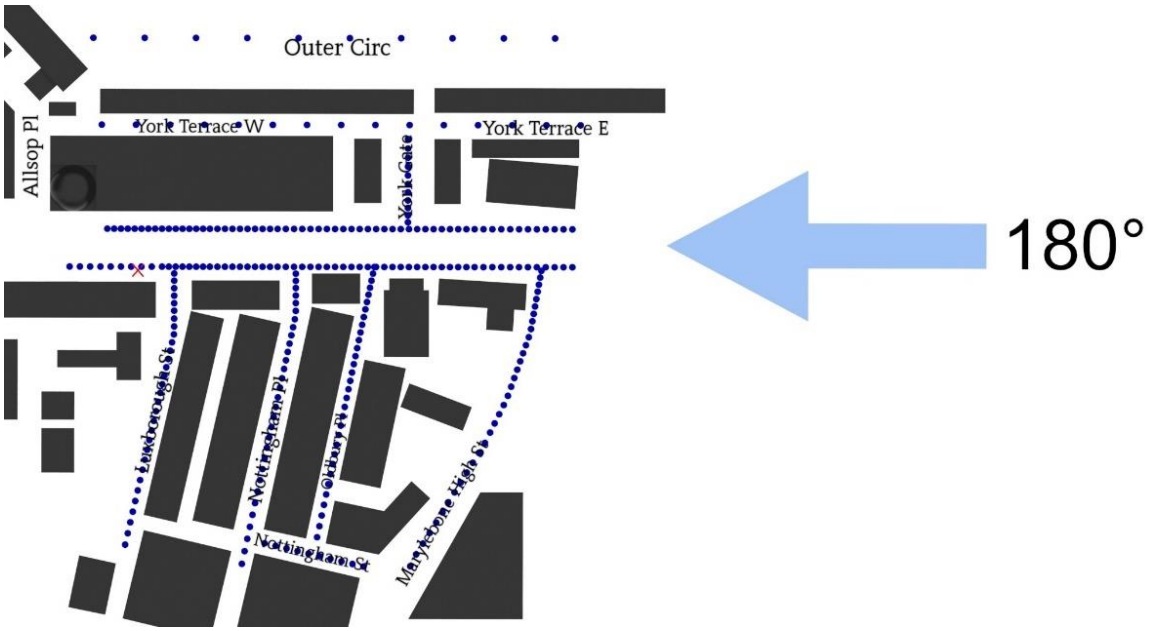

Figure 30: *Measurement locations for 180° forward modelling case*

In general, measurements were taken along the centre of each road that was traversable with the traversing systems to simulate traffic emission, although, in some cases, measurements were also taken at open spaces to be able to determine a holistic view of the results from each wind direction.

Due to the FFID being fixed very close to the right hand lane of Marylebone Road, it was not possible to move the source to areas surrounding the station. However, due to the proximity of the plume, the peak concentration levels are important and thus, the concentrations were measured using an alternative trace gas releasing device (shown in Figure 31) that was moved into each inaccessible position manually.

When taking manual measurements, to account for the impact of the traverse that originally released the source gas on the boundary layer, the EnFlo Stack traverse was positioned close to the last attainable measurement point for each wind direction, but at an elevated height of 50 mm as shown in Figure 31.

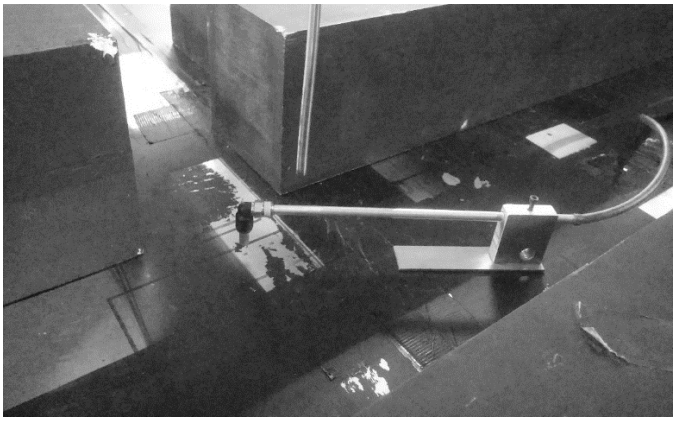

Figure 31: *Manual source release set-up for Experiment Set 2*

To reduce the likelihood of signal clipping where the data acquisition device was incapable of detecting the full strength of the tracer concentration, the flow rate and strength were reduced to 1 l/min and 0.5 % respectively. At points near the monitoring station, the results had to be repeated due to the high concentration levels.

4.2.2. INVERSION MODELLING

The resolution of measurement points were halved for this set of experiments compared to the forward modelling scenario and the positions of the FFID and the source gas emission system were reversed which imposed new limits to the movement of each device. Additionally, the wind direction was inverted apart from which, measurements were taken in the same manner as the forward modelling case. The source gas was released at (202.5, -74, 10) while the FFID moved across the measurement points as shown in Appendix A (Figure A4 to Figure A7) at a height of 10 mm off the tunnel floor. In this case, manual measurements were not taken.

The purpose of this experiment is to check if the inversion modelling results are linear compared to the forward modelling results. For this to be the case, there must be symmetry in the building geometry and road layout, else, the turbulence profiles can vary greatly. With the wide range of geometries involved in this study, it is expected for the turbulence profiles to differ in forward and inverse cases and the results to not being directly comparable. Thus, a fully linear relationship is not expected between the results. This experiment was conducted as the differences between the two can further help develop understanding of flow behaviour at Marylebone Road.

5. RESULTS AND DISCUSSION

This section presents the results and analysis conducted based on the wind tunnel experiments.

All measurements are transformed from a time-averaged concentration to a non-dimensional concentration, C* for comparison with previous studies. The difference to the equation shown in the literature review, Equation (2) is due the use of reference velocity rather than roof level velocity.

$$C^* = \frac{C_{ppm} U_{ref} {H_{BH}}^2}{Q_{trace}} \quad (4)$$

Where:

C_{ppm} is the mean concentration in parts per million (ppm).

U_{ref} is the mean reference velocity (m/s).

H_{BH} is the average building height (m).

Q_{trace} is the volumetric flow rate from the source (m^3/s).

Furthermore, the straight-line distance, R between the source and the receptor is calculated using:

$$R = \sqrt{\delta x^2 + \delta y^2 + \delta z^2} \quad (5)$$

Where:

$\delta x, \delta y \; and \; \delta z$ are the deltas in their respective directions.

All coordinates within this section are measured in millimetres and for indicated flow directions and coordinate system, refer to Figure 28.

5.1. Data Quality

The results in this subsection analyses the uncertainties found in a sample of data gathered in this study. Even though these evaluations have been conducted for cases other than the sample shown in this subsection including different wind directions and streets, these have been omitted due to the level of similarity that can be found between them. However, any anomalous results and exceptions to the trends shown in the sample data have been clearly identified.

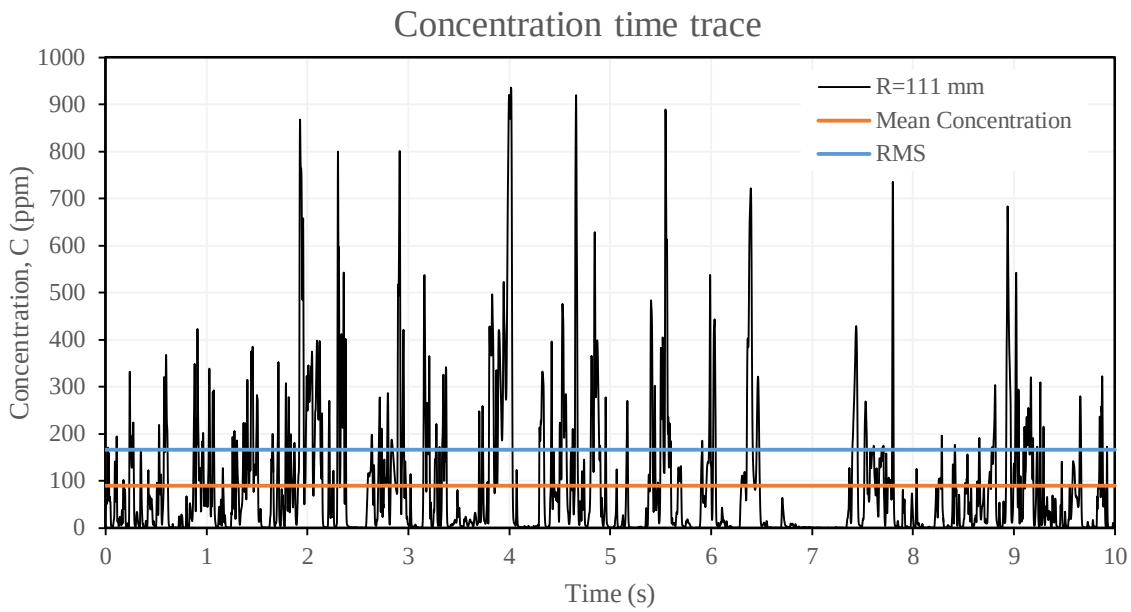

Figure 32: *Plot showing concentration time trace at 180° wind direction as measured by FFID at (312.79, 63.36) with a straight line distance, R of 111 mm*

A plot showing a typical time trace over a period of 10 seconds obtained during the course of this study, as measured directly by the FFID, is plotted in Figure 32. The mean concentration for this sample data is 90 ppm with a standard deviation of 140 ppm – giving an RMS value of 166 ppm. The maximum is located roughly six standard deviations (σ) away from the mean while the minimum is located under a single σ. This result is for a very short source/receptor distance (R=111 mm) with very high concentration fluctuations with time. Thus, the large deviations from the mean are expected in this case with measurements from other locations and wind directions typically

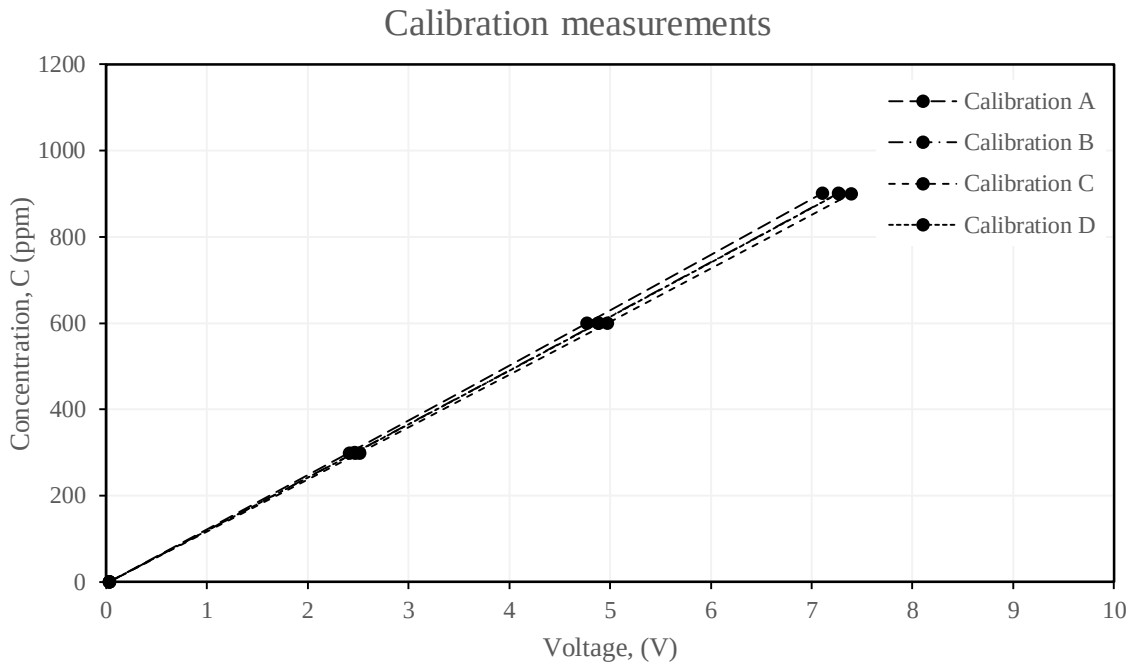

Figure 33: *Plot showing four sample linearity fits of concentrations calibrated against FFID voltage*

As stated in Section 3.2, the FFID was calibrated at four concentrations for accurate measurements. This was completed intermittently every two hours and at the start and end of each experiment. Figure 33 displays a plot showing four such calibrations taken during the experiments. This plot is characteristic of all calibrations conducted in this study with any anomalous measurements repeated and resulting erroneous data omitted from the results presented herein. All results presented were based on a calibrated FFID with linearity errors consistently below 0.5%. The errors are so insignificant that they are indistinguishable from the measurement points shown in the figure.

It should be noted that a number of concentration measurements, taken when the tracer gas was released by the device shown in Figure 31 had the signal clipped when the distance between the source and receptor was at its lowest as the results exceeded a certain threshold set by the sampling equipment. Thus, certain high values were omitted from the mean concentration calculation in the software. Further analysis of these anomalous readings has shown that the absence of signal clipping can lead to an increase in mean concentration of up to 10%. As stated in section 4.2, repeats were conducted on signal clipped regions to overcome this issue. However, the source strength was not sufficiently reduced for the fluctuations to remain below the threshold at points that were extremely close to the FFID.

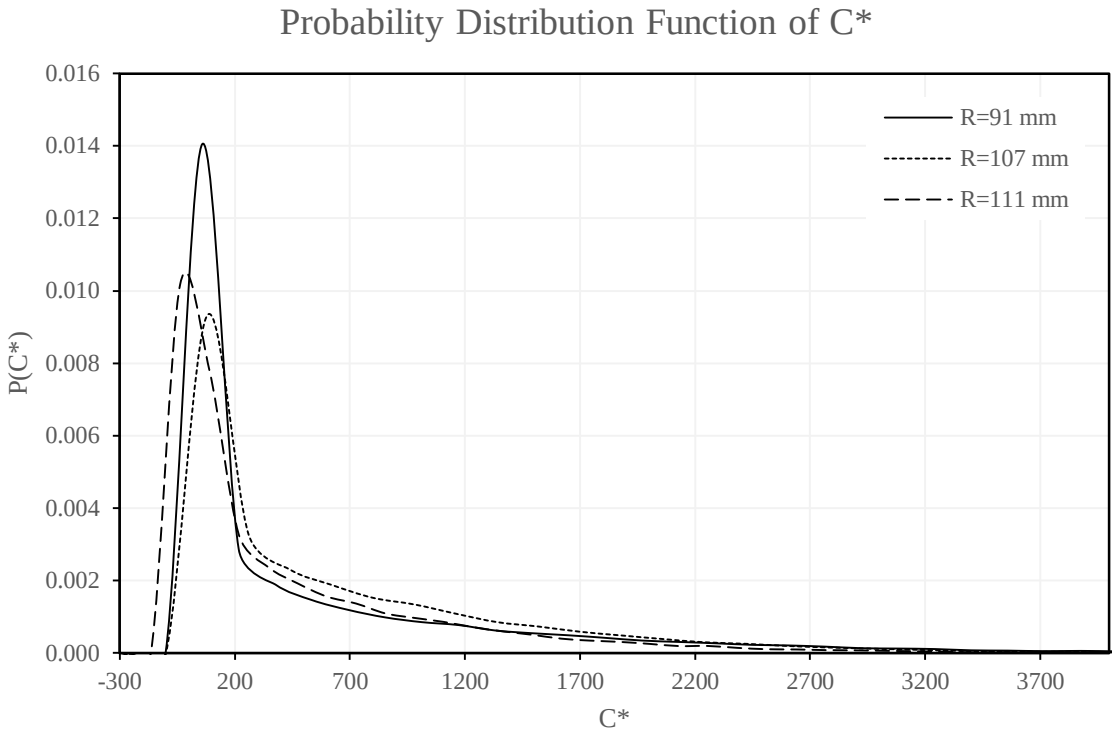

Figure 34: *Probability Distribution Function (PDF) plot of non-dimensional concentration, C* from the 180° forward modelling scenario for three measurement points near to the receptor, where R is the straight line distance between the source and receptor as shown in Equation (5).*

Figure 34 plots the probability distribution function for concentration measurements taken at three points located close to the FFID from the 180° forward modelling case along the right-hand side (RHS) of Marylebone Road which gave some of the highest concentration measurements. These results do not follow any known distributions in general. However, all results show a region with

high probability that is characteristic of the concentration measurements. This plot is representative of the probability distribution for all measurements taken. This was validated for a large scatter of points at different locations for all wind directions.

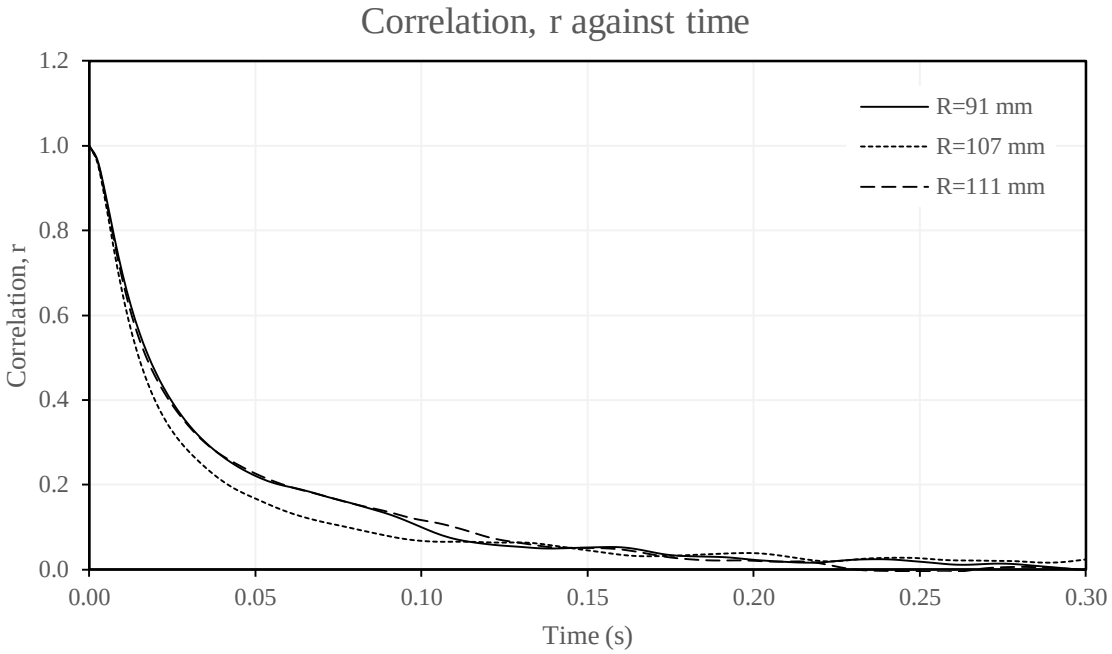

Figure 35: *Plot showing correlation coefficient, r against time for six measurement points from the 180° forward modelling scenario, where R is the straight line distance between the source and receptor as shown in Equation (5).*

Figure 35 plots correlation coefficient, r against time for the same measurement locations as Figure 34 for a sample of the measured dataset. It plots a statistical trend showing the level of similarity between results with a separation in distance or time. The correlation is said to be perfect (r=1) with a distance or time separation of zero and this decreases with increased separation. The results are akin to an inverse exponential relationship, as expected with the difference being that the results are limited and does not tend towards infinity. The correlation coefficient at a time step of zero is limited to one in all measured cases due to the physical size of the smallest eddies which prohibits resolving anything smaller than its size (Thus, the plot curves to r=1). This trend is common to all measurements taken in this study.

5.2. Experiment Set 1 - Monitoring station

Wind tunnel experiments were conducted as detailed in 4.1 with tracer gas emissions from two lanes of Marylebone Road for each wind direction considered in this study.

A ratio of the average concentration across a surface with and without the station is used to evaluate the impact of the station on the results as shown below:

$$P = \frac{Surface\ average\ C^*\ with\ station}{Surface\ average\ C^*\ without\ station} \tag{6}$$

Additionally, a ratio of the concentration at the centre of a surface with and without the station is used to evaluate the results as shown below:

$$Q = \frac{Surface\ central\ C^*\ with\ station}{Surface\ central\ C^*\ without\ station} \tag{7}$$

5.2.1. 180° WIND DIRECTION

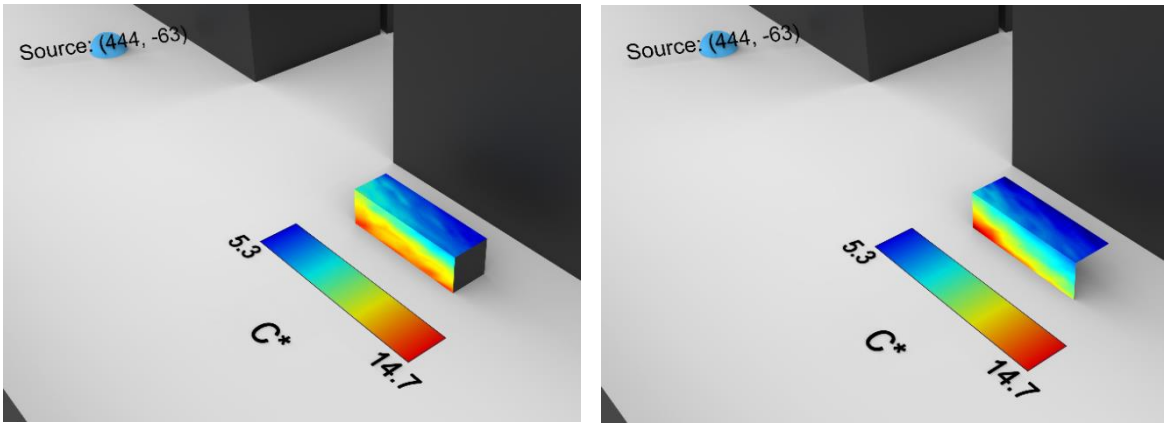

(a) with station (b) without station

Figure 36: *3D Contour plot of non-dimensional concentration, C* at a wind direction of 180° with source gas released at (444, -63) mm. (a) with the station in place (b) without the station*

Figure 36 displays 3D contour plots for the 180° case with the tracer gas released from the RHS of Marylebone Road. The ratios P and Q are 1.10 and 1.08 across the top surface and 1.07 and 1.13 across the front respectively. Thus, it can be seen that the average and central results are in good agreement in both cases. It can also be seen from Figure 36a that with the station, the base of the frontal surface has a clearly visible concentration layer rather than a high concentration region towards the bottom left, as seen without the station in Figure 36b.

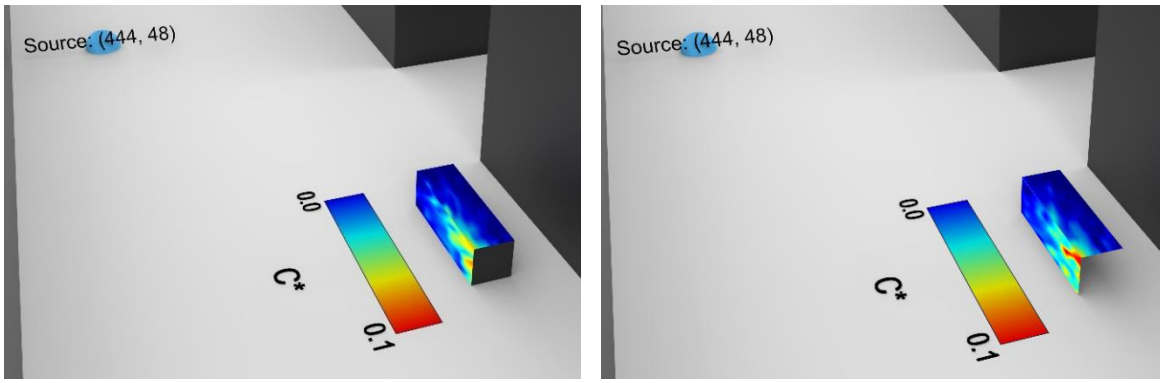

(a) with station (b) without station

Figure 37: *3D Contour plot of non-dimensional concentration, C* at a wind direction of 180° with source gas released at (444, 48) mm. (a) with the station in place (b) without the station*

Figure 37 shows 3D contour plots across the station surfaces with the tracer gas released from the left-hand side (LHS) of Marylebone Road. The ratios P and Q are 0.93 and 1.17 across the top surface and 0.87 and 0.84 across the front respectively. Contrary to the LHS release, the removal of the station has resulted in a marked increase in the concentration region. However, the concentrations from this LHS release are minimal, as can be seen in the ranges in Figure 37a and Figure 37b. This is probably due to the air simply passing through the road in a straight line with little mixing occurring at the intersections. This causes the emissions to travel downstream along the LHS with little to no interaction with the station.

5.2.1. -45° WIND DIRECTION

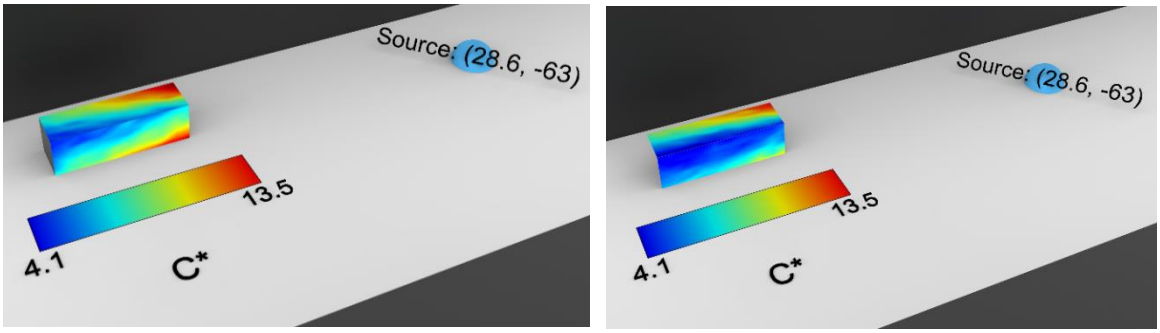

(a) with station (b) without station

Figure 38: *3D Contour plot of non-dimensional concentration, C* at a wind direction of -45° with source gas released at (28.6, -63) mm. (a) with the station in place (b) without the station*

3D contour plots showing C* for a -45° wind direction and RHS tracer release along with the release coordinates can be found in Figure 38. The ratios P and Q are 1.08 and 1.17 across the top surface and 1.24 and 1.27 across the front respectively. The concentration levels have decreased in general with the station in place. In this case, the average and central results between the surfaces are similar, and even more so without the station. The top surface shows good agreement with and without the station, but with a slightly larger concentrated region with the station in place across

both surfaces. It is likely that the concentrated region has formed due to flow recirculation caused by the upstream buildings, which was intensified slightly by the presence of the station.

Compared to previous experiments shown in Figure 20a and Figure 20b, the scale is higher, as expected, because the source is released closer to the monitoring station. However, the contours do not present any similarity either with or without the station due to the varying turbulence profile closer to the station surface, as these measurements were taken 2.5 mm closer to the surface than the unpublished work introduced in section 2.4.

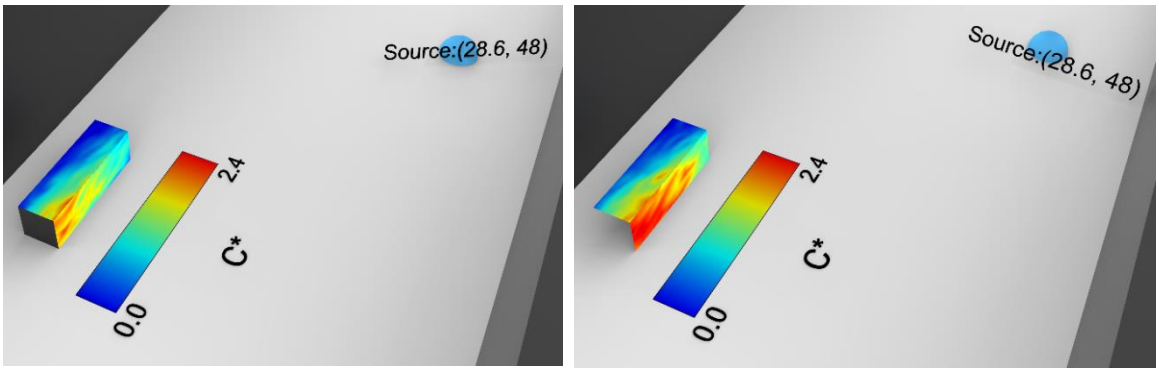

(a) with station (b) without station

Figure 39: *3D Contour plot of non-dimensional concentration, C* at a wind direction of -45° with source gas released at (28.6, 48) mm. (a) with the station in place (b) without the station*

3D contour plots of C* for a -45° wind direction with emission from the LHS of Marylebone Road are shown in Figure 39 along with the specific release coordinates. The ratios P and Q are 0.89 and 0.87 across the top surface and 0.77 and 0.84 across the front respectively. There is an increase in the average and central concentration values in both cases. Similarly to the 180° case, but to a much larger extent, the removal of the station has resulted in a substantial increase in the area with high concentration, especially along the top left of the frontal surface, as can be seen in Figure 39a and Figure 39b. This is due to the high level of mixing caused by the diagonal flow of air, which developed rotating flow that directed the concentration to act in the manner described.

These results are at a lower scale than the experiments conducted previously, as shown in Figure 20c and Figure 20d. This is because the gas is being emitted further along Marylebone Road and there is little interaction between either lane in this region.

5.2.2. -90° WIND DIRECTION

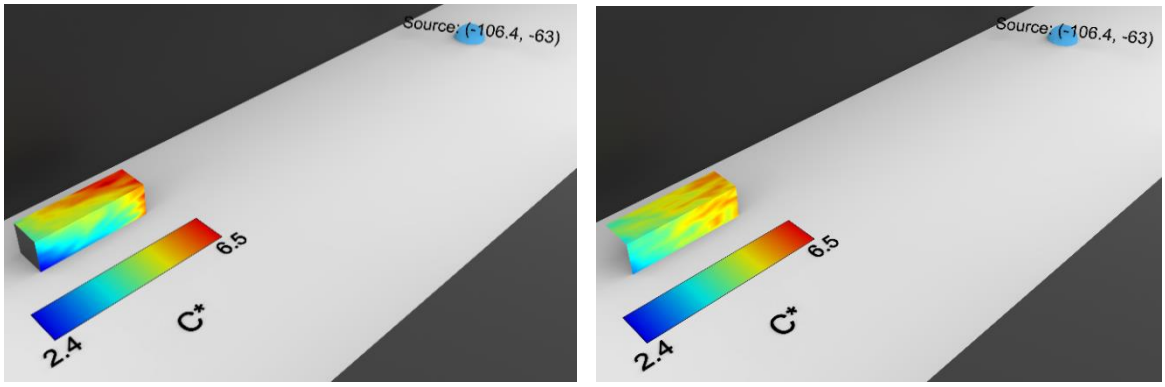

(a) with station (b) without station

Figure 40: *3D Contour plot of non-dimensional concentration, C* at a wind direction of -90° with source gas released at (-106.4, -63) mm. (a) with the station in place (b) without the station*

Figure 40 shows 3D contour plots of C* with trace gas emission from RHS of Marylebone Road along with specific release coordinates for -90° wind direction. The ratios P and Q are 1.06 and 1.05 across the top surface and 0.93 and 0.93 across the front respectively. The ratios are remarkably consistent across each surface even though there is a clear increase in the concentration scale with the presence of the station. The air flow is directed from behind the station and the presence of the station causes a sharp increase in concentration across the top right of both surfaces. The flow is more dispersed without the station in place. This is probably due to the air flow colliding with the side of the station when present and creating a displacement zone as discussed in 2.1.2.1 within which the pollutant is of a higher concentration, although, in this case, the flow is not completely perpendicular to the modelled station.

These results are on a similar scale to previous work shown in Figure 20e and Figure 20f as the source was released at the same location. As mentioned previously, the difference in contours is probably due to the increased proximity to the station surfaces.

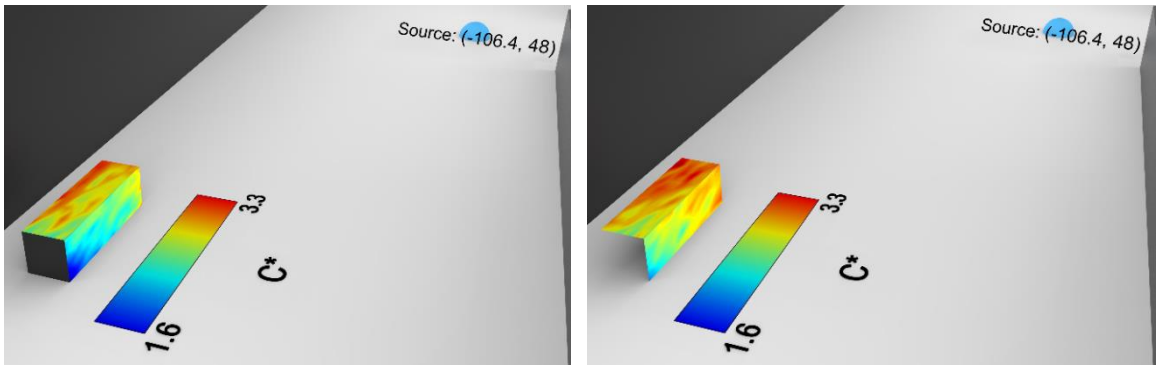

(a) with station (b) without station

Figure 41: *3D Contour plot of non-dimensional concentration, C* at a wind direction of -90° with source gas released at (-106.4, 48) mm. (a) with the station in place (b) without the station*

Figure 41 shows 3D contour plots of C* for -90° wind direction from the LHS of Marylebone Road with specific release coordinates illustrated. The ratios P and Q are 0.97 and 0.91 across the top surface and 0.91 and 0.90 across the front respectively. Both surfaces have larger areas of high concentration without the station present. It can be seen from Figure 41a and Figure 41b that the top surface has lower concentration levels with the station. This decline is probably due to a reduction in the suction zone across the top of the modelled station, as established in experiments conducted previously and described in 2.1.2.1 that occurs when air flow hits the station diagonally.

To summarise the first set of experiments, the P ratio ranges between 6% and 11%, while the Q ratio ranges between 5% and 17% across all wind directions, although, most of the results are below or around 10% which shows good agreement to the average concentration across the surface. The outlier being a ratio of 17% from -45° and 180° wind directions where the source was released along the LHS (y=48). Thus, considering the fact that the majority of the results were below 10%, the impact of the station can be presumed to be minimal across the top surface.

Contrary to the top surface, the P ratio ranges between 7% and 33% which is a considerably wide range. Similarly, the Q ratio also shows a wide range in dimensionless concentration, ranging between 8% and 27%. The -90° case shows the least impact with P and Q ratios of less than 10%, followed by 180° with an impact of less than 15%. Thus, the -45° case showed the most impact, with ratios greater than 16% and up to 33% in all measurements.

It can be seen from the plots in this subsection that the results follow the theory introduced in section 2.1.2 and that in certain cases, the flow around the monitoring station behaves in such a manner that the station itself can be considered to be an isolated building surrounded by building arrays. Furthermore, situations where a series of high concentration results are immediately preceded or proceeded by low concentration readings is probably due to the formation of helical vortices by upstream buildings as described in section 2.1.2. The presence of the station breaks down the strength of the flow and stops the vortex from proceeding downstream, whereas in its absence, the flow continues along in a helical manner before interacting with and dissipating along downstream intersections.

5.3. Experiment Set 2

This section presents the results from the second set of wind tunnel experiments and discusses the spatial relationship between air pollutants and areas of interest, primarily, Marylebone Road.

5.3.1. FORWARD MODELLING

This section presents the results based on the procedure detailed in 4.2.1. The source gas was emitted from different locations while the receptor was kept fixed at the centre of the monitoring station, at a height of 10 mm above the tunnel floor. Herein, the location of the FFID will be referred to as either the receptor or monitoring station location.

5.3.1.1. 180° Wind Direction

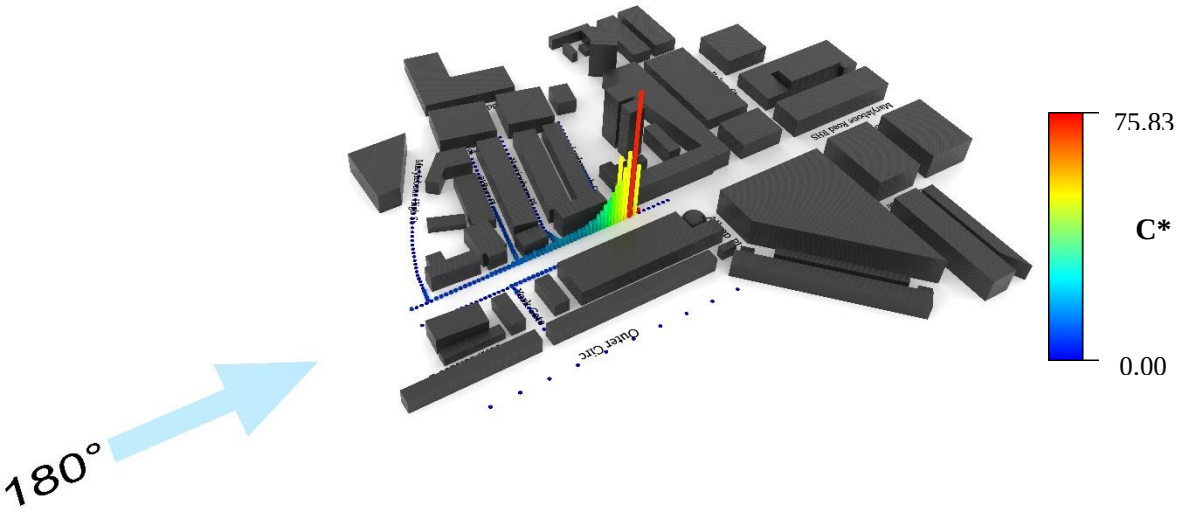

Figure 42: *3D Plot of non-dimensional concentration, C* at a wind direction of 180° with varied source release location and fixed FFID at (202.5, -74, 10) mm*

The 180° wind, approximately a westerly wind is along the axis of Marylebone Road. The concentration levels are shown in Figure 42. A gradual drop in concentration can be seen along each of the intersections except for Nottingham Place which is probably due to recirculation caused by the leading building along this road. There is little interaction between the two lanes on Marylebone Road as the LHS has low concentration levels along its entirety while the RHS has a region of high concentration surrounding the receptor location, as expected. These results would align well with street network based models as based on these results, the air is simply passing through Marylebone Road with minimal interaction with the buildings, although, an ADMS model would better handle the narrow streets that form street canyons such as Chiltern St and Nottingham Pl.

5.3.1.2. -45° Wind Direction

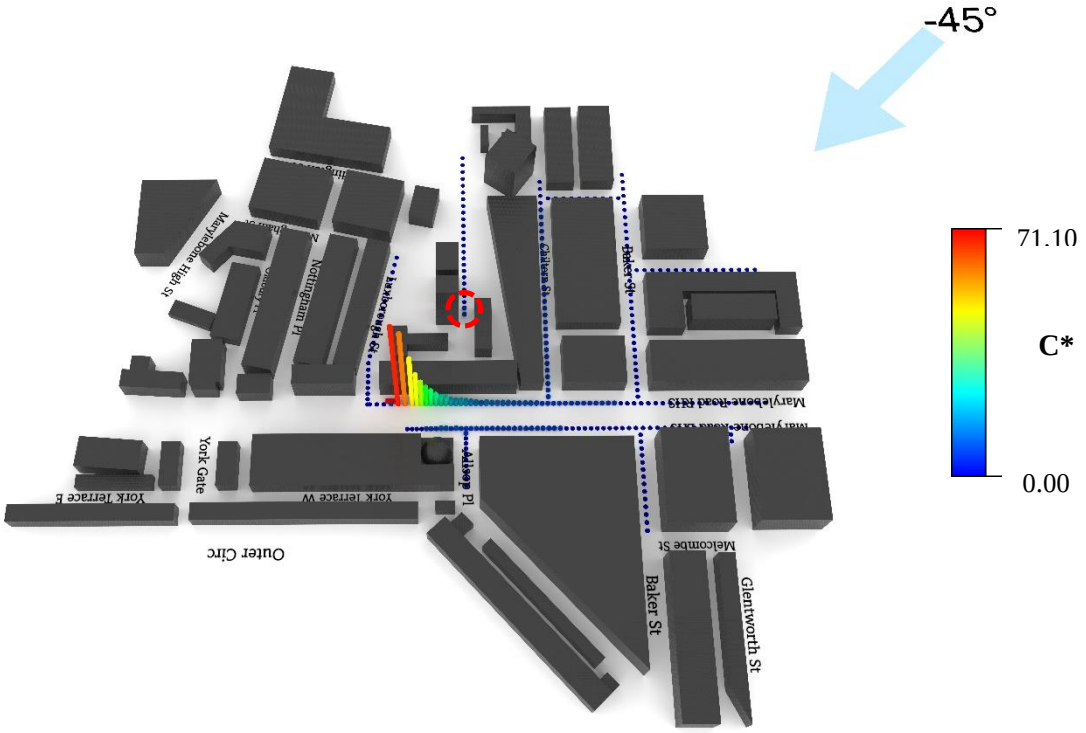

Figure 43: *3D Plot of non-dimensional concentration, C* at a wind direction of -45° with varied source release location and fixed FFID at (202.5, -74, 10) mm*

Interestingly, at a -45° wind direction, the majority of the high concentration area is localised to the RHS of Marylebone Road as can be seen in Figure 43 with limited interaction from the LHS area directly opposite the monitoring station. A sharp decrease in concentration can be seen along the RHS of Marylebone Road before almost completely declining completely past Baker St. Furthermore, there is little to no pollutant dispersion from any of the side streets affecting the station location and there is little to no mixing at any of the intersections. Though it may be difficult to see in the figure, the area circled in red provides quantifiable contribution to the receptor. This is probably due to helical vortices hitting the tall buildings beside it, before traversing over the downstream buildings and towards the receptor location.

5.3.1.3. -90° Wind Direction

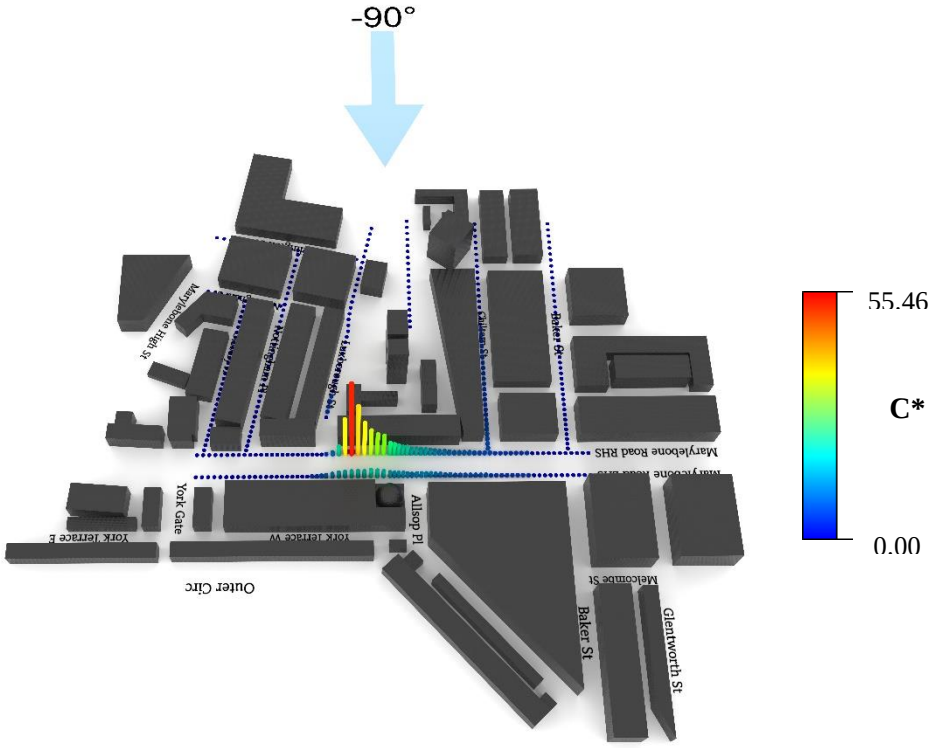

Figure 44: *3D Plot of non-dimensional concentration, C* at a wind direction of -90° with varied source release location and fixed FFID at (202.5, -74, 10) mm*

Figure 44 displays the concentration contribution across measured points from a -90° wind direction. The air converges towards the receptor location from the buildings behind it. Apart from the peaks, both sides of the road follow the same profile, and the LHS has considerable impact on the monitoring station location compared to the RHS, more so than any other wind direction considered in this study. In terms of side roads, Chiltern St has the highest impact and the closest points along Luxborough St provides a quantifiable amount of contribution while the other roads provide little to no contribution. Although, looking at the results, it is possible that the intersection between Marylebone Road and Allsop Pl and also the road itself could have had a substantial contribution had its impact been measured.

5.3.1.4. +45° Wind Direction

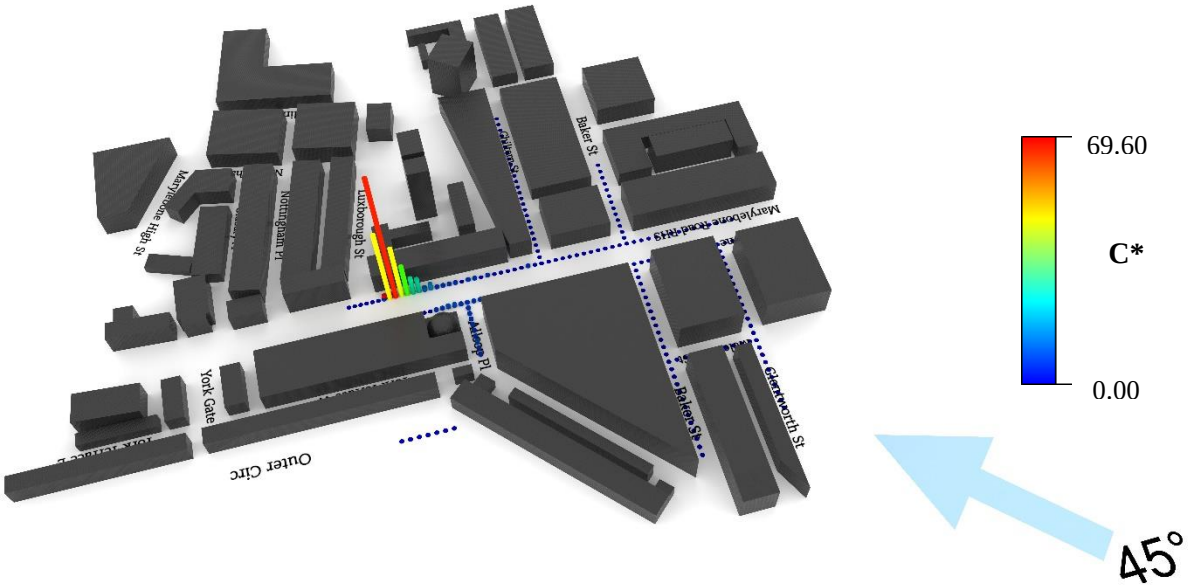

Figure 45: *3D Plot of non-dimensional concentration, C* at a wind direction of 45° with varied source release location and fixed FFID at (202.5, -74, 10) mm*

Figure 45 shows the concentration contribution at a +45° wind direction. This wind direction has a much tighter cluster of high concentration measurements near the receptor location. There are quantifiable results located sporadically along the RHS of Marylebone Road but limited contribution from the LHS. It should be noted that source gas emission along Baker St and Glentworth St do not have a significant impact at the receptor location even though the air should flow along these streets and into Marylebone Road. This is most likely due to the wind speed being too low for the flow to overcome the height of the adjacent buildings and traverse its way towards the receptor. However, Allsop Pl does have a noticeable contribution which is most likely due to the geometry of the building alongside it that channels the flow along its path.

5.3.1.5. Combined Data

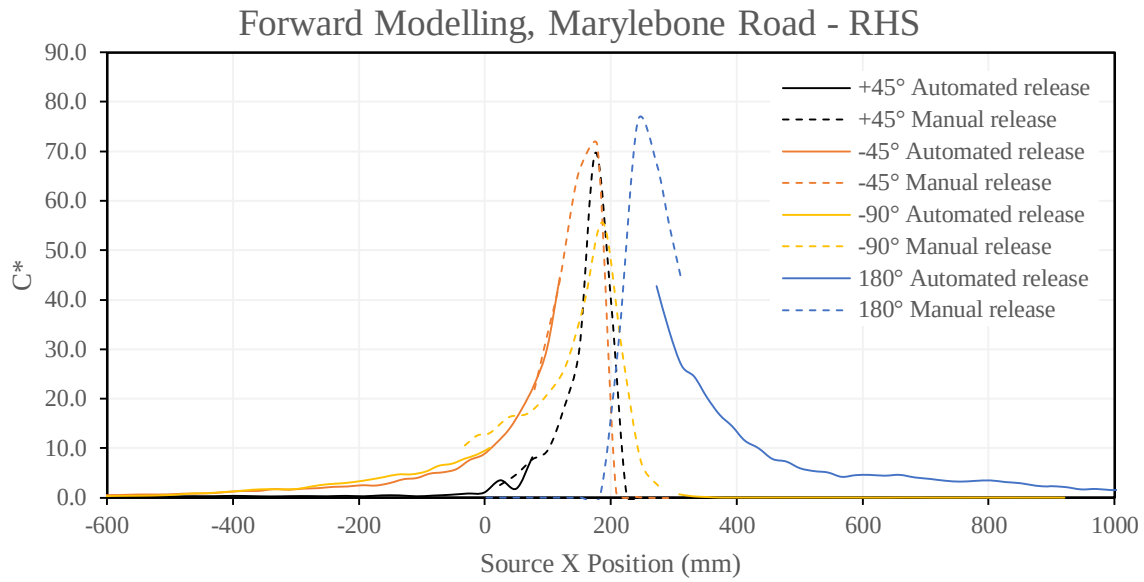

Figure 46: *Dimensionless concentration, C* plotted against source emission X position along Marylebone Road RHS – comparing forward modelling scenarios from four wind directions with both automated and manual source releases.*

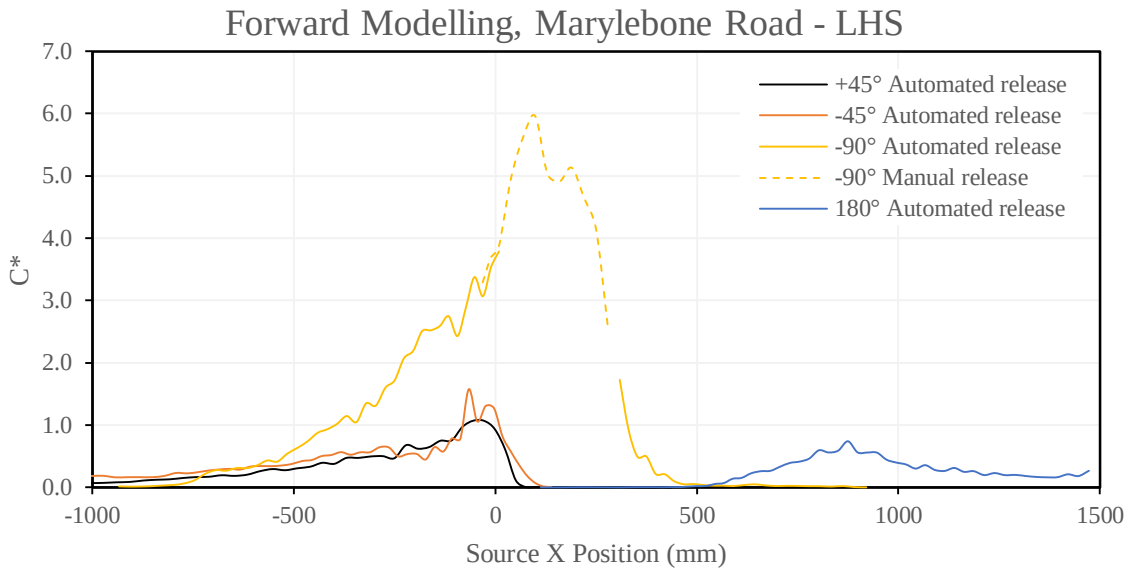

Figure 47: *Dimensionless concentration, C* plotted against source emission X position along Marylebone Road LHS – comparing forward modelling scenarios from four wind directions with both automated and manual source releases.*

Sensitivity of the locations being measured manually was investigated by repeating three points that were previously recorded using the automated traverse and comparing the results. Figure 46 and Figure 47 plots dimensionless concentration for the RHS and LHS of Marylebone Road respectively including comparative curves of automated and manual releases. The plots show results from the main road as it is one of the most polluted roads in London as stated in the introduction with the variability of these results ranging between 2% and 8%. However, with the 180° case, a difference of up to 64% was recorded.

From these figures, it can be seen that the peak concentrations are located within a confined region for all wind directions, especially when the source was released along the RHS of Marylebone Road – where the monitoring station is situated with the notable exception being the 180° case where a delta exists along x. On the whole, the delta could be due to positional errors and/or due to interference caused by the manual release mechanism shown in Figure 31. Additionally, the change in geometry caused by the removal of the traverse overhead of the release position could have also altered the flow fields. Furthermore, as expected, the results show that at 180° there is little interaction between the two lanes as the flow is simply passing through the road without any obstructions and also for this reason, it has the highest concentration contribution.

5.3.2. INVERSE MODELLING

This section presents and discusses the results from experiments conducted as described in 4.2.2. This set of experiments had the source located at the centre of the monitoring station and the receptor moving along the different streets – contrary to the forward modelling scenario.

5.3.2.1. 0° Wind Direction (Inverse of 180°)

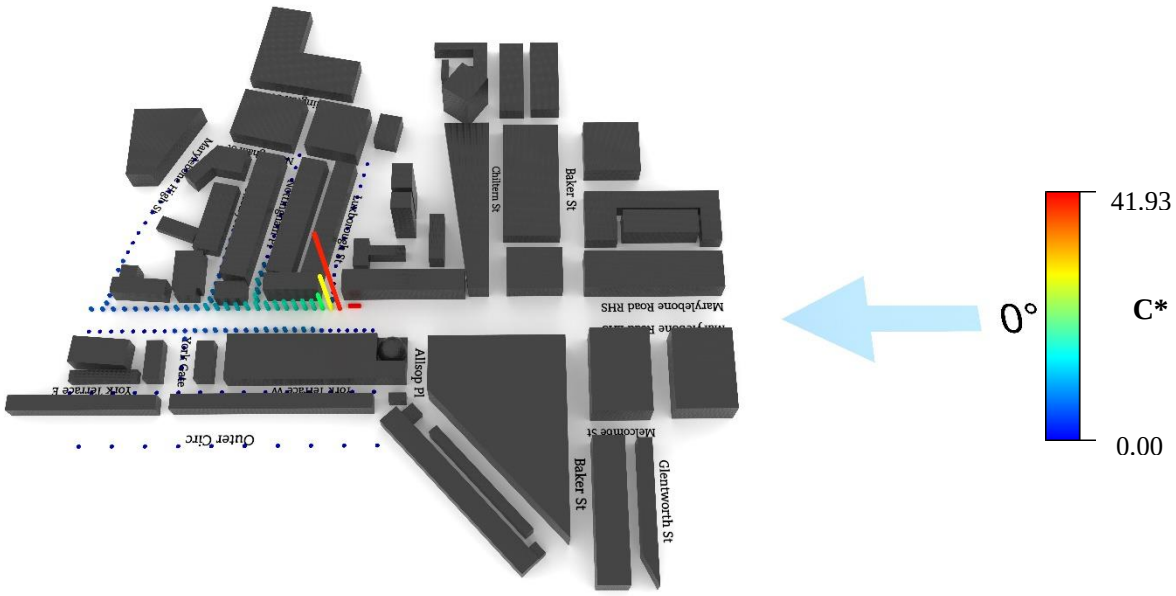

Figure 48: *3D Plot of non-dimensional concentration, C* at a wind direction of 0° with varied FFID location and fixed source release at (202.5, -74, 10) mm*

Figure 48 shows the concentration contribution at an angle of 0° - the inverse case of 180°. There is little to no contribution from any of the side roads located along the positive y axis and the majority of the impact is due to the side roads located in the negative y axis (refer to Figure 28 for coordinate system). This is because most of the buildings located along the negative x axis are organised along the x and y axes without any orientation which allows the flow to be simply channelled along the main road without diversion. This could not be verified by taking measurements across roads located in the negative x axis due to traverse limitations outlined in section 3.1.

Compared to the forward modelling case shown in Figure 42, the intensity along Luxborough St is much lower and the peak concentration is 45%, but the rest of the streets show good agreement in both cases, although, comparing the two experiments, the results clearly do not show any linearity as expected, but do show similar trends along each street apart from the aforementioned Luxborough St. With the measurement locations considered in this experiment and plotted in Figure D1 and Figure D2, the RHS of Marylebone Road follows a similar profile in both forward and inverse cases, whereas, the LHS has a peak located 400 mm further along the negative x direction than the forward case.

5.3.2.2. 135° Wind Direction (Inverse of -45°)

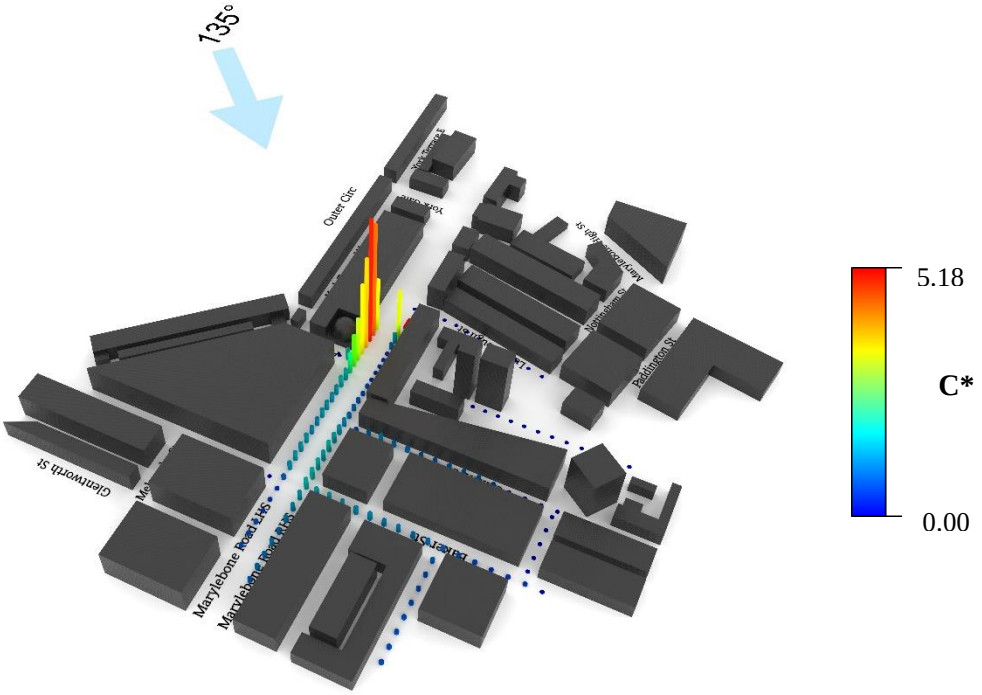

Figure 49: *3D Plot of non-dimensional concentration, C* at a wind direction of 135° with varied FFID location and fixed source release at (202.5, -74, 10) mm*

A plot of concentration at a wind direction of 135° is shown in Figure 49. Along the RHS of Marylebone Road, the concentration levels show bimodal behaviour due to the development of helical vortices across the street. While along the LHS, the concentration contribution increases gradually with these vortices having little effect to the mean due to the high concentration levels. In this case, the high concentration region is found along the LHS than the RHS as opposed to the forward case due to the opposite direction of oncoming flow. The peak concentration is roughly 7% that of the forward -45° case shown in Figure 43. This is due to the length of the buildings adjacent to the Outer Circ that are obstructing the flow from circulating along Marylebone Road and proceeding further downstream.

There exists no common trend between this wind direction and the forward -45° case shown in Figure 43. This is due to the significant difference in the geometry of the leading buildings the oncoming flow collides with in both cases as well as the far narrower and limiting layout of the

leading roads. Furthermore, unlike the forward case, the pollutant is dispersed over a larger region and provides quantifiable readings at the most downstream of measurement locations.

Contrary to the 180° case and its inverse found in sections 5.3.1.1 and 5.3.2.1, the peak along the RHS for this case is so minor compared to the forward case, as shown in Figure D3, that its profile cannot be distinguished without further experimentation at a higher resolution. Meanwhile the LHS follows a similar profile in both forward and inverse cases, but with a marked increase in the peak concentration, as shown in Figure D4.

5.3.2.3. 90° Wind Direction (Inverse of -90°)

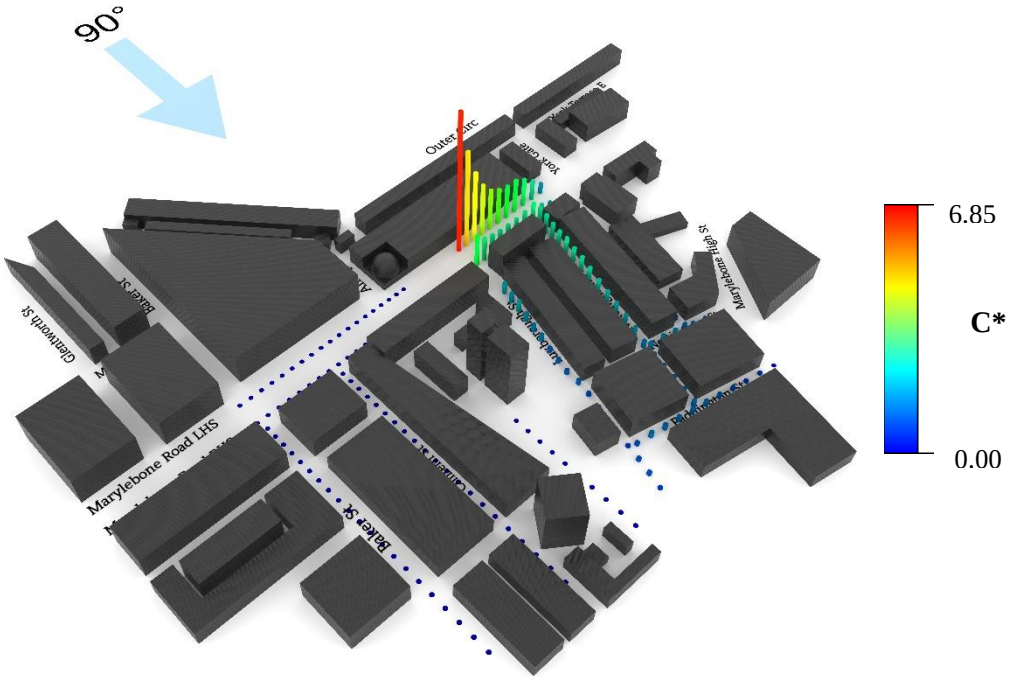

Figure 50: *3D Plot of non-dimensional concentration, C* at a wind direction of 90° with varied FFID location and fixed source release at (202.5, -74, 10) mm*

The concentration contribution from a wind direction of 90° is shown in Figure 50 and its counterpart, the forward modelling case at -90°, in Figure 44. The peak contribution in this case is 12% that of the forward case. In both cases, both sides of Marylebone Road have quantifiable measurements. It should be noted that with the inverse scenario, the decrease in pollutant contribution is gradual along the side roads (e.g. Luxborough St and Nottingham Pl), whereas, with the forward scenario, there is a sharp drop in concentration along Marylebone Road with no significant impact from any of the side roads.

In a similar manner to the 135° inverse case, the concentration impact along Marylebone Road RHS is extremely low compared to the forward case plotted in Figure D5 and there is no similarity between the forward and inverse cases at this wind direction in this lane. However, the peak contribution is within 15% of each other along the LHS and they follow a similar profile as shown in Figure D6. However, the increase is more gradual with the forward case than the inverse and with the inverse, there is a bias of roughly 230 mm towards the positive X direction.

5.3.2.4. -135° Wind Direction (Inverse of +45°)

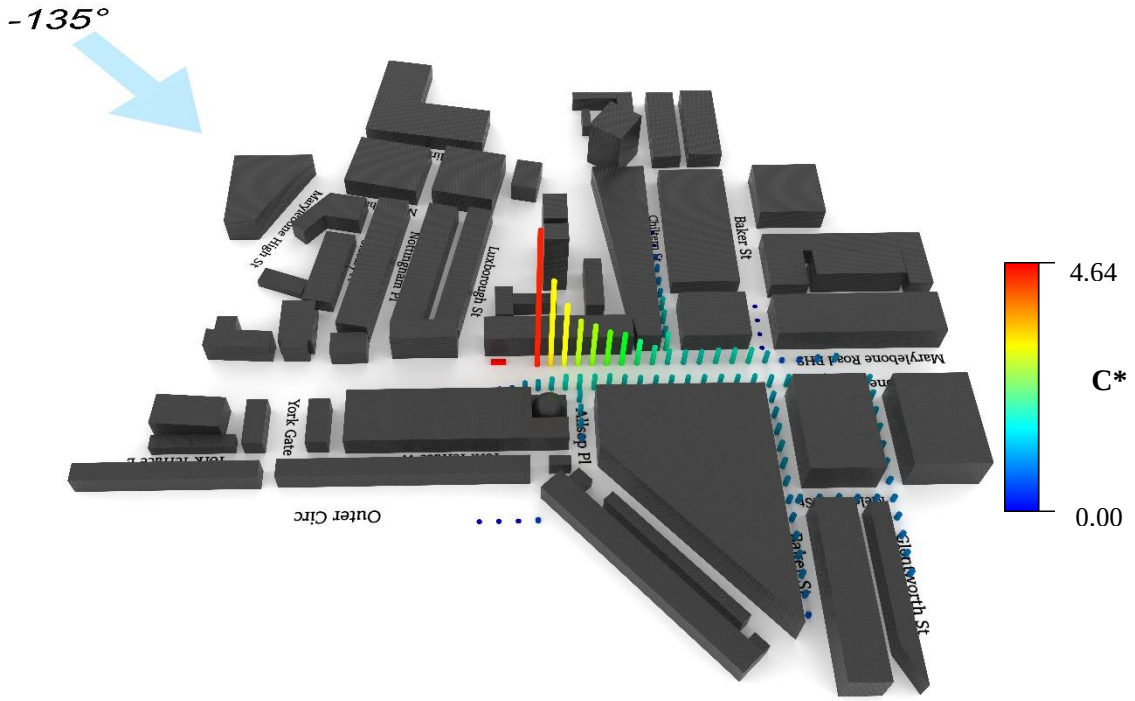

Figure 51: *3D Plot of non-dimensional concentration, C* at a wind direction of -135° with varied FFID location and fixed source release at (202.5, -74, 10) mm*

Figure 51 shows a plot of concentration contribution from a wind direction of -135°, its counterpart, the 45° forward case, is shown in Figure 45. Unlike the forward case, where the highest concentration is located as a cluster with little contribution from any of the side roads, with the inverse, there is a substantial contribution to all of the side roads apart from Allsop Pl and the south side of Baker St. The contribution to Glentworth St and Baker St is almost constant across its length, whereas, Chiltern St and Allsop Pl sees a steadier drop in contribution with increasing distance from Marylebone Road.

The peak contribution is only 7% that of the forward case which is the lowest out of all the inverse scenarios studied. Also, not enough measurements have been taken across the Marylebone Road RHS to determine profile similarity between the forward and inverse scenarios. However, the measurements that were taken do suggest that there is some level of similarity at least from X=-1100 through to X=0, as shown in Figure D7. Additionally, unlike the inverse cases discussed so far, the forward case of 45° has a larger peak contribution across the LHS than its inverse of -135°, as plotted in Figure D8.

5.3.2.5. Combined Data

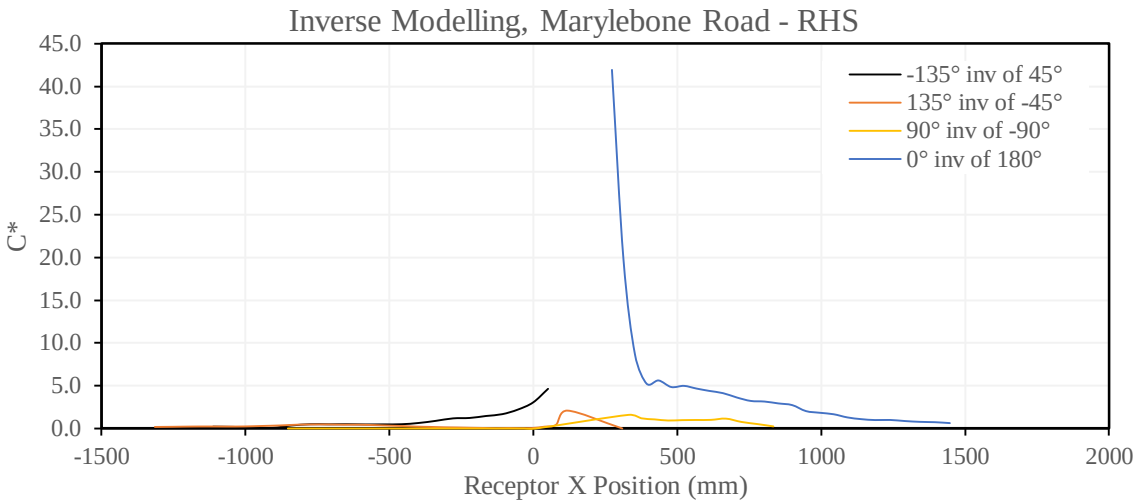

Figure 52: *Dimensionless concentration, C* plotted against receptor X position along Marylebone Road RHS - comparing inverse modelling from four wind directions with automated source releases.*

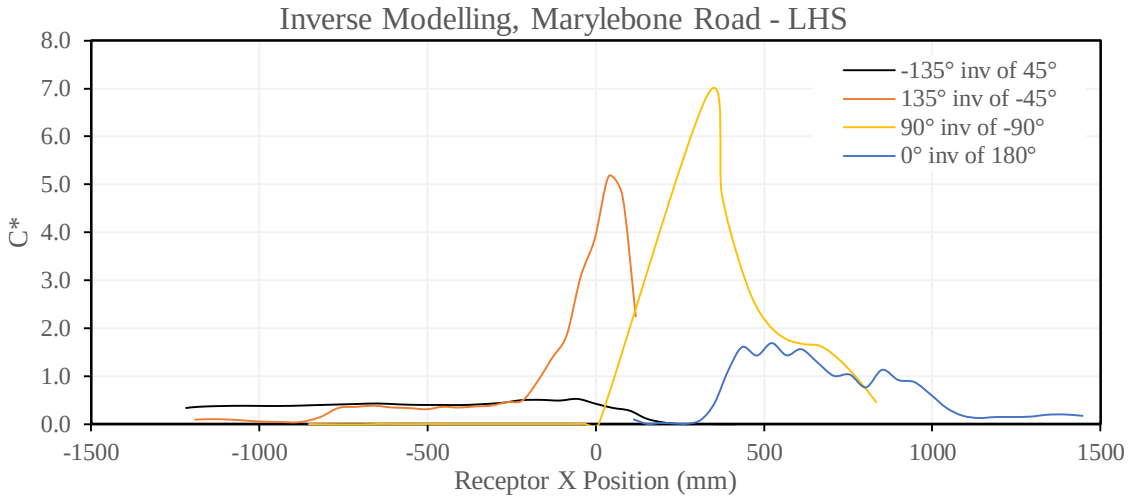

Figure 53: *Dimensionless concentration, C* plotted against receptor X position along Marylebone Road LHS - comparing inverse modelling from four wind directions with automated source releases.*

Figure 52 and Figure 53 plot non-dimensional concentration against the receptor X position along the main road for the RHS and LHS respectively. With the RHS, due to the lack of obstruction, 0° sees the highest concentrations and due to traverse limitations, measurements could not be taken until a clear peak was established with both 0° and -135° cases. The contribution from 135° and 90° inverse cases is very low due to the geometry of the obstructions. With the LHS, 135° and 0° sees very little contribution due to little mixing along Marylebone Road which does not allow the pollutant to pass from one lane to the next where the FFID is located. The peak is biased to a slightly positive X position due to turbulence created by the side roads causing a reversing flow towards the FFID. -135° and 90° sees higher levels of contribution as the flow recirculates within this region which increases the pollutant contribution to the FFID.

5.3.3. FURTHER ANALYSIS

5.3.3.1. Majority Concentration Contribution Map

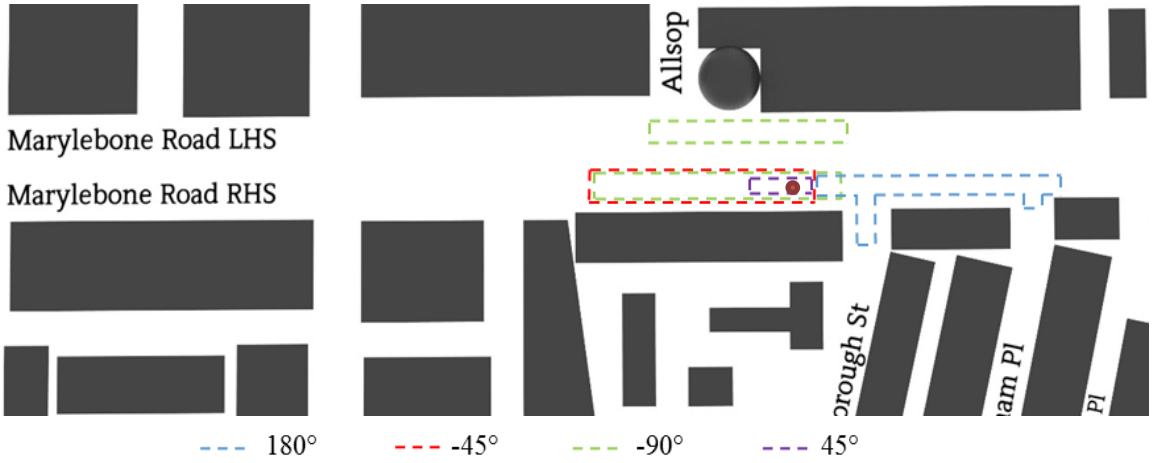

Figure 54: *Truncated plan view showing region responsible for 80% of concentration releases from forward modelling for four wind directions, (red dot signifies FFID location)*

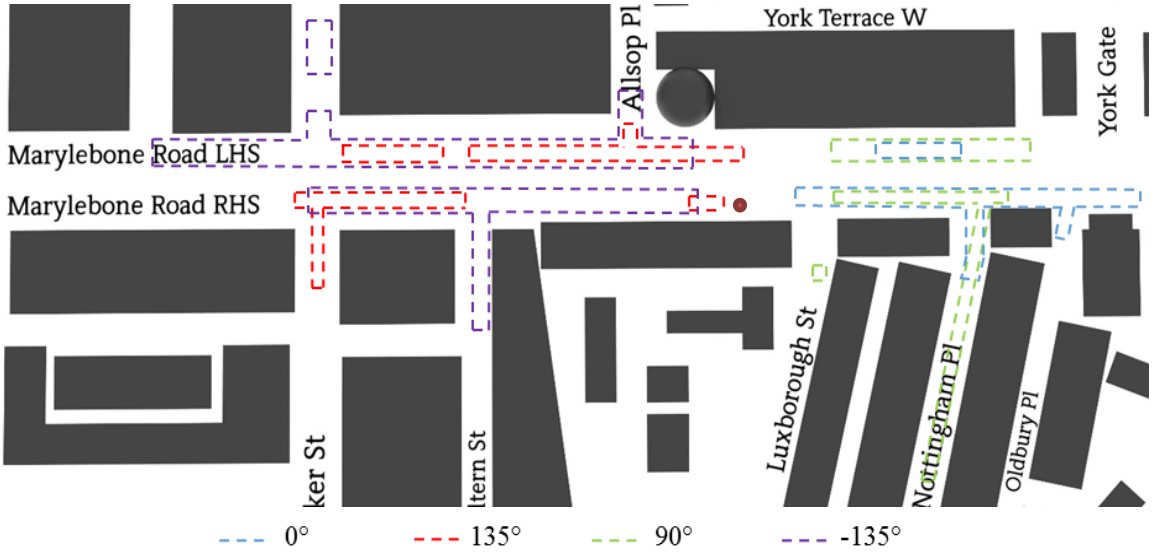

Figure 55: *Truncated plan view showing region responsible for 80% of concentration releases from inverse modelling for four wind directions, (red dot signifies FFID location)*

Figure 54 and Figure 55 show truncated plan views of the Marylebone site along with a colour-coded overlay for four wind directions presenting the region responsible for the majority of the concentration contribution to and from the receptor location under forward and inverse modelling scenarios respectively. With the forward case, there is a clear overlap between all wind directions very close to the measurement location. Whereas, with the inverse case, the contribution is spread out over a larger area, including intersections at side roads and in this case, there is no clear overlap between wind directions. The spreading of the results is partially due to the halving of the measurement points for the inverse than the forward case. From these results, no clear trend can be seen linking the forward and inverse scenarios due to the lack of symmetry in building geometry

and road layout along each axis. If this was the case, then there would be a sense of linearity between the results from both cases.

Refer to Appendix B for 3D concentration plots showing these truncated regions in greater detail for each wind direction along with the measurement scale in the same manner as those shown in sections 5.3.1 and 5.3.2.

5.3.3.2. Concentration Fields

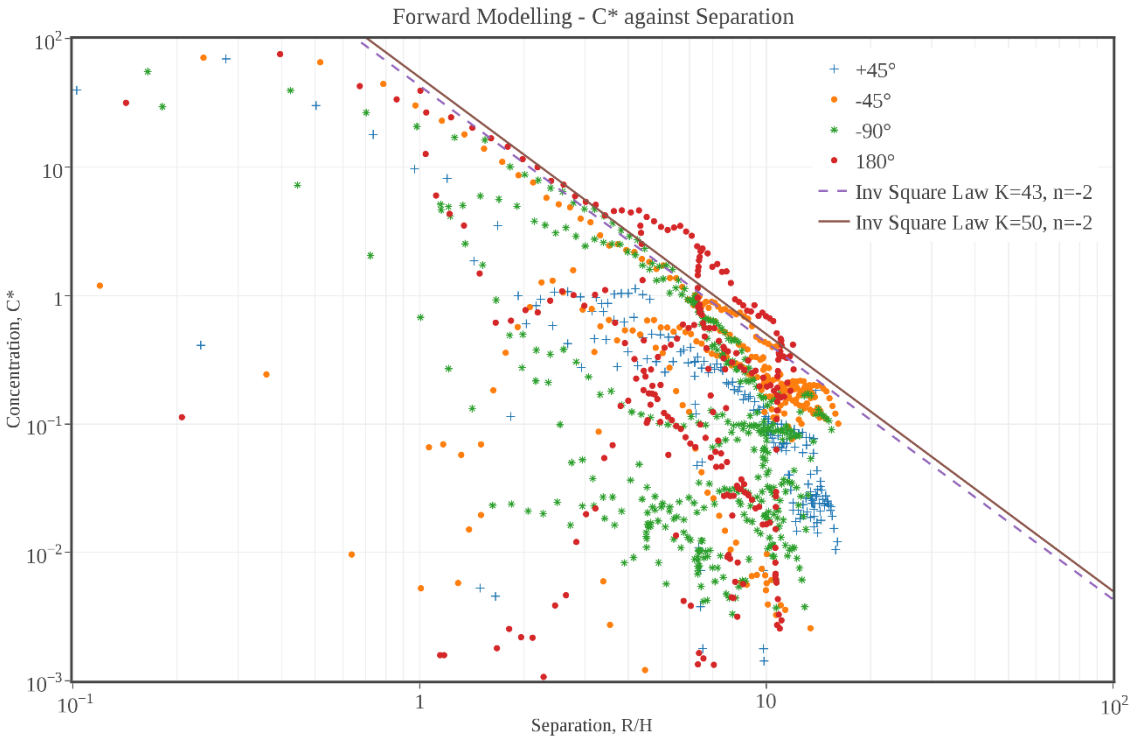

Figure 56: *Variation of non-dimensional concentration, C* from forward modelling scenario plotted against source-receptor separation, R/H for four wind directions compared to the inverse-square law with constants K=43, n=-2 and K=50, n=-2 in Equation (4).*

Figure 56 shows a plot of all the concentration measurements gathered in this study against the straight line separation distance between the tracer gas emission and the FFID. There is a recognisable upper bound for the majority of the data which is consistent the inverse square law shown in Equation (3), with constants K = 50 and n = -2. The results obtained by (Robins et al., 2010) plotted in Figure 18 also showed a recognisable upper bound with K = 12 and n = -2. Using a ratio of 0.28 for the roof level velocity to tower velocity translates to a predicted K value of ~43 as this study uses the reference wind speed rather than the roof level speed to calculate C* which the tower velocity represents. The results from this study are thus consistent to a certain degree to previous results.

The plot shows that at the smaller separation distance, concentration values are much lower than the expected trend due to the limited mixing of the pollutant with the flow. Concentration increases with larger distances when the pollutant mixes in uniformly with the flow before dropping off again when the mixed flow is greatly dispersed. Certain results from the 180° clearly shows an exception

which is most likely due to the lack of obstruction to generate turbulence and uniformly mix the pollutant with the flow. The work conducted by (Robins et al., 2010) studied larger distances where the inverse square law was in full effect and the flow was well mixed which may account for the slight discrepancy in the trend. While this study investigates a near field region with much closer source/receptor distances where the flow is not well mixed.

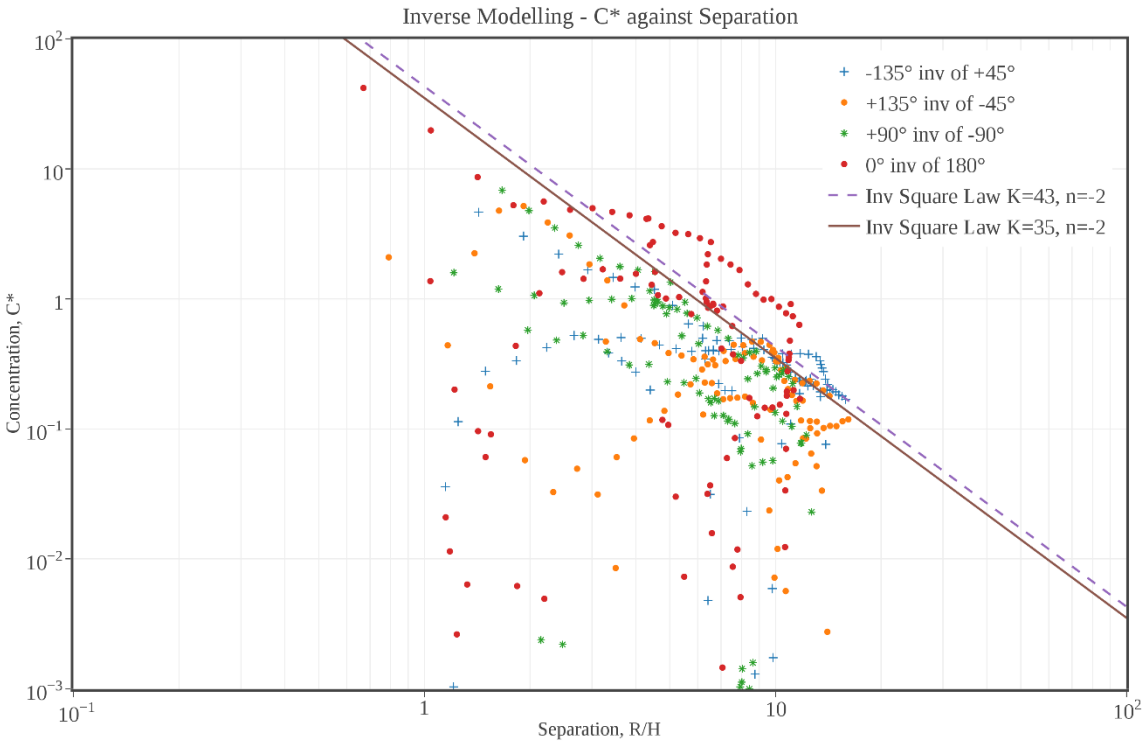

Figure 57: *Variation of non-dimensional concentration, C* from inverse modelling scenario plotted against source-receptor separation, R/H for four wind directions compared to the inverse-square law with constants K=43, n=-2 and K=35, n=-2 in Equation (4).*

In a similar manner, a plot of the results from the inverse modelling scenario is shown in Figure 57. These results also show a clear upper bound to the majority of the data, but with constants K = 35 and n = -2 instead in Equation (3) which is still near the expected trend. There are again certain exceptions to the general trend in this case. Certain results from -135° have higher concentrations at larger distances and once more, the inverse of the 180° case - 0°, falls outside the projected range.

Interestingly, in both the forward and inverse modelling scenarios the 180° case and its inverse behaves in a similar manner, once again, this is most probably due to the relatively wide spacing along Marylebone Road which allows flow to pass through with a distinct lack of obstructions.

5.3.3.3. Fluctuation Fields

The fluctuation in concentrations is important as the concentration an individual can experience can be a lot larger or smaller than the mean values. For example, an asthmatic individual exposed to a pollutant may react to a release with mean concentration values that have been deemed safe but the fluctuation varies widely between safe and unsafe limits. This factor cannot be seen by analysing only the mean values.

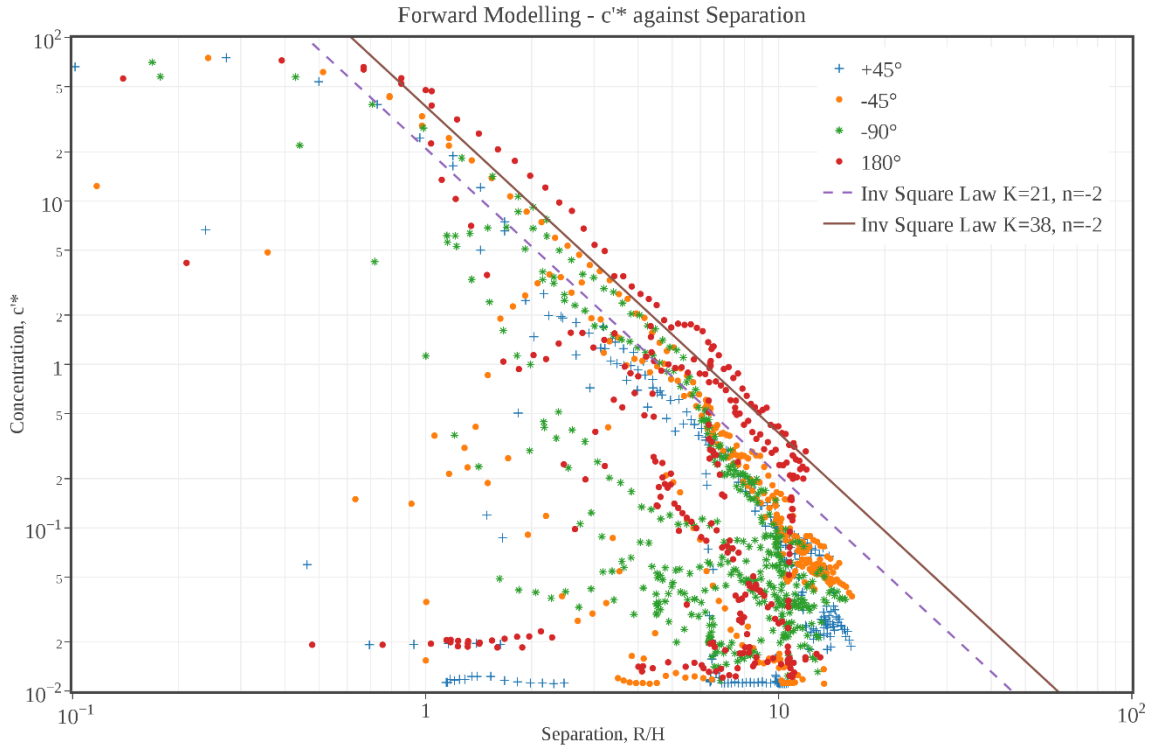

Figure 58: *Variation of non-dimensional standard deviation of concentration fluctuations, c'* from forward modelling scenario plotted against source-receptor separation, R/H for four wind directions compared to the inverse-square law with constants K=21, n=-2 and K=38, n=-2 in Equation (4).*

As with the dimensionless concentrations, the standard deviation of concentration fluctuations, c'* were made dimensionless using Equation (4). Similarly to the concentration plot in Figure 57, there is a clear upper bound to the results with a value of K = 38 and n = -2 in Equation (3). The results obtained by Robins et al. (2010), shown in Figure 18, translates to a K value of ~21 and n of -2 using the ratio of roof level to BT tower height wind speed of 0.28. In this case, there is less similarity between the predicted and projected results which is probably caused by the difference in set ups, such as the addition of aerodynamic curves to the traverse to minimise its impact on the results and the change in origin leading to an increase in buildings modelled in the tunnel.

Nevertheless, the 180° forward case is still deviant from the other results. Once again, this is most likely due to the flow not interacting with the buildings, mixing the pollutants a great deal, and just flowing in a straight line. In this case, like the concentration graph in Figure 56, the fluctuations are much lower than the expected trend at closer distances before joining the projected line and dropping down at greater distances.

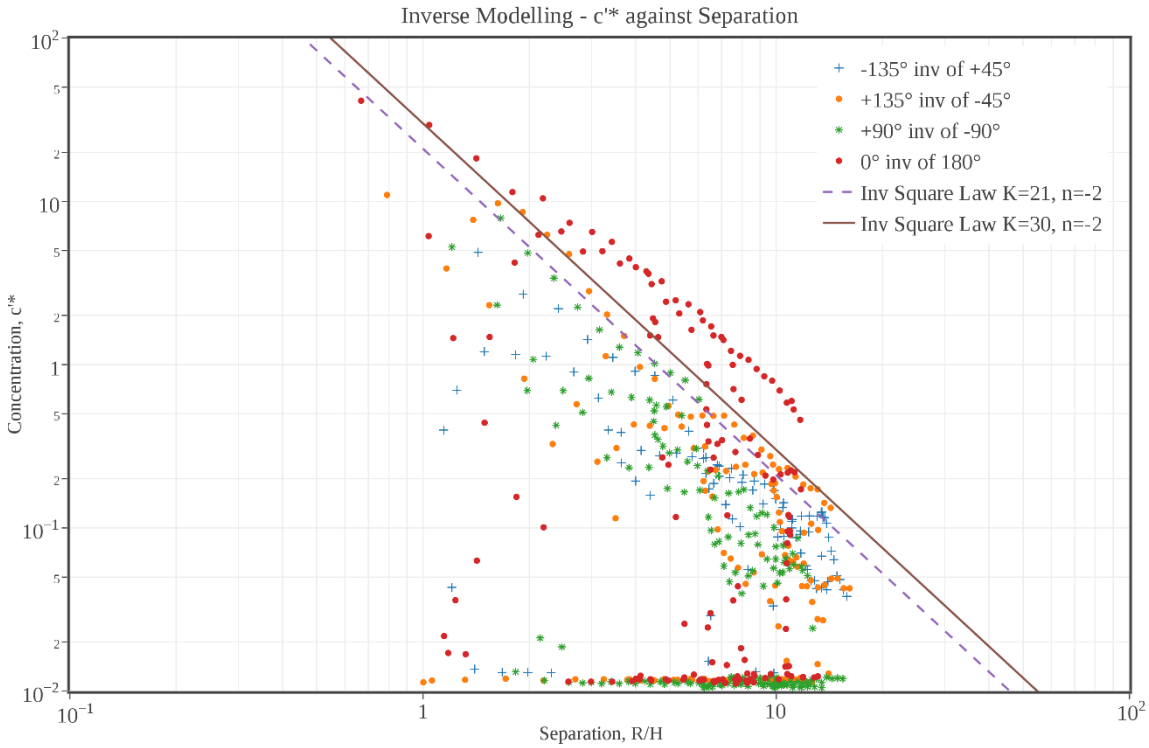

Figure 59: *Variation of non-dimensional standard deviation of concentration fluctuations, c'* from forward modelling scenario plotted against source-receptor separation, R/H for four wind directions compared to the inverse-square law with constants K=21, n=-2 and K=38, n=-2 in Equation (4).*

Figure 59 plots the standard deviation of concentration fluctuations, c'* for the inverse case. These results once again show an upper bound for all wind directions except for the 0° case which strays from the trend most probably due to the high intensity of pollutants the FFID is exposed to by a direct flow with little obstacles to dissipate its strength. The constants K = 30 and n = -2 in Equation (3) covers the majority of the results and is close to the predicted result of K = 21 from previous experiments. There is a clear cluster of concentration results located towards the bottom for both the forward and inverse cases caused by extreme amounts of flow dispersion and there remains little pollutant to be detected.

Comparing figures from Appendix B and Appendix C for the same wind directions, large variations in fluctuations can be seen in regions that were identified as being responsible for the majority of the concentration contribution (in section 5.3.3.1) to and from the monitoring station for forward and inverse cases respectively. In general, large variations in fluctuations occur in regions with high concentrations, and areas in which the tracer gas has become well mixed with the flow exhibits little variation in fluctuation, as expected. The fluctuations for the forward cases are remarkably similar with c'* ranging from 70 to 75, whereas, fluctuations in the inverse cases show a greater range that follows their respective concentration values.

6. CONCLUSIONS AND FURTHER WORK

Existing methods of analysing pollutant dispersion behaviour include field experiments, CFD modelling and wind tunnel simulations. The latter two methods have been developed significantly over the past few decades due to the statistically unsteady nature of results obtained from field experiments and the impracticality of repeating results as environmental conditions can vary a great deal with time. With advancements in computational architecture and processing power, the use of CFD has surged ahead. However, the time spent on setting up models is still intensive and the time scales involved for completion of a modelling scenario is extremely high. Conversely, wind tunnel testing allows for rapid changes to flow conditions and adjustments to the model without any additional set up time. Additionally, results from wind tunnel testing are repeatable and statistically steady which allows for relatively straightforward analysis, enabling the detection of any underlying distributions.

The target of this study was to address two primary areas of interest. The first was to determine the impact the monitoring station can have on results and the second was to understand the relationship between pollutant releases and areas of interest, both of which will provide additional context to field experiments. For the achievement of these targets, two sets of experiments were conducted for each goal. The first set investigated the effect of the monitoring station and the second analysed the source-receptor relationships at the Marylebone Road site.

The use of a similar experimental set-up as well as methodology as previous DAPPLE work allowed for a relatively direct comparison of results. The data recorded throughout this study is of good quality as demonstrated in section 5.1 and can be added to existing datasets for validating computational models, although, as noted in the same section, two to three points in each wind direction reported mean concentrations that were up to 10% lower than the actual values due to signal clipping. This issue occurred even after the source strength was reduced to account for it, as the region in question was located extremely close to the receptor, which caused large amounts of trace gas to enter the FFID and affect the results.

6.1. Experiment Set 1

For the range of wind directions considered in this study, the ratio of average concentration across the top surface with and without the station were below 10%. Similarly, the ratio of concentration at the centre of the top surface with and without the station was also generally below 10% with only a limited number of results exceeding it. The outlier in this case was from -45° and 180° wind directions where the source was released along the LHS of Marylebone Road (y=48). However, considering the range in concentration for the 180° case being from 0.0 to 0.1, the impact is insignificant. Thus, the impact that needs to be taken into consideration for any future field studies conducted is when the wind is coming from an angle of -45°, which matches the theory introduced in section 2.1.2 of wind flow around buildings at an angle. The air flow directly collided with the sharp corners which accelerated the flow, creating a pressure difference which in turn formed eddies

of high strength at the leading edge. This led to a significant amount of mixing leading to a greater interaction between lanes than other wind directions.

Contrary to the top surface, the ratio of average concentration across the front surface with and without the station ranges had a significantly wider range, going up to 33%. The ratio of concentration at the centre of the front surface with and without the station also shows a similarly wide range, going up to 27%. The -90° and 180° showed only moderate to low amounts of impact with the presence of the station as the ratios were relatively low. However, the -45° case showed results that were consistently above 16% and peaked at 33%, suggesting a substantial level of impact to the flow, which again, was due to the higher level of mixing caused by the flow angle. This impact must be considered in any future field experiments.

In general, with the ratios consistently remaining below or around 10% across the top surface bodes well for field studies as this shows a low level of impact on the measurements, especially considering the fact that the physical monitoring station located along Marylebone Road conducts sampling measurements via devices located at the top of the station. Furthermore, all cases showed a marked increase in average and central concentration values when the tracer gas was released from the LHS and a decrease in both when released from the RHS. The front surface, on the other hand, showed a marked reduction in concentration with the station in place in the majority of the cases due to redirection of the polluted flow.

To summarise, the flow is less concentrated with the station in place when the source gas is emitted from the LHS of Marylebone Road in all cases considered. Furthermore, with the exception of the 180° wind direction, emissions from the RHS shows a larger region of high concentration with the station in place. Thus, the station has contrasting levels of impact depending on which side of Marylebone Road the emission originates. Likewise, from the concentration ranges shown in section 5.2 for each wind direction, it is clear that in general, the concentration contribution to the station from the left hand side of Marylebone Road is relatively low compared to the right which shows a low level of interaction between the two lanes.

6.2. Experiment Set 2

The second stage of experiments were divided into two subsets. The first took concentration measurements at the centre of the monitoring station while a tracer gas was released along traversable roads and in some cases, along park areas at wind directions of 180°, -45°, -90° and +45° (forward modelling). The second reversed the position of the receptor and the tracer gas, i.e. the pollutant was released from the centre of the station and the receptor traversed along the roads, taking concentration measurements at the reversed wind directions (inverse modelling).

Concentration measurements from the forward modelling showed a tight cluster of results near to the monitoring station location common to all wind directions with little concentration detected in any of the side streets, whereas, the inverse modelling showed a much greater spread of concentration for all wind directions with the appearance of bimodal behaviour along Marylebone Road at a wind direction of 135°. It should be noted that in the inversion modelling scenario, results from 0° had peak concentrations that were greater than all other inverse cases by up to a factor of

eight, which was probably due to the large spacing between the buildings that enabled the flow to pass directly through Marylebone Road with little mixing of the trace gas. It can be deduced from these results that the level of similarity between the forward and inverse modelling scenarios are negligible. This is due to the high level of asymmetry found in the model geometry, which resulted in the flow behaving in a completely different manner when oncoming flow arrives from the opposite direction as predicted in section 4.2.2.

Analysis conducted to find the points responsible for contributing up to 80% of the concentration showed an overlapping region between all wind directions which was within a very short distance from the receptor. This demonstrated that, as expected, areas surrounding the receptor, i.e. the monitoring station, had the highest concentrations in all wind directions. The fluctuation results in general also overlaps with this region due to high level of concentrations in the area. The fluctuations vary significantly in regions of high concentrations, where the presence of vortices (of varying strengths), generates an intermittent concentration of pollutants within the region and further downstream. Regions of low concentration were mainly found to be mostly situated at the side streets, excluding intersections, where sharp corners generated vortices and increased flow mixing. Low concentration regions such as these show a minimal change in fluctuations, where the tracer gas has not fully mixed in with the flow.

Previous DAPPLE work plotting dimensionless results against separation distance (introduced in section 2.4) showed that all recorded results fell below an upper bound, determined by an inverse square relationship with a fixed constant for concentration, C*, and another constant for standard deviation fluctuations, c'*. The results in this study show a similar trend, where, apart from certain results obtained at 180° and its inverse 0°, all results behaved in the predicted manner and stayed below the projected inverse square relationship line. However, it should be noted that the constant in front of the inverse square relationship varied slightly with the forward and inverse dimensionless concentration measurements and even more so with the fluctuations. This variation was caused by the several changes made to the original model site as described in section 3.5, such as the inclusion of buildings that are at an angle to the main road, unlike previous studies, which in turn changed the average building height, affecting the behaviour of the flow greatly. Additionally, the source-receptor distances considered in this study are much shorter than those conducted previously.

In conclusion, all results are highly sensitive to wind direction due to the difference in geometry the flow is exposed to, with the immediate vicinity of the monitoring station constantly showing high levels of concentration contribution, as is to be expected due to the proximity to the receptor. The impact of the monitoring station has been summarised in the section for the first set of experiments. Thus, both primary and secondary objectives listed in the introduction have been achieved through the completion of these two sets of experiments.

6.3. Recommendations

In addition to the first set of experiments conducted in this study, as well as previous DAPPLE work, future work should take concentration measurements across the omitted sides of the monitoring station with an increased resolution and at varying distances from the surface. This would enable a better understanding of the flow behaviour surrounding the station and provide a more holistic view of the impact it has on the measurements taken onsite. Furthermore, trace gas should be emitted in front of the station along both lanes to account for the bus lanes located directly in front of the station as well as the large number of coaches that are present in front of Madam Tussauds. Based on the results of the second set of experiments, such an experiment may yield significant concentrations at a wind direction of -90°.

Throughout the study, a constant source release rate and strength was assumed at each point. In real life, however, the pollutant concentration strength will vary with location. There are several factors to take into consideration, e.g. traffic flow rates will vary at different times of day, intersections and locations with traffic lights will accumulate a higher concentration of pollutants than any other areas due to emissions from stationary cars. Furthermore, the releases will be greatly condensed in this situation due to the high density of cars, i.e. the level of quality of the air will be at its poorest. Thus, further work could emit the tracer gas with greater strength and proximity at locations with traffic lights and conversely, lower strength at areas with low traffic density to simulate this situation.

An additional change in operating parameter could be the tunnel wind speed, as the entire study was completed at a constant reference wind speed of 2 m/s. Varying wind speeds of 3 m/s and 1 m/s, for example, would help develop a better understanding of the Marylebone Road site's response to change in wind conditions, other than simply the wind direction. In addition, the wind tunnel analysis completed in this study is limited to a two-dimensional understanding of the source-receptor relationship, as all measurements were taken at a height of 10 mm. Pollutant sources are not limited to traffic flows, exhausts from buildings, especially in industrial areas, can also add to the pollutant contribution. To account for this situation, this work could be developed further to include roof level releases and also analyse the source-receptor relationship at varying heights. Additionally, an LDA, as introduced in section 3.4, could be used to provide a better understanding of the flow field by measuring flow velocities at different regions.

One of the fundamental assumptions made in this study was that the boundary layer generated was neutral, which is rarely ever encountered in the environment. Thus, future work should conduct a similar set of experiments with stable and unstable boundary layers and perform a comparative analysis against the results provided in this report. Lastly, the wind tunnel model of the Marylebone Road site used in this study omits all trees present. Their impact on the results may be significant and thus, a separate sensitivity study could help elevate the quality of these results.

BIBLIOGRAPHY

Allen, D. and Durrenberger, C. (1995) *Gaussian Plume Modeling.* Available at: http://www.utexas.edu/research/ceer/che357/PDF/Lectures/gaussian_plume_modeling.pdf (Accessed: 20 April 2015).

Arnold, S.J., ApSimon, H., Barlow, J., Belcher, S., Bell, M., Boddy, J.W., Britter, R., Cheng, H., Clark, R., Colvile, R.N., Dimitroulopoulou, S., Dobre, A., Greally, B., Kaur, S., Knightes, A., Lawton, T., Makepeace, A., Martin, D., Neophytou, M., Neville, S., Nieuwenhuijsen, M., Nickless, G., Price, C., Robins, A., Shallcross, D., Simmonds, P., Smalley, R.J., Tate, J., Tomlin, A.S., Wang, H. and Walsh, P. (2004) 'Introduction to the DAPPLE Air Pollution Project', *Science of the Total Environment*, 332(1-3), pp. 139-153.

Bakker, A. (2006) *Lecture 10 - Turbulence Models.* Available at: http://www.bakker.org/dartmouth06/engs150/10-rans.pdf (Accessed: 21 April 2015).

Berkowicz, R. (2000) 'OSPM – A parameterised street pollution model', *Environmental Monitoring and Assessment*, 65(1-2), pp. 323-331.

Berrone, S., De Santi, F., Pieraccini, S. and Marro, M. (2012) 'Coupling traffic models on networks and urban dispersion models for simulating sustainable mobility strategies', *Computers & Mathematics with Applications*, 64(6), pp. 1975-1991.

Bonner, C.S., Ashley, M.C.B., Cui, X., Feng, L., Gong, X., Lawrence, J.S., Luong-van, D.M., Shang, Z., Storey, J.W.V., Wang, L., Yang, H., Yang, J., Zhou, X. and Zhu, Z. (2010) 'Thickness of the Atmospheric Boundary Layer Above Dome A, Antarctica, during 2009', *The Astronomical Society of the Pacific*, 122(895), pp. 1122-1131.

Bredberg, J. (2001) *On Two-equation Eddy-Viscosity Models.* Available at: http://www.tfd.chalmers.se/~lada/postscript_files/jonas_report_lowre.pdf (Accessed: 21 April 2015).

Britter, R.E. and Hanna, S.R. (2003) 'Flow and Dispersion in Urban Areas', *Annual Review of Fluid Mechanics*, 35, pp. 469-496.

Cambustion (2014) *Fast FID Principles.* Available at: http://www.cambustion.com/products/hfr500/fast-fid-principles (Accessed: 08 April 2015).

Carpentieri, M., Salizzoni, P., Robins, A. and Soulhac, L. (2012) 'Evaluation of a neighbourhood scale, street network dispersion model through comparison with wind tunnel data', *Environmental Modelling & Software*, 37, pp. 110-124.

Carruthers, D.J., Holroyd, R.J., Hunt, J.C.R., Weng, W.S., Robins, A.G., Apsley, D.D., Thompson, D.J. and Smith, F.B. (1994) 'UK-ADMS: A new approach to modelling dispersion in the earth's atmospheric boundary layer', *Journal of Wind Engineering and Industrial Aerodynamics*, 52(0), pp. 139–153.

Carruthers, D.J., Mckeown, A.M., Hall, D.J. and Porter, S. (1999) 'Validation of ADMS against wind tunnel data of dispersion from chemical warehouse fires', *Atmospheric Environment*, 33(12), pp.1937-1953.

Carruthers, D.J. and Hunt, J. (2008) *ADMS - Atmospheric Dispersion Modelling System.* Available at: http://www3.imperial.ac.uk/pls/portallive/docs/1/52391701.PDF (Accessed: 19 April 2015).

Casey, M. and Wintergerste, T. (2000) *European Research Community On Flow, Turbulence And Combustion Best Practice Guidelines*

CERC (2015) *Environmental software.* Available at: http://www.cerc.co.uk/environmental-software.html (Accessed: 19 April 2015).

Cheng, W.K., Summers, T. and Collings, N. (1998) 'The Fast-Response Flame Ionization Detector', *Progress in Energy and Combustion Science*, 24(2), pp. 89-124.

Counihan, J. (1971) 'Simulation of an adiabatic urban boundary layer in a wind tunnel', *Atmospheric Environment*, 7(7), pp. 673-689.

Crosby, C.J., Fullen, M.A., Booth, C.A., Searle, D.E. (2014) 'A dynamic approach to urban road deposited sediment pollution monitoring (Marylebone Road, London, UK)', *Journal of Applied Geophysics*, 105, pp. 10-20.

Dantec Dynamics (2013) *Measurement principles of LDA.* Available at: http://www.dantecdynamics.com/measurement-principles-of-lda (Accessed: 09 April 2015).

DEFRA (2011) *Brief history*. Available at: http://uk-air.defra.gov.uk/networks/brief-history (Accessed: 15 May 2015)

Di Sabatino, S., Kastner-Klein, P., Berkowicz, R., Britter, R.E. and Fedorovich, E. (2003) 'The Modelling of Turbulence from Traffic in Urban Dipsersion Models - Part I: Theoretial Considerations', *Environmental Fluid Mechanics*, 3(2), pp. 129-143.

Di Sabatino, S., Buccolieri, R., Pulvirenti, B. and Britter, R.E. (2008) 'Flow and Pollutant Dispersion in Street Canyons using FLUENT and ADMS-Urban', *Environmental Modeling & Assessment*, 13(3), pp. 369-381.

Eisenbud, M. and Gesell, T.F. (1997) *Environmental Radioactivity from Natural, Industrial and Military Sources: From Natural, Industrial and Military Sources.* 4th ed. Academic Press.

EnFlo (2015) *Meteorological Wind Tunnel.* Available at: http://www.surrey.ac.uk/mes/research/aef/enflo/facilities/meteorological/ (Accessed: 29 March 2015).

Exploring the Environment Project (2015) *Layers of Earth's Atmosphere.* Available at: http://ete.cet.edu/gcc/?/volcanoes_layers/ (Accessed: 22 April 2015).

Fedorovich, E. (2015) *Physical modelling of atmospheric boundary layer flows*. Available at: http://www.researchgate.net/publication/235436617_Physical_modeling_of_atmospheric_boundary_layer_flows_Part_I_Overview_of_modeling_concepts_and_techniques_Part_II_Modeling_neutrally_stratified_boundary_layer_flows (Accessed: 20 April 2015).

Fenger, J., Hertel, O. and Palmgren, F. (1998). *Urban Air Pollution - European Aspects*. Dordrecht: Springer Netherlands.

Foster, P.M. and Robins, A.G. (1985) *The Effects of Buildings on Low-Level Atmospheric Discharges (Nuclear science & technology)*. Luxembourg: Springer.

Franke, J., Hellsten, A., Schlünzen, H. and Carissimo, B. (2007). *Best practice guideline for the CFD simulation of flows in the urban environment*. Hamburg: Meteorological Inst.

Garratt, J.R. (1994) *The Atmospheric Boundary Layer*. 1st ed. Cambridge University Press.

Geernaert, G.L. (2003) 'Surface Layer', *Encyclopedia of Atmospheric Sciences*, 9, pp. 305-310.

Google Earth v7.1.2.2041 (2015) *Marylebone Road, London, 51°31'20.75" N, 0°09'19.96" W, elev 47 m, eye alt 1.03 km, The GeoInformation Group*, Available at: http://code.google.com/apis/earth/ (Accessed: 18 April 2015).

Hanna, S.R., Egan, B.A., Purdum, J. and Wagler, J. (2001) 'Evaluation of the ADMS, AERMOD and ISC3 models with the Optex, Duke Forest, Kincaid, Indianapolis and Lovett field data sets', *International Journal of Environment and* Pollution, 16, pp. 301–314.

Hosker, R.P. (1984) 'Flow and Diffusion Near Obstacles', *Atmospheric Science and Power Production*, pp. 241-326.

Hunt J.C.R. and Fernholz, H. (1975) 'Wind-tunnel simulation of the atmospheric boundary layer: a report on Euromech 50', *Journal of Fluid Mechanics*, 70(3), pp. 543-59.

Hunt J.C.R, Abell, C.J., Peterka, J.A. and Woo, H. (1978) 'Kinematical studies of the flows around free or surface mounted obstacle; applying topology to flow visualisation', *Journal of Fluid Mechanics*, 86(1), pp. 179-200.

Irwin, H.P.A.H. (1981) 'The Design of Spires for Wind Simulation', *Journal of Wind Engineering and Industrial Aerodynamics*, 7(3), pp. 361-366.

Kakosimos, K.E., Hertel, O., Ketzel, M. and Berkowicz, R. (2010) 'Operational Street Pollution Model (OSPM) – a review of performed application and validation studies, and future prospects', *Environmental Chemistry*, 7(6), pp. 485-503.

King's College London (2015) *LAQN Monitoring Sites*. Available at: http://www.londonair.org.uk/london/asp/publicdetails.asp?region=0&site=MY1&details=general&mapview=CO&la_id=20&network=AURN&MapType=Static (Accessed: 21 May 2015)

Mitchell, G., Namdeo, A., Lockyer, J., May, T. and Kay, D. (2002) *Technical Report of an EPSRC Link-Future Integrated Transport Project.* Available at: http://www.geog.leeds.ac.uk/projects/airquality/reports/reports.htm (Accessed: 20 April 2015).

Moreira, D. and Vilhena, M. (2009) *Air Pollution and Turbulence: Modeling and Applications.* 1st ed. CRC Press.

Namdeo, A.K. and Colls, J.J. (1996) 'Development and evaluation of SBLINE, a suite of models for the prediction of pollution concentrations from vehicles in urban areas', *Science of The Total Environment*, 189–190, pp. 311-320.

NASA (2010) *Atmospheric Structure.* Available at: http://disc.sci.gsfc.nasa.gov/ozone/additional/science-focus/about-ozone/atmospheric_structure.shtml (Accessed: 22 April 2015).

Oke, T.R. (1988) *Boundary Layer Climates.* 2nd ed. Routledge.

Plate, E.J. (1971) *Aerodynamic characteristics of atmospheric boundary layers.* Washington, D.C.: U.S. Atomic Energy Commission.

Riddle, A., Carruthers, D., Sharpe, A., McHugh, C. and Stocker, J. (2003) 'Comparisons between FLUENT and ADMS for atmospheric dispersion modelling', *Atmospheric Environment*, 38(7), pp. 1029-1038.

Robins, A., Castro, I., Hayden, P., Steggel, N., Contini, D. and Heist, D. (2001) 'A wind tunnel study of dense gas dispersion in a neutral boundary layer over a rough surface', *Atmospheric Environment*, 35(13), pp. 2243-2252.

Robins, A. (2003) 'Wind tunnel dispersion modelling some recent and not so recent achievements', *Journal of Wind Engineering and Industrial Aerodynamics*, 91(12-15), pp. 1777-1790.

Robins, A.G., Cheng, H. and Hayden, P. (2010) 'DAPPLE wind tunnel studies', *Final Report to Home Office*, University of Surrey.

Salem, N.B., Garbero, V., Salizzoni, P., Lamaison, G. and Soulhac, L. (2015) 'Modelling Pollutant Dispersion in a Street Network', *Boundary-Layer Meteorology*, 155(1), pp. 157-187.

Sargison, J.E., Walker, G.J., Bond, V. and Chevalier, G. (2004) *Experimental review of devices to artificially thicken wind tunnel boundary layers.* Available at: http://www.aeromech.usyd.edu.au/15afmc/proceedings/papers/AFMC00091.pdf (Accessed: 27 April 2015).

Shallcross, D.E., Petersson, K.F., White, I.R., Martin, D and Robins, A.G. (2010) 'The 2007 tracer dispersion experiments at the DAPPLE field site', *Final Report to Home Office*, University of Surrey.

Sodja, J. (2007) *Turbulence models in CFD.* Available at: http://mafija.fmf.uni-lj.si/seminar/files/2006_2007/Turbulence_models_in_CFD.pdf (Accessed: 21 April 2015).

Soulhac, L., Salizzoni, P., Cierco, F.-X. and Perkins, R. (2011) 'The model SIRANE for atmospheric urban pollutant dispersion; part I, presentation of the model', *Atmospheric Environment*, 45(39), pp. 7379-7395.

Soulhac, L., Salizzoni, P., Mejean, P., Didier, D. and Rios, I. (2012) 'The model SIRANE for atmospheric urban pollutant dispersion; PART II, validation of the model on a real case study', *Atmospheric Environment*, 49(0), pp. 320-337.

Stull, R.B. (1988) *An Introduction to Boundary Layer Meteorology.* 1st ed. Springer.

Tominaga, Y. and Stathopoulos, T. (2011) 'CFD modeling of pollution dispersion in a street canyon: Comparison between LES and RANS', *Journal of Wind Engineering and Industrial Aerodynamics*, 99(4), pp. 340-348.

Ubald, B.N. (2014) *DAPPLE - Dispersion of air pollutants and their penetration into the local environment*, Unpublished EPSRC summer project, University of Surrey.

University of Surrey (2015) *Research.* Available at: http://www.surrey.ac.uk/mes/research/aef/enflo/research/index.htm (Accessed: 19 May 2015).

Vardoulakis, S., Fisher, B.E.A., Pericleous, K. and Gonzalez-Flesca, N. (2003) 'Modelling air quality in street canyons: a review', *Atmospheric Environment*, 37(2), pp. 155-182.

World Health Organisation (2006) *WHO Air quality guidelines for particulate matter, ozone, nitrogen dioxide and sulphur dioxide. Summary of risk assessment*, Geneva: WHO Press.

Wood, C.R., Barlow, J.F., Belcher, S.E., Dobre, A., Arnold, S.J., Balogin, A.A., Lingard, J.J.N., Smalley, R.J., Tate, J.E., Tomline, A.S., Britter, R.E., Cheng, H., Martin, D., Petersson, F.K., Robins, A.G., Shallcross, D.E., Smalley, R.J., Tate, J.E., Tomlin, A.S. and White, I.R. (2009) 'Dispersion Experiments in Central London: The 2007 DAPPLE Project', *American Meteorology Society*, 90, pp. 955-969

Xie, Z.-T. and Castro, I.P. (2009) 'Large-eddy simulation for flow and dispersion in urban streets', *Atmospheric Environment*, 43(13), pp. 2174-2185.

Xie, Z.-T. (2011) 'Modelling Street-Scale Flow and Dispersion in Realistic Winds - Towards Coupling with Mesoscale Meteorological Models', *Boundary-Layer Meteorology* , 141(1), pp. 53-75.

Xie, Z.-T., Hayden, P. and Wood, C.R. (2013) 'Large-eddy simulation of approaching-flow stratification on dispersion over arrays of buildings', *Atmospheric Environment*, 71, pp. 64-74.

Yuan, C., Ng, E. and Norford, L.K. (2014) 'Improving air quality in high-density cities by understanding the relationship between air pollutant dispersion and urban morphologies', *Building and Environment*, 71(0), pp. 245-258.

Zhang, A., Gao, C. and Zhang, L. (2005) 'Numerical simulation of the wind field around different building arrangements', *Journal of Wind Engineering and Industrial Aerodynamics*, 93(12), pp. 891-904.

Zhang, Z. (2010) *LDA Application Methods: Laser Doppler Anemometry for Fluid Dynamics*. 1st ed. Berlin: Springer.

APPENDICES

Appendix A: MEASUREMENT POINTS

This section of the appendix shows a plan view of the AURN site with the blue circles representing the source gas release locations for forward modelling at -45° (Figure A), -90° (Figure A) and +45° (Figure A) wind directions. The red cross shows the location of the FFID.

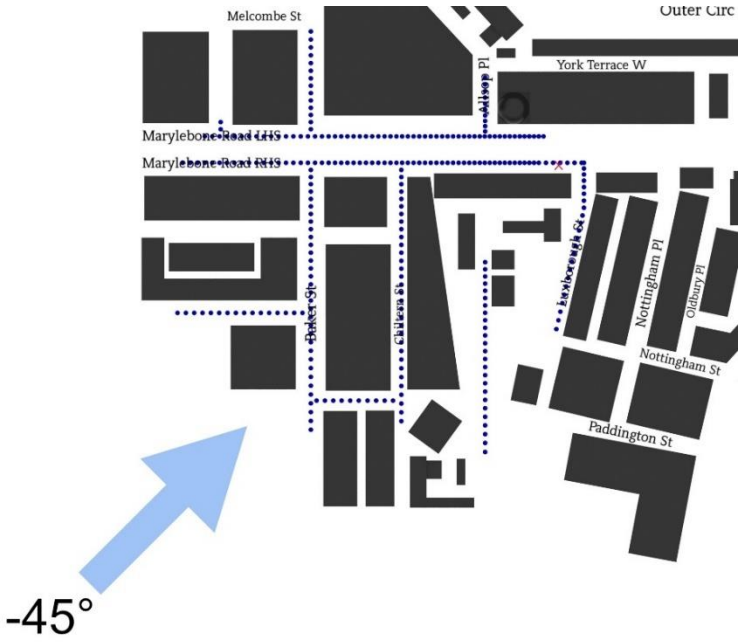

Figure A1: *Measurement locations for -45° forward modelling case*

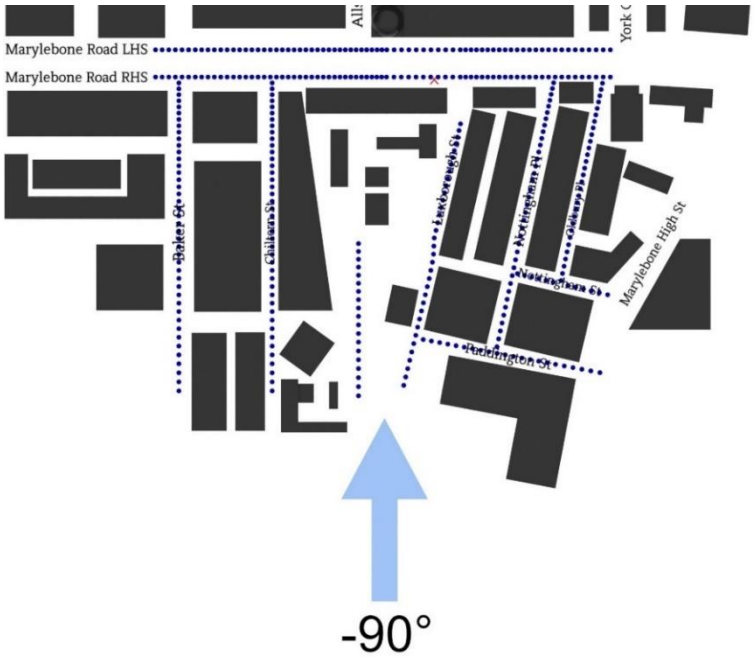

Figure A2: *Measurement locations for -90° forward modelling case*

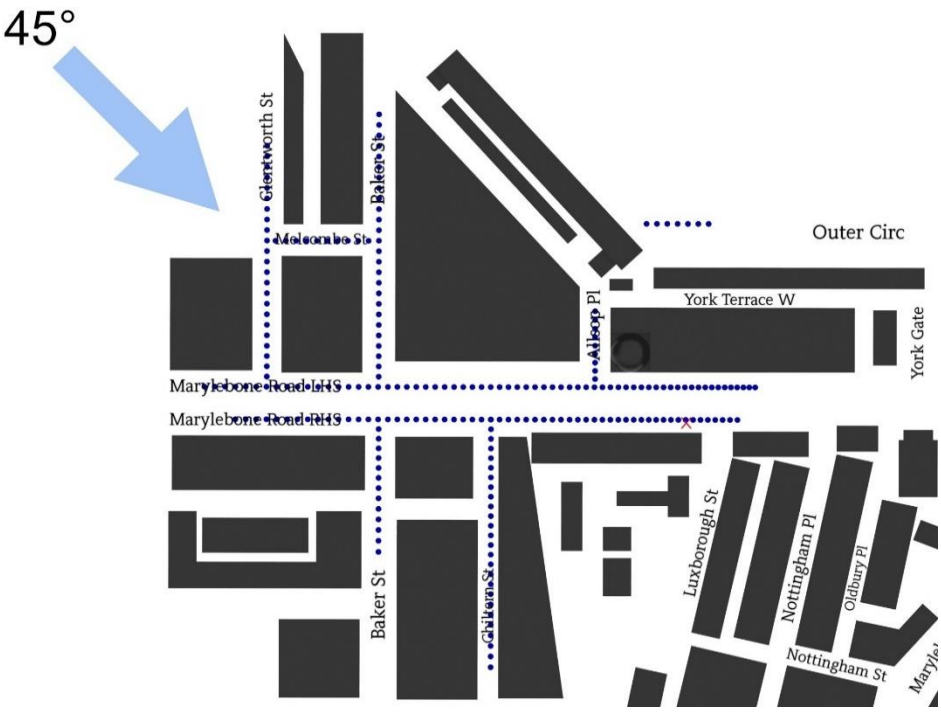

Figure A3: *Measurement locations for 45° forward modelling case*

The figures from here to the next appendix section shows the measurement points for inverse modelling as described in Section 4.2.2.

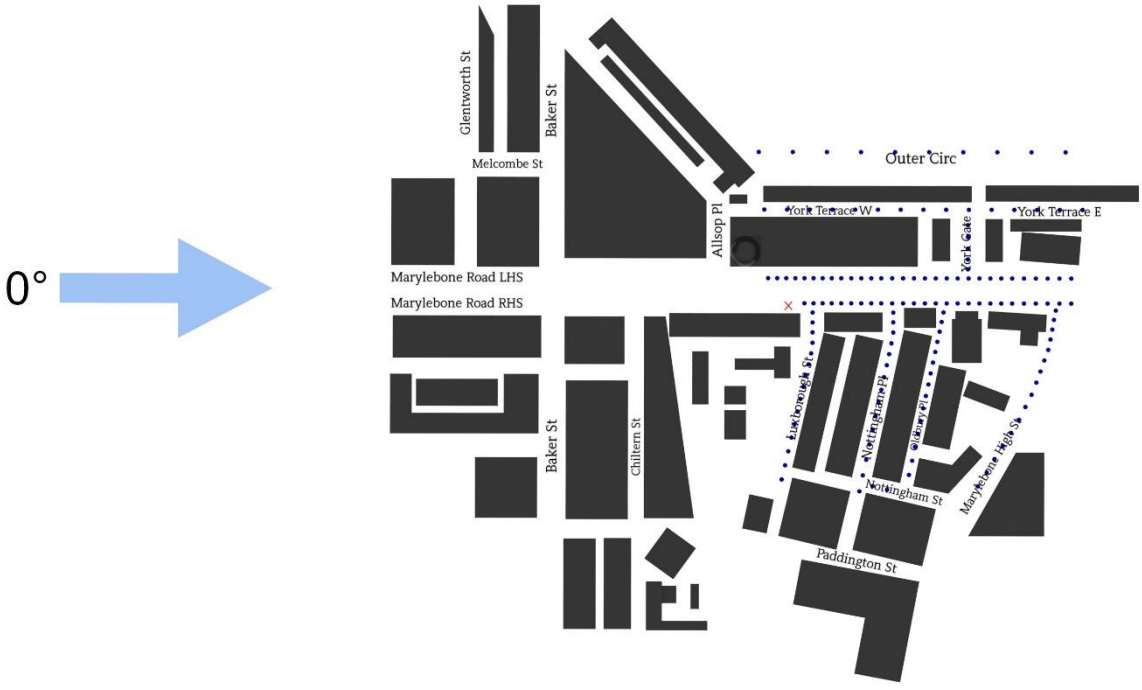

Figure A4: *Measurement locations for 0° inverse modelling case (Inverse of 180°)*

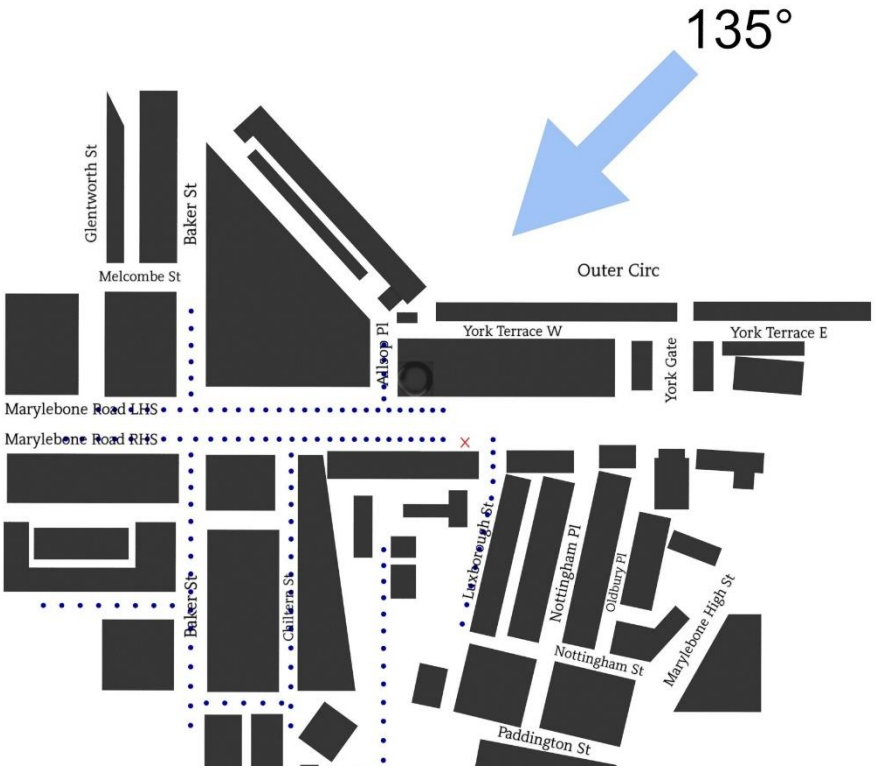

Figure A5: *Measurement locations for 135° inverse modelling case (Inverse of -45°)*

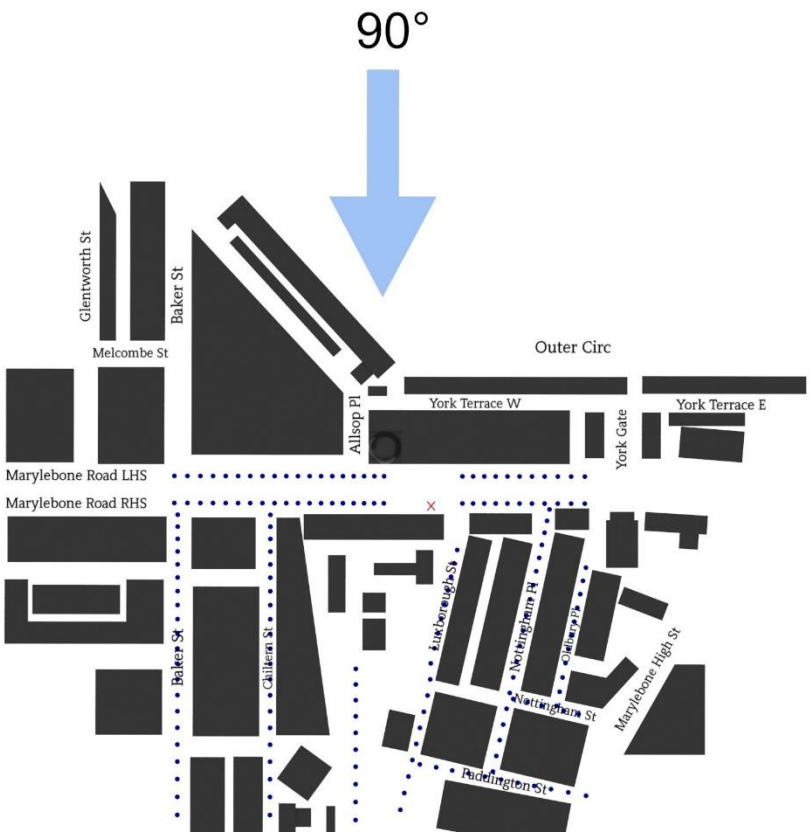

Figure A6: *Measurement locations for 90° inverse modelling case (Inverse of -90°)*

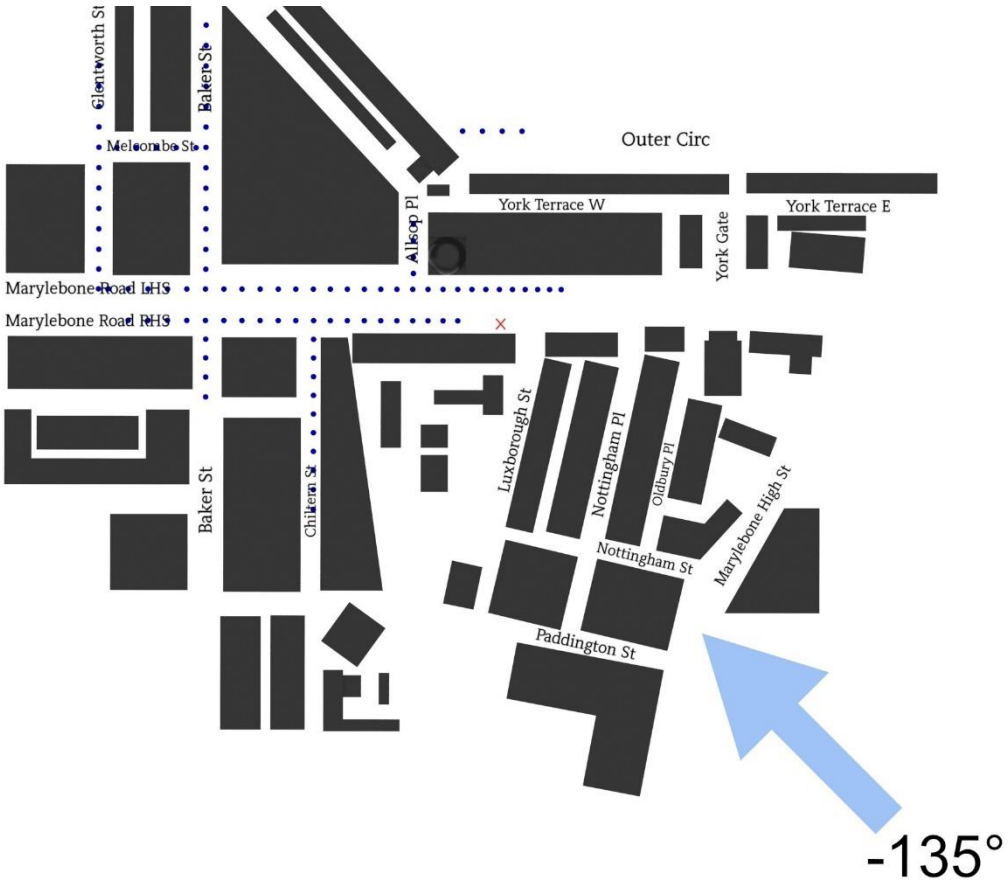

Figure A7: *Measurement locations for -135° inverse modelling case (Inverse of 45°)*

Appendix B: AREA RESPONSIBLE FOR 80% CONCENTRATION CONTRIBUTION

This section shows 3D plots for a range of forward and inverse modelling wind directions where 80% of the contribution originated. These plots show greater detail than those outlined in Figure 54 and Figure 55 in section 5.3.3.

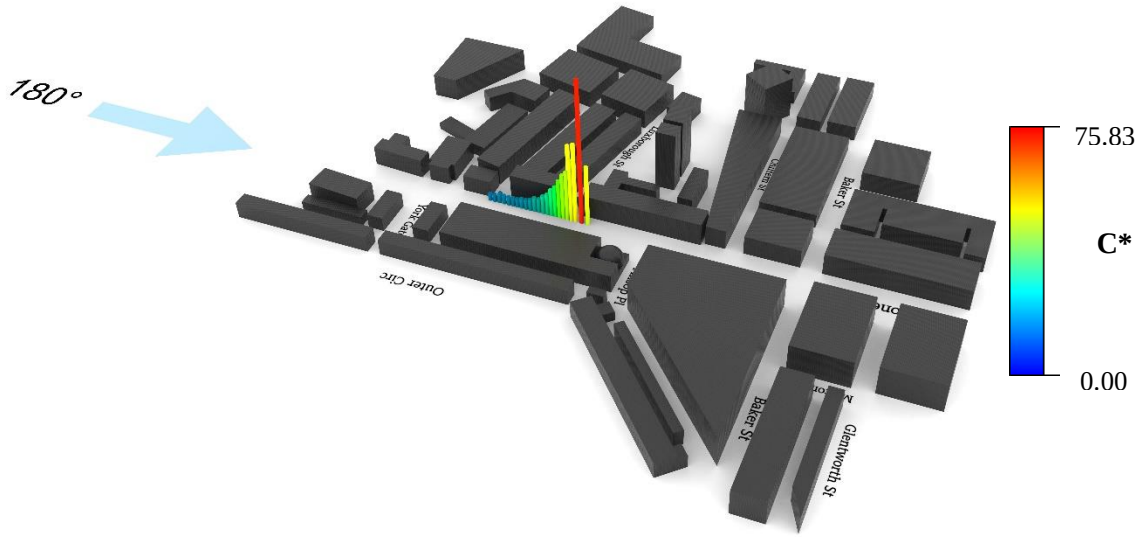

Figure B1: *3D bar plot showing region responsible for 80% of concentration measurements as recorded at (202.5, -74, 10) mm from 180° wind direction (Forward Modelling)*

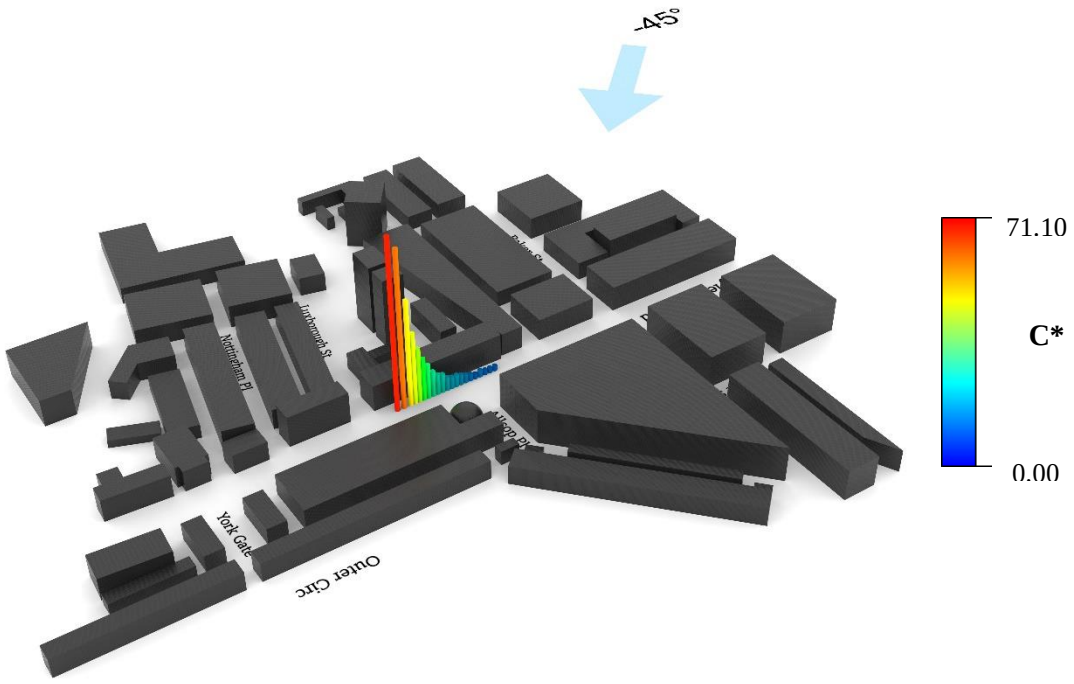

Figure B2: *3D bar plot showing region responsible for 80% of concentration measurements as recorded at (202.5, -74, 10) mm for -45° wind direction (Forward Modelling)*

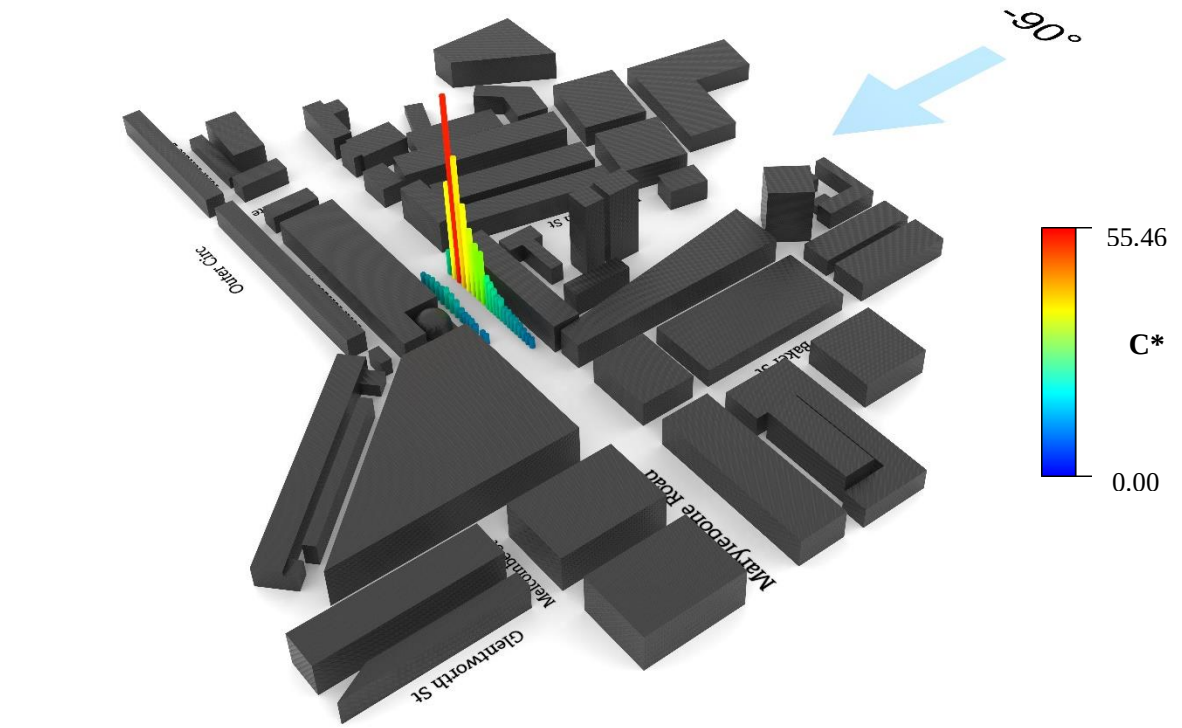

Figure B3: *3D bar plot showing region responsible for 80% of concentration measurements as recorded at (202.5, -74, 10) mm from -90° wind direction (Forward Modelling)*

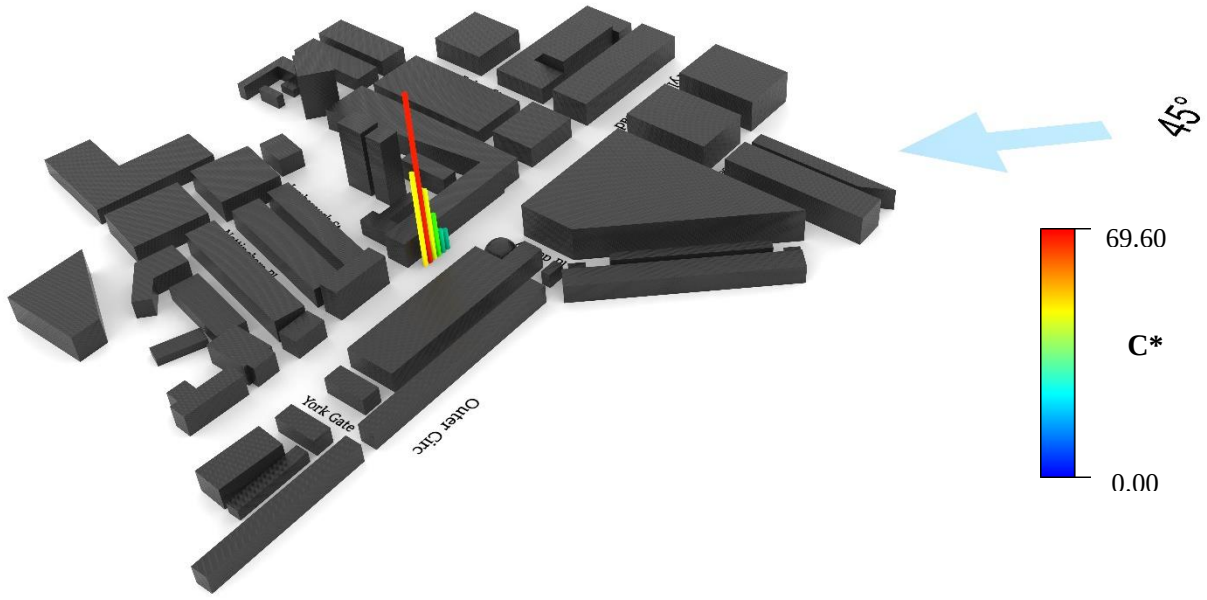

Figure B4: *3D bar plot showing region responsible for 80% of concentration measurements as recorded at (202.5, -74, 10) mm from 45° wind direction (Forward Modelling)*

The figures from here to the next section covers the inversion modelling scenario as described in Section 4.2.2.

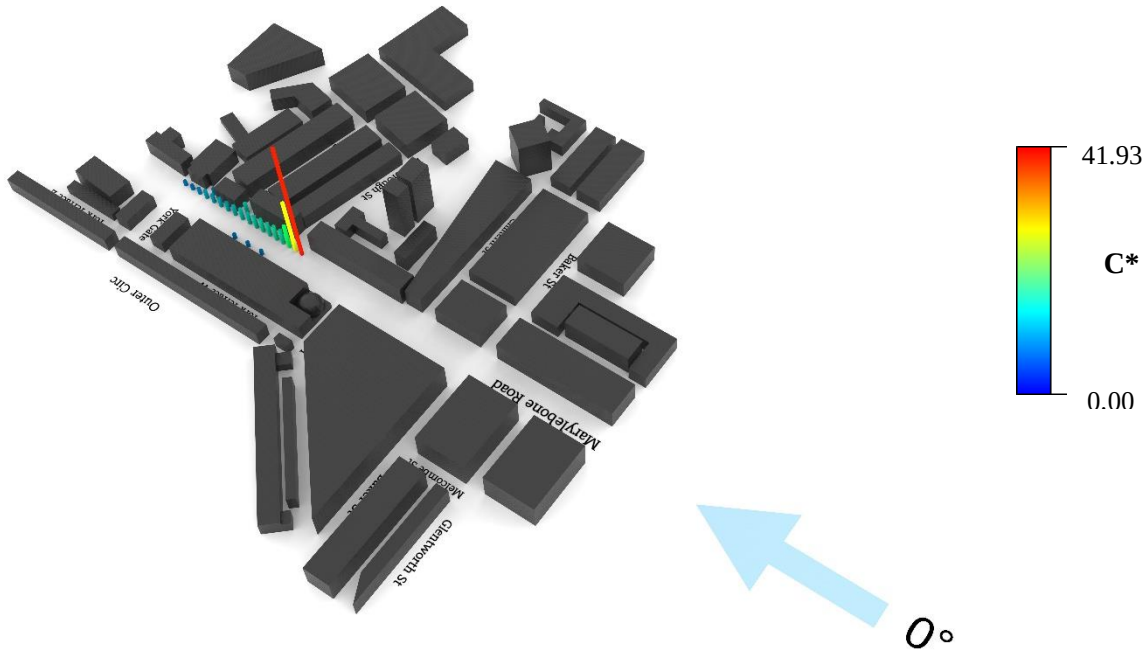

Figure B5: *3D bar plot showing region responsible for 80% of concentration measurements with source gas emission at (202.5, -74, 10) mm from 0° wind direction (inverse of 180°) (Inverse Modelling)*

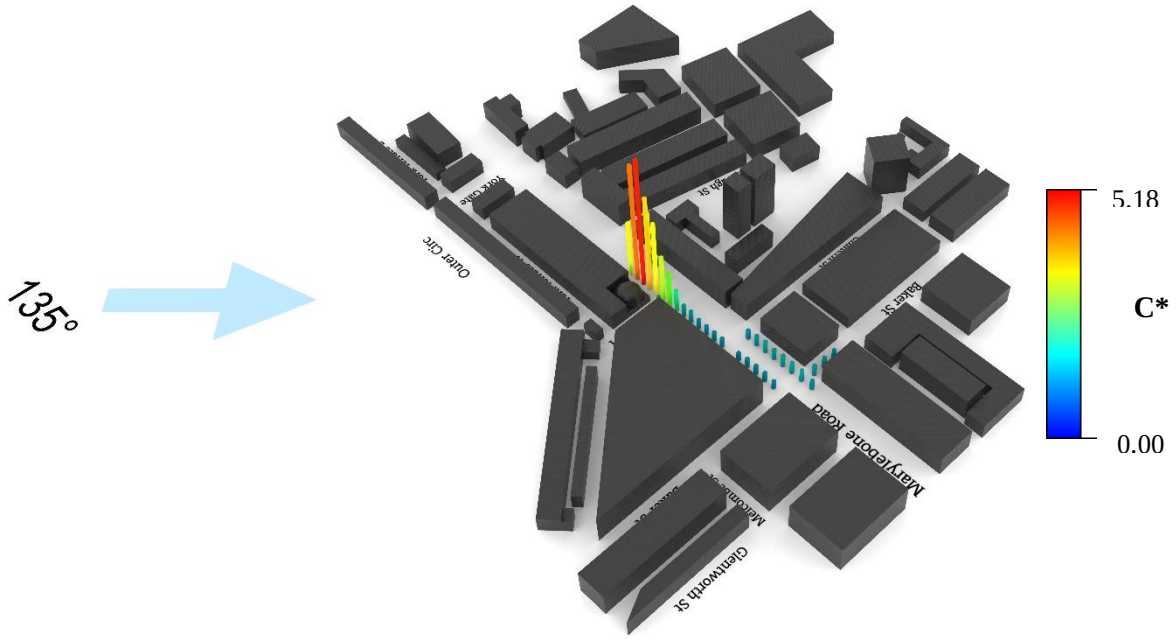

Figure B6: *3D bar plot showing region responsible for 80% of concentration measurements with source gas emission at (202.5, -74, 10) mm from 135° wind direction (inverse of -45°) (Inverse Modelling)*

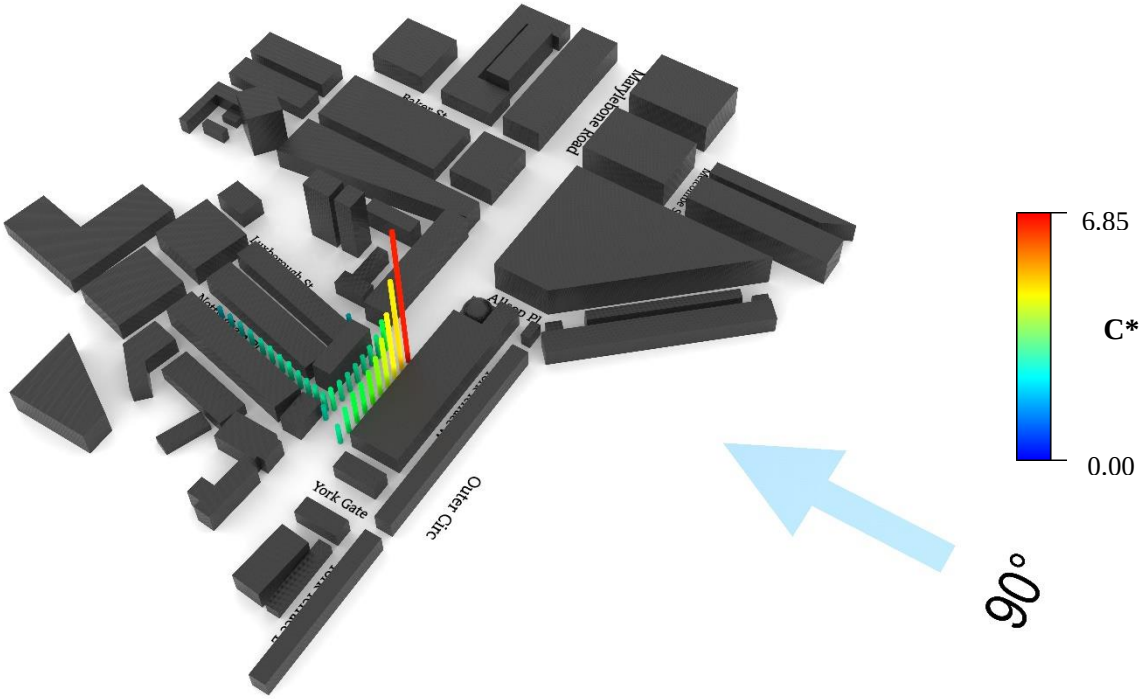

Figure B7: *3D bar plot showing region responsible for 80% of concentration measurements with source gas emission at (202.5, -74, 10) mm from 90° wind direction (inverse of -90°) (Inverse Modelling)*

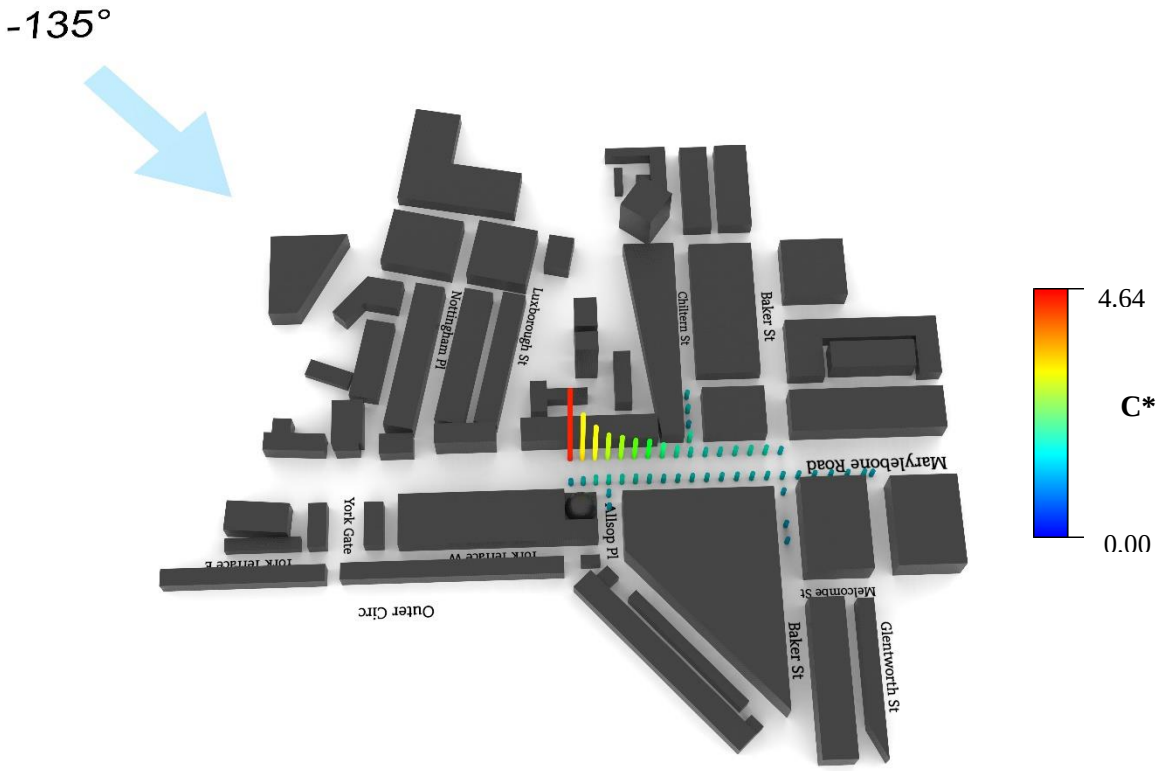

Figure B8: *3D bar plot showing region responsible for 80% of concentration measurements with source gas emission at (202.5, -74, 10) mm from -135° wind direction (inverse of 45°) (Inverse Modelling)*

Appendix C: 3D BAR PLOTS SHOWING FLUCTUATIONS (C'*)

This appendix presents 3D bar plots similar to those presented in Section 5.3, but for non-dimensional standard deviation of concentration fluctuations, c'*. The first four figures presents bar plots for the forward modelling scenario.

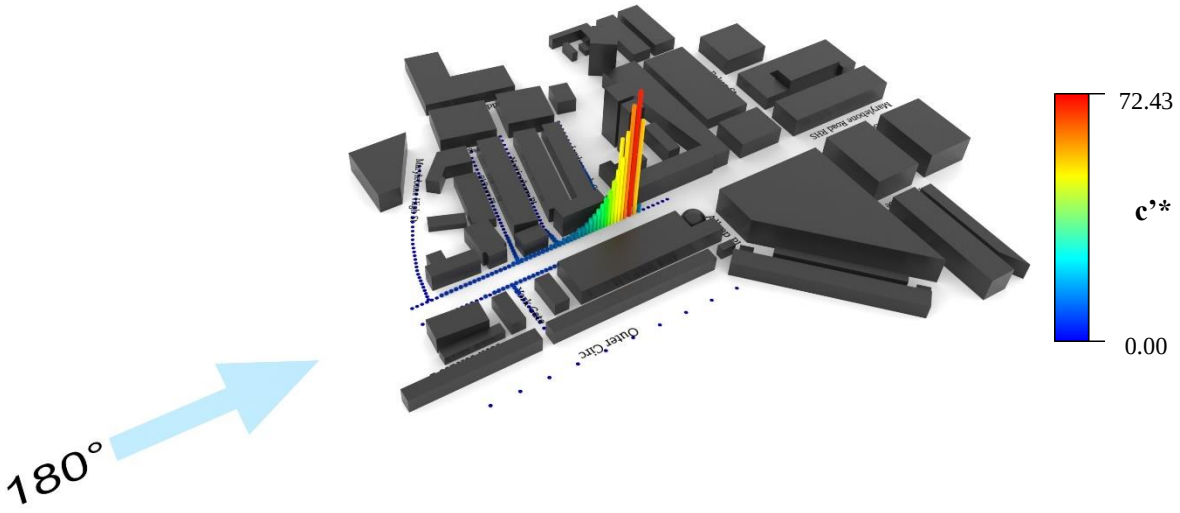

Figure C1: *3D plot of non-dimensional standard deviation of concentration fluctuations, c'* from forward modelling at a wind direction of 180° with varied source release location and fixed FFID at (202.5, -74, 10) mm*

Figure C2: *3D plot of non-dimensional standard deviation of concentration fluctuations, c'* from forward modelling at a wind direction of -45° with varied source release location and fixed FFID at (202.5, -74, 10) mm*

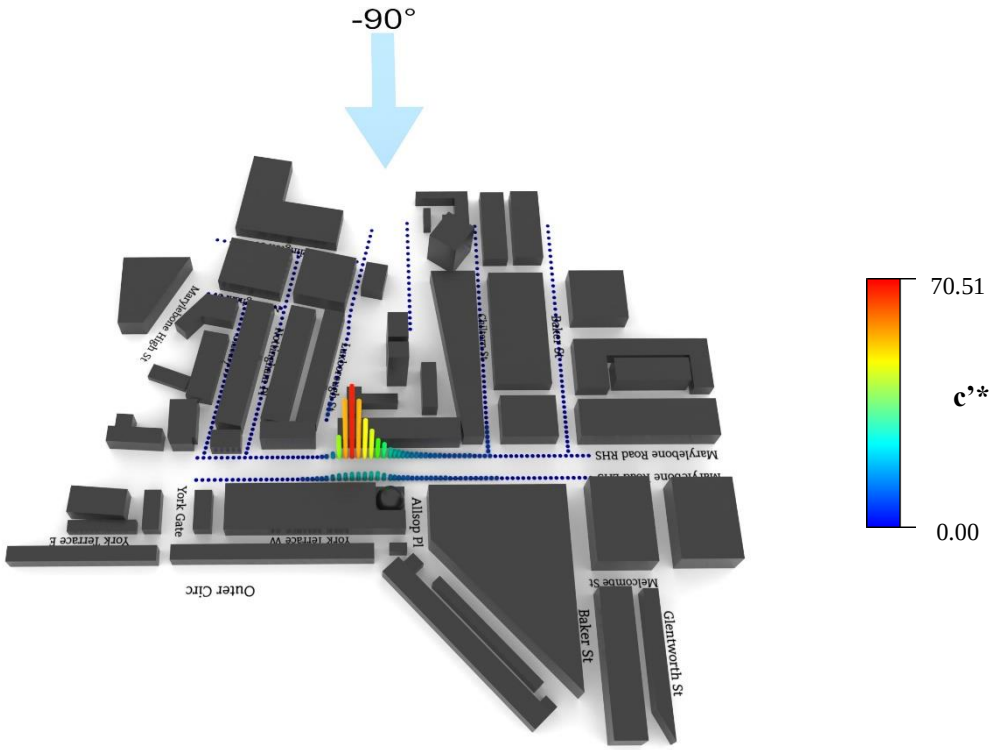

Figure C3: *3D plot of non-dimensional standard deviation of concentration fluctuations, c'* from forward modelling at a wind direction of -90° with varied source release location and fixed FFID at (202.5, -74, 10) mm*

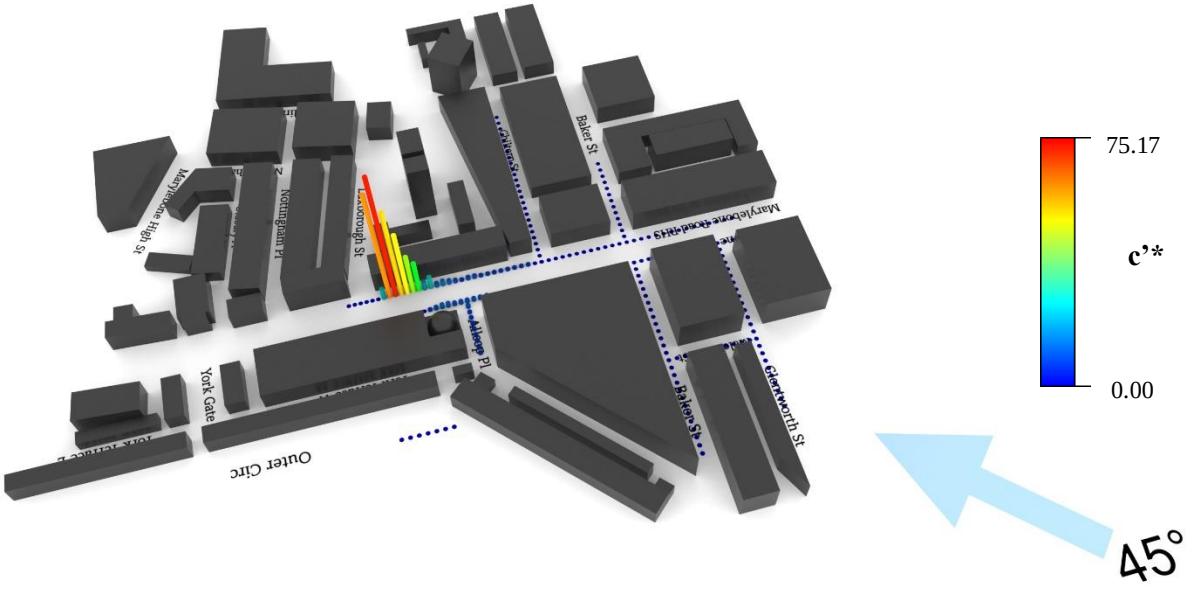

Figure C4: *3D plot of non-dimensional standard deviation of concentration fluctuations, c'* from forward modelling at a wind direction of 45° with varied source release location and fixed FFID at (202.5, -74, 10) mm*

The four figures herein plots the fluctuations for the inversion modelling scenario as described in Section 4.2.2.

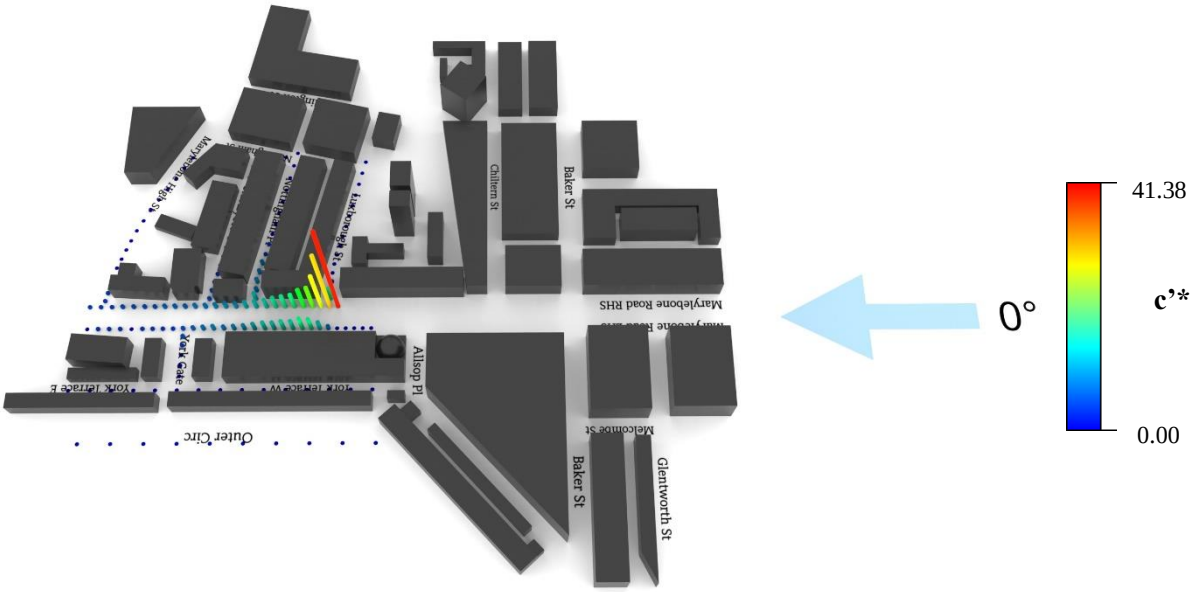

Figure C5: *3D plot of non-dimensional standard deviation of concentration fluctuations, c'* from inverse modelling at a wind direction of 0° with varied FFID location and fixed source release at (202.5, -74, 10) mm*

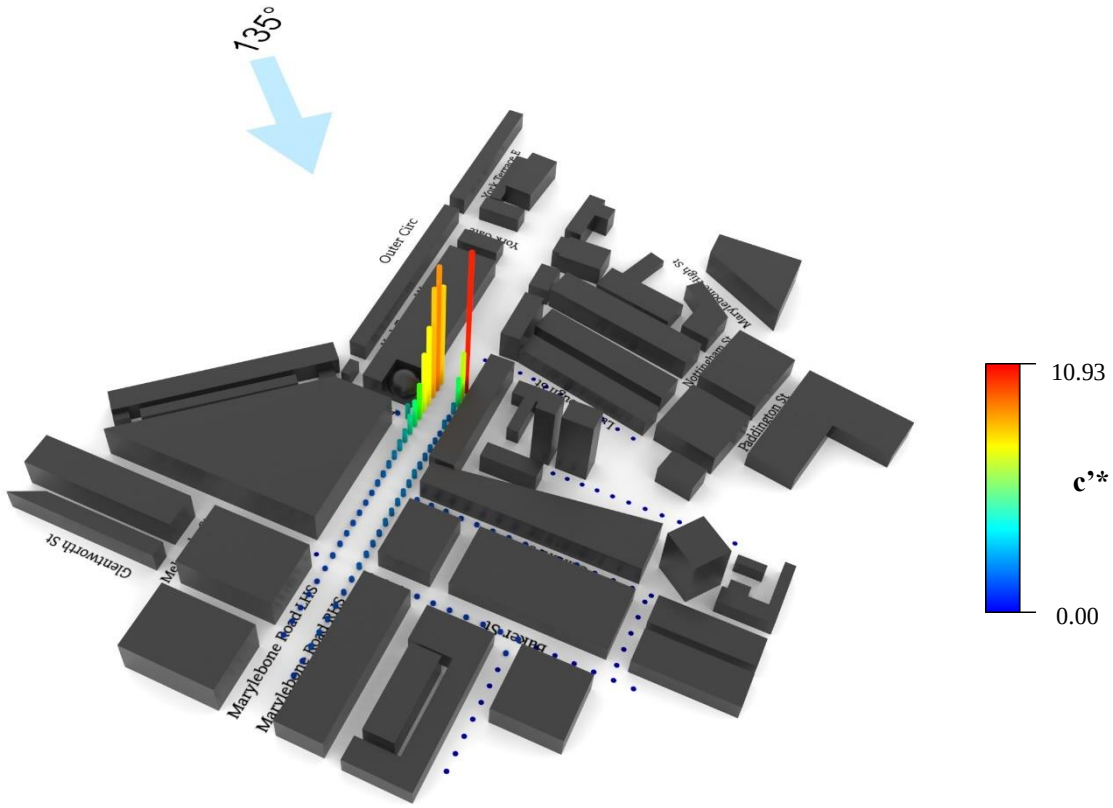

Figure C6: *3D plot of non-dimensional standard deviation of concentration fluctuations, c'* from inverse modelling at a wind direction of 135° with varied FFID location and fixed source release at (202.5, -74, 10) mm*

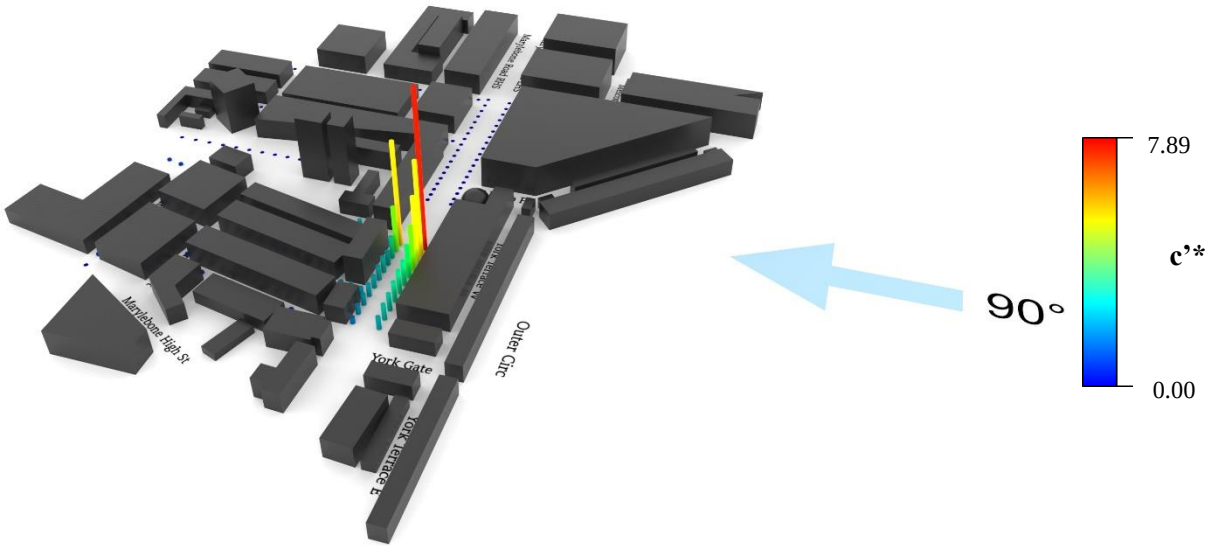

Figure C7: *3D plot of non-dimensional standard deviation of concentration fluctuations, c'* from inverse modelling at a wind direction of 90° with varied FFID location and fixed source release at (202.5, -74, 10) mm*

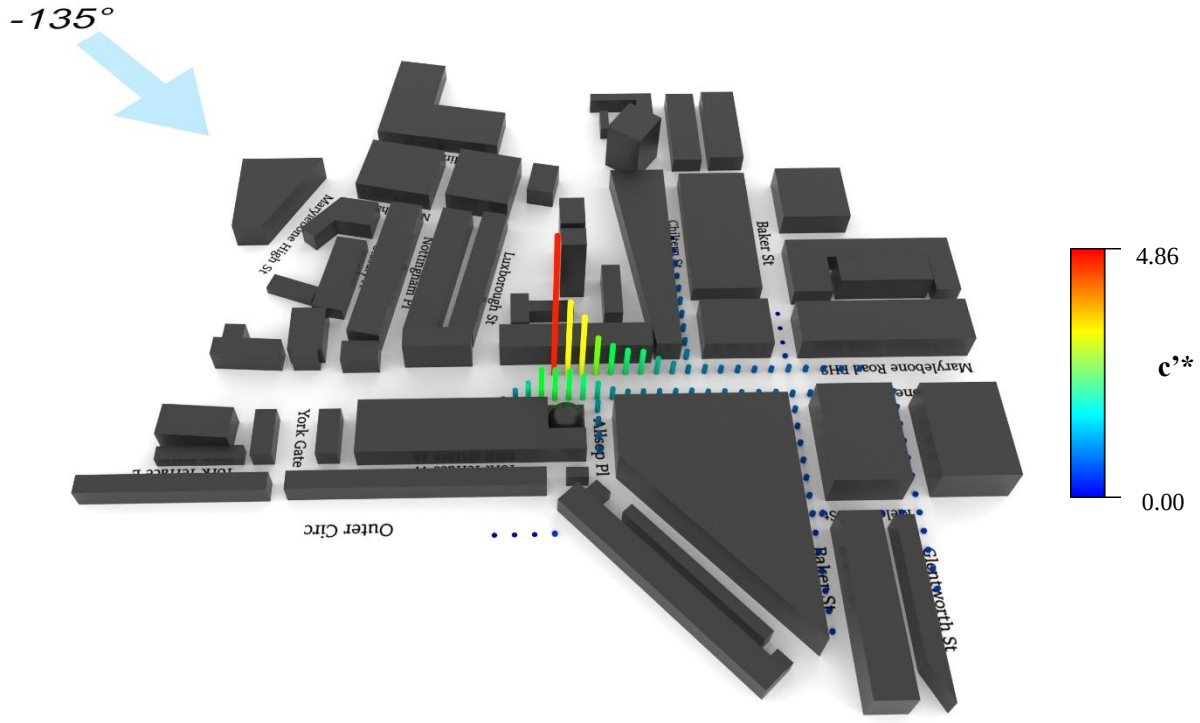

Figure C8: *3D plot of non-dimensional standard deviation of concentration fluctuations, c'* from inverse modelling at a wind direction of -135° with varied FFID location and fixed source release at (202.5, -74, 10) mm*

Appendix D: FORWARD AGAINST INVERSE MODELLING COMPARISON

Graphs plotting C* against X position along Marylebone Road with origin as defined in Figure 28 for a LHS, (y=48) and a RHS, (y=-63) across 180°, -45°, -90°, 45° and their respective inverse cases.

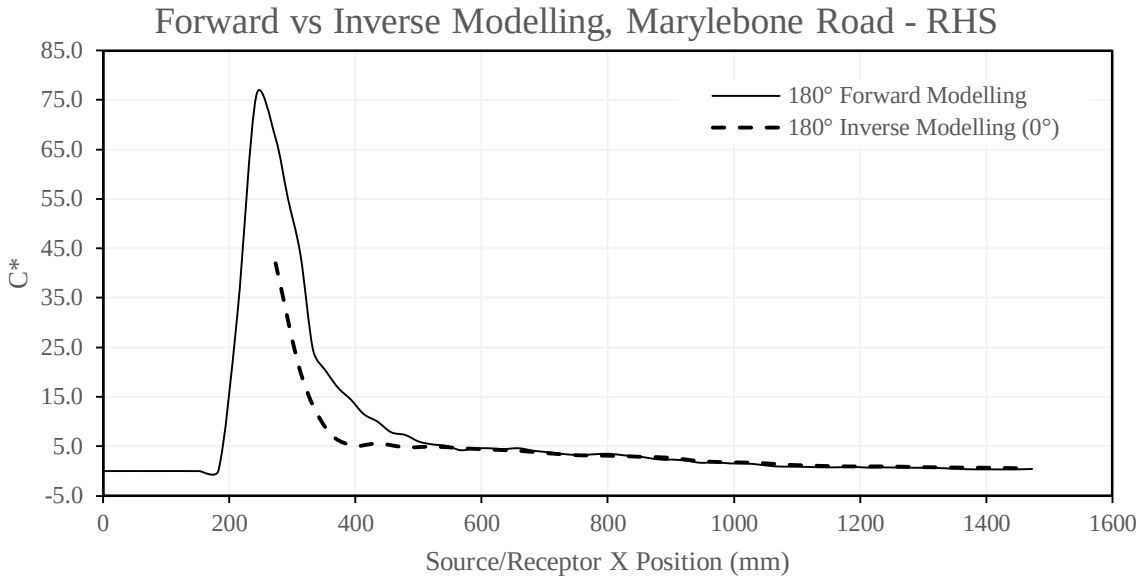

Figure D1: *Graph plotting C* against source/receptor position along Marylebone Road, RHS - comparing forward and inverse modelling scenarios for 180° wind direction*

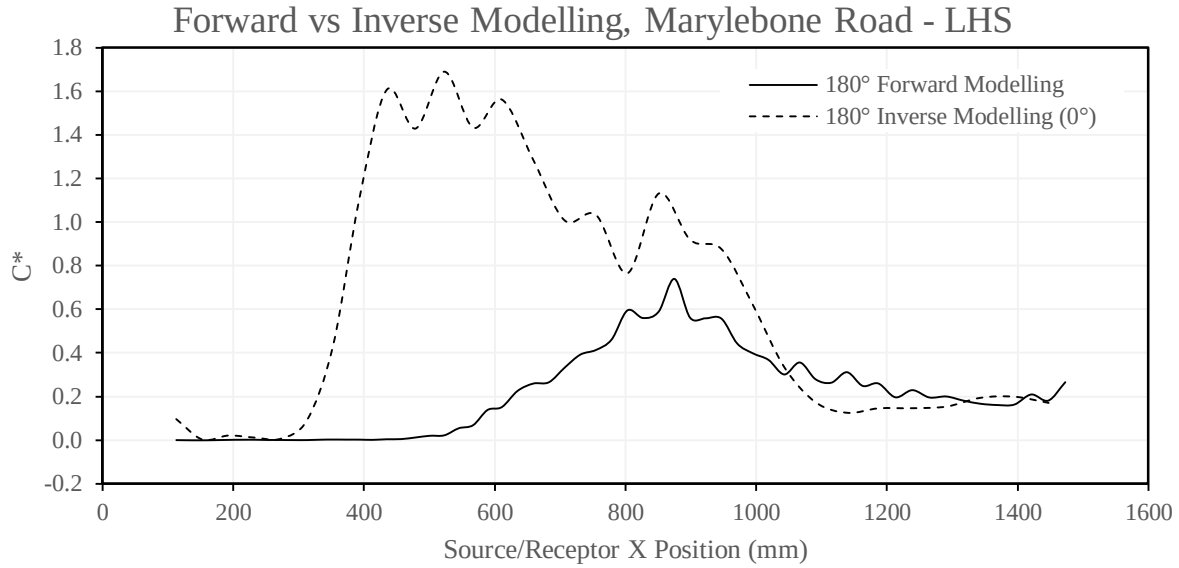

Figure D2: *Graph plotting C* against source/receptor position along Marylebone Road, LHS - comparing forward and inverse modelling scenarios for 180° wind direction*

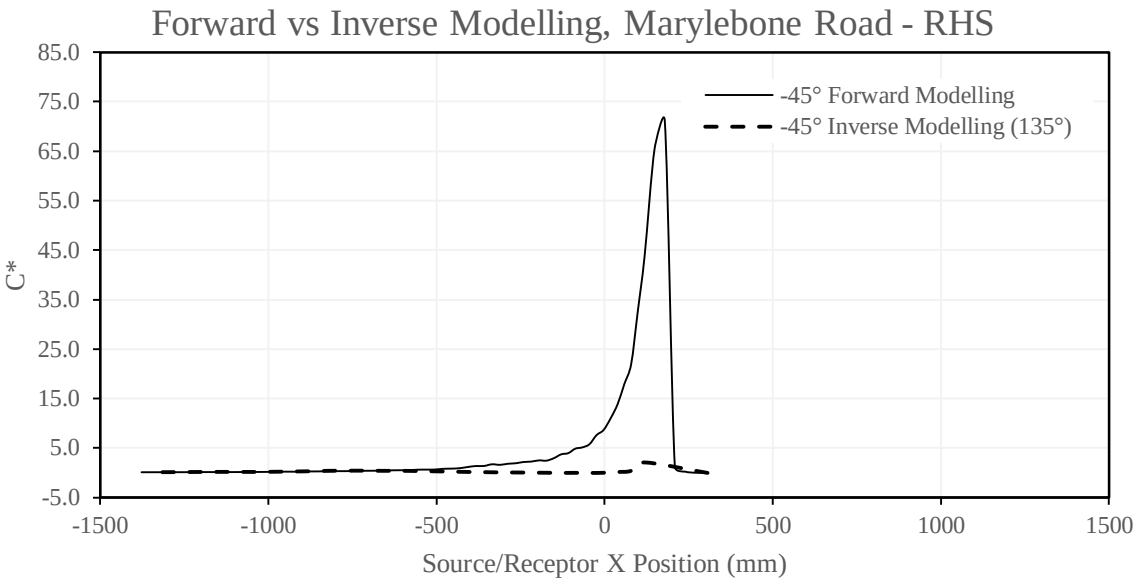

Figure D3: *Graph plotting C* against source/receptor position along Marylebone Road, RHS - comparing forward and inverse modelling scenarios for -45° wind direction*

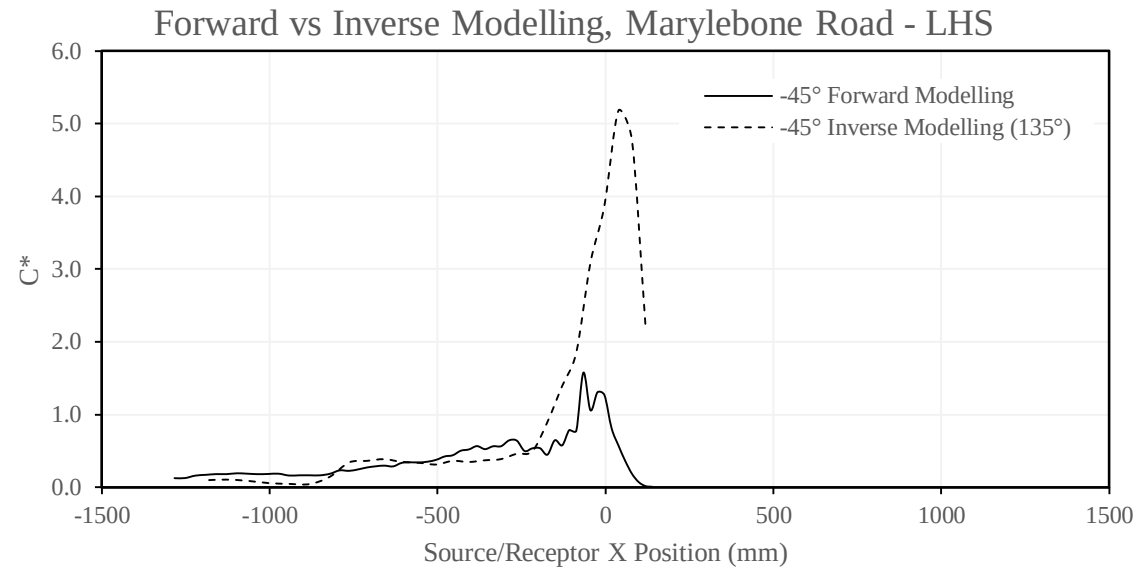

Figure D4: *Graph plotting C* against source/receptor position along Marylebone Road, LHS - comparing forward and inverse modelling scenarios for -45° wind direction*

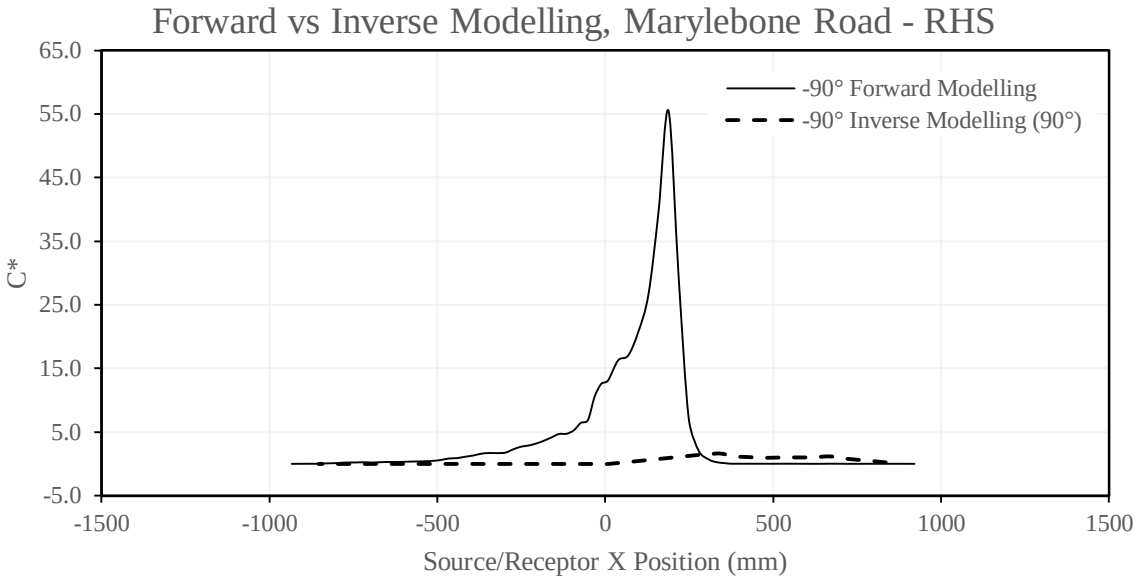

Figure D5: *Graph plotting C* against source/receptor position along Marylebone Road, RHS - comparing forward and inverse modelling scenarios for -90° wind direction*

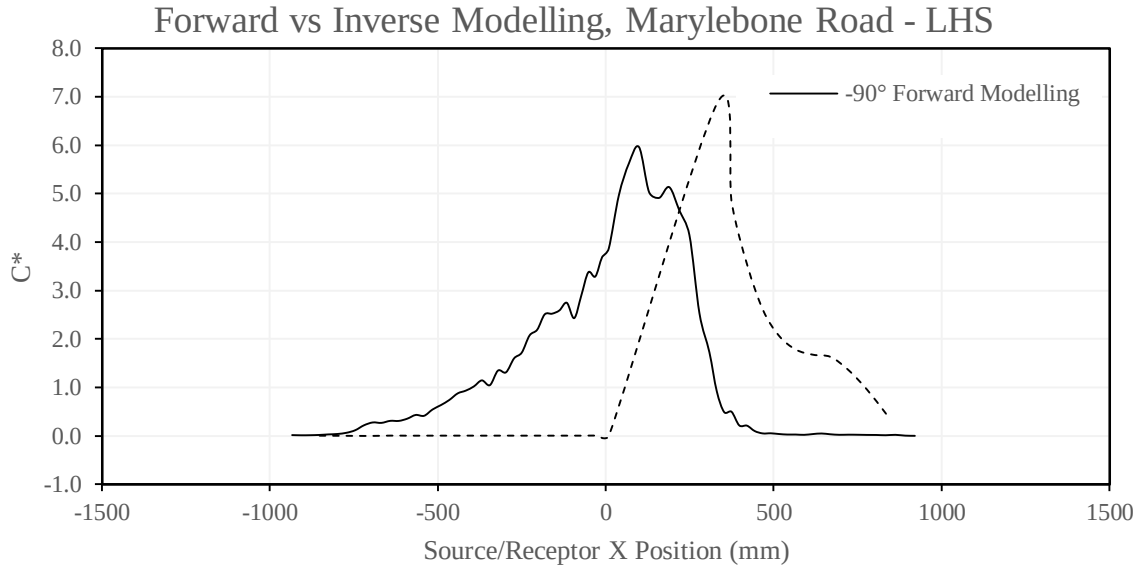

Figure D6: *Graph plotting C* against source/receptor position along Marylebone Road, LHS - comparing forward and inverse modelling scenarios for -90° wind direction*

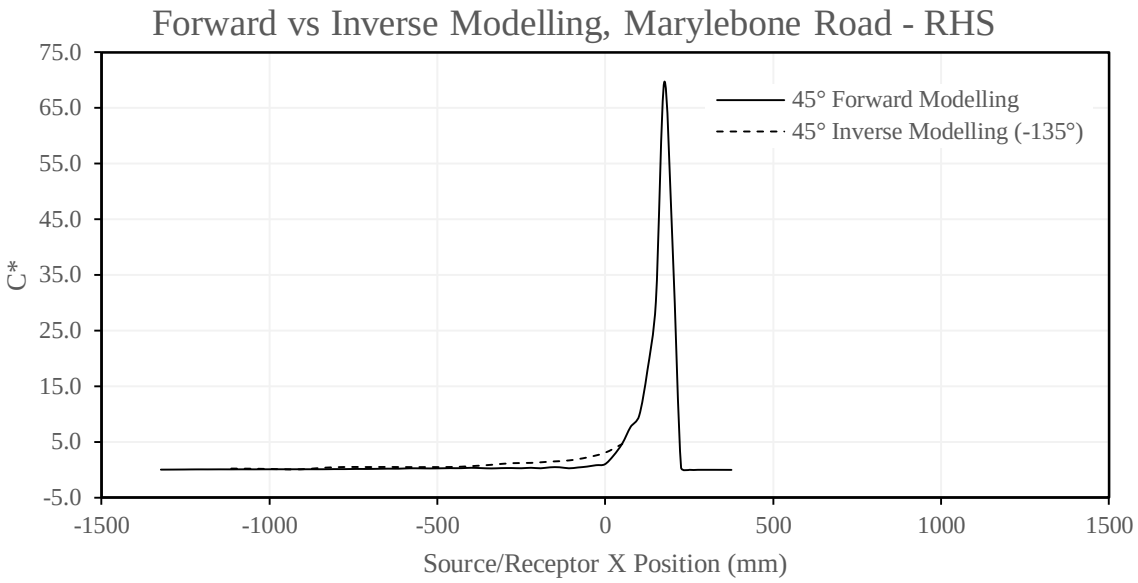

Figure D7: *Graph plotting C* against source/receptor position along Marylebone Road, RHS - comparing forward and inverse modelling scenarios for 45° wind direction*

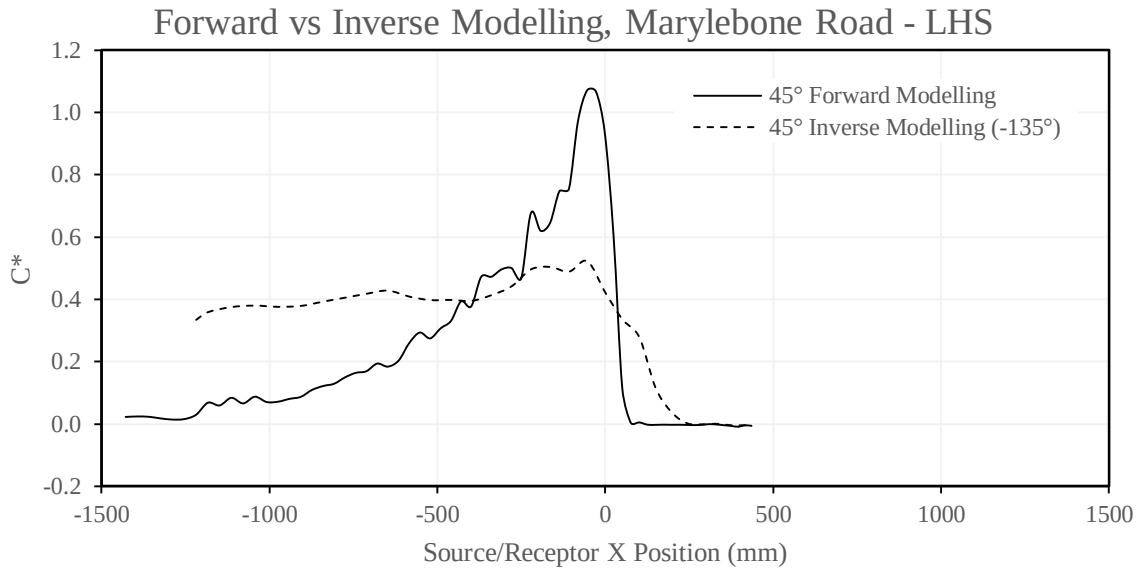

Figure D8: *Graph plotting C* against source/receptor position along Marylebone Road, LHS - comparing forward and inverse modelling scenarios for 45° wind direction*

Appendix E: PROJECT GANTT CHART

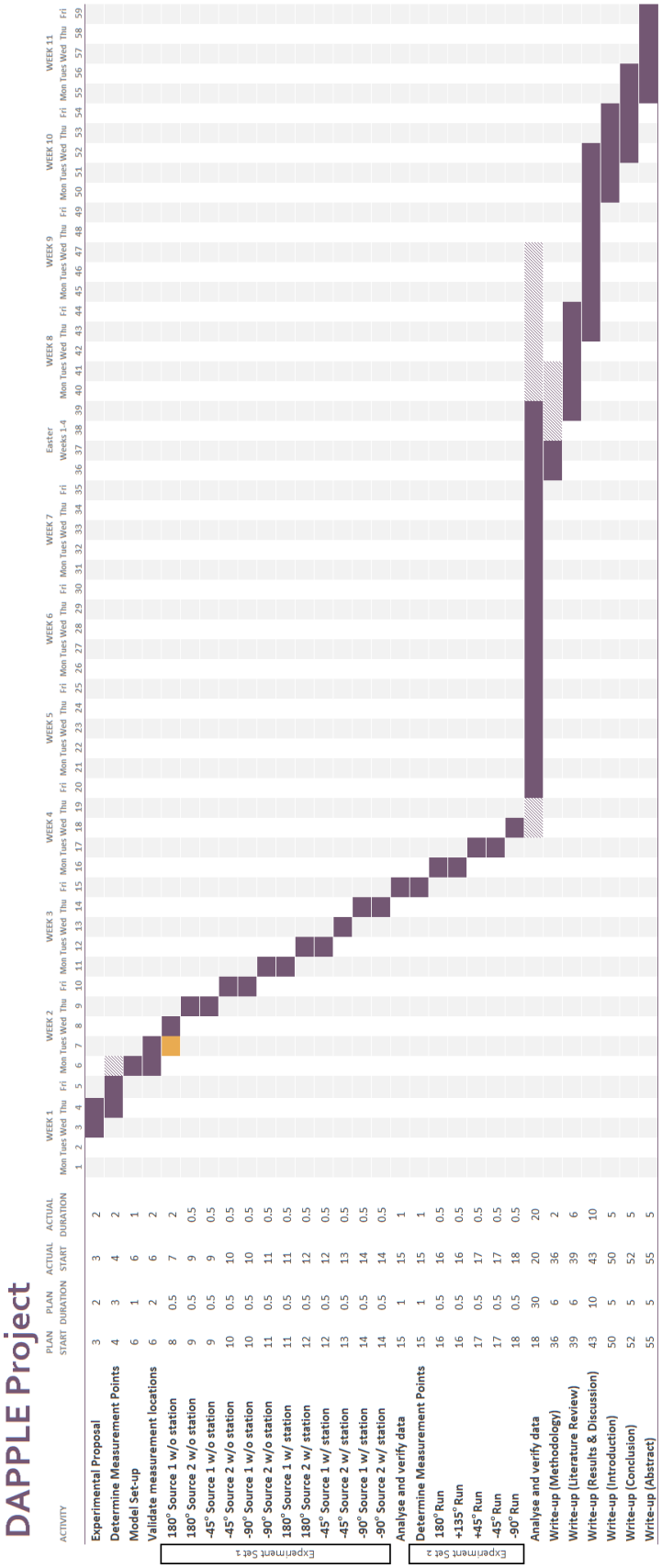

Figure E1: *Project Gantt chart*